2015-01-01

Heat Absorption Analysis By Falling Particles At High Temperatures For Concentrating Solar Power Systems

Arturo Sepulveda Fernandez
University of Texas at El Paso, asepulveda4@miners.utep.edu

HEAT ABSORPTION ANALYSIS BY FALLING PARTICLES AT HIGH TEMPERATURES FOR CONCENTRATING SOLAR POWER SYSTEMS

ARTURO SEPULVEDA FERNANDEZ

DOCTORAL PROGRAM IN ENVIRONMENTAL SCIENCE AND ENGINEERING

APPROVED:

Vinod Kumar Ph.D., Chair

Arturo Bronson Ph.D., Co-Chair

Barry Benedict Ph.D.

Norman D Jr. Love, Ph.D.

Bill Tseng Ph.D.

Zhiwen Ma Ph.D.

Charles Ambler, Ph.D.
Dean of the Graduate School

Dedication

To God my Family and Friends

HEAT ABSORPTION ANALYSIS BY FALLING PARTICLES AT HIGH TEMPERATURES FOR CONCENTRATING SOLAR POWER SYSTEMS

by

Arturo Sepulveda Fernandez, MS

DISSERTATION

Presented to the Faculty of the Graduate School of

The University of Texas at El Paso

in Partial Fulfillment

of the Requirements

for the Degree of

DOCTOR OF PHILOSOPHY

ENVIRONMENTAL SCIENCE AND ENGINEERING

THE UNIVERSITY OF TEXAS AT EL PASO

MAY 2015

Acknowledgements

I would like to deeply thank my advisor Dr. Vinod Kumar for his trust, and giving me the opportunity to work besides him and provide all the support to complete this project, as well I am very grateful to the Department of Energy (DOE FOA # DE-EE0004008), the Department of Mechanical Engineering, and the University of Texas at El Paso for partially supporting my work.

Abstract

High temperature Heat Transfer Fluid (HTF) with Thermal Energy Storage (TES) for the Concentrated Solar Power (CSP) technology can provide a large and relatively cheaper storage option, as opposed to limited and expensive electrical battery storage with PV technology, and hence, it has potential to maintain a constant production when no sunlight is available. Research of material like aluminum, silicon, graphite could be potential candidates to work as thermal energy storage. Currently, nitrate and chloride molten salts are widely used as the TES medium for a CSP plant. However, molten salt, especially chlorides, must be handled carefully at high temperature (800ºC-1200ºC) because of their corrosive nature or decomposition. At high temperature, the electricity generated from a CSP power plant is expected to be cost competitive with conventional sources of power generation system if supplemented with efficient high temperature thermal energy storage (TES) system. In addition, a CSP plant depends only on renewable and clean (i.e., negligible carbon footprint) sources of natural energy resources.

High temperature storage increases power cycle efficiency, which is equivalent to reduce the solar field cost and size, and increases storage energy density. However, the high temperature storage is still not technologically viable at this moment. Our study presents preliminary studies on developing an innovative approach to develop an engineered material that possess high heat capacity and thermal conductivity for temperatures from 700ºC to 1000ºC. The engineered material is achieved by assuming an alloy melt encapsulated in graphite capsules of 10-15mm diameter at approximately 1000ºC. The encapsulated alloy melt uses the enthalpy of fusion/solidification, as well as its heat capacity transfer; it stores and releases heat from 800ºC to 1200ºC during the day time. The storage media uses low-cost, highly-stable solid material (sand, silica) that can be made to behave like a fluid using fluidization and other solid-particle transport

mechanism. For charging/discharging processes, air is directly set in contact with the storage media which provides a heat transfer medium for the particles. In the storage mode, stagnant solid particles can be self-insulated to hold the heat. Also for the simulation study, materials falling at an ambient condition will be considered as a main focus.

Table of Contents

List of Tables

List of Figures

List of Illustrations

Chapter 1: Introduction

Thermal energy storage (TES) is a great channel to develop and help renewable energy demands to improve its usage. With today energy demand levels there is a need for systems with capabilities to produce and store energy with higher efficiencies compared what fossil fuels can give. In the generation of energy with concentrated solar power systems, the thermal energy storage has been playing a great role in the process. TES typically has been using molten salts with different mixtures and one of the most common combinations are with KNO_3 and $NaNO_3$; these combinations have been selected in the past and used because of their thermal properties consisting primarily heat capacity and, thermal conductivity, as well as density, viscosity, availability, and cost. Molten salts can operate in a temperature reaching 600°C, so the need to use materials that can work on higher levels of temperature is required to provide electricity cost at a competitive rate compared to fossil fuels sources. I can assume that there is a need to have a sustainable, cheaper, and available medium that has the desired thermal properties. According to other studies and papers, adjusting particles sizes have the potential to improve thermal energy storage for concentrating solar power (CSP) systems. Ho's paper for TES, it is advantageous to look at new metallic, polymetallic, or alloy and inorganic salt nanoparticles combined with encapsulation processes to facilitate the operation of the CSP process and increase efficiencies due to the particular characteristics of each element combined. There is ample data from experiments that show that the phase-change behavior of nanoscale metals and salts can be different from that of bulk materials. In general, it is found that for small aggregates, the phase transitions occur at significantly lower temperatures than for the bulk material. Further, the transitions extend over a broad temperature range, rather than at a fixed temperature as is found for the bulk material. Both of these characteristics are important for the thermal storage application (1).

Thermal energy storage has several benefits and some of these are fewer turbine startups, better utilization of balance of plant, better utilization of collector field, better match of power

output to demand with an increase in plant revenue, and consistent power output makes CSP plants work with better performance and reduce conventional generation backups (2)(3).

The DOE has set up cost targets for the energy with CSP between $0.05 and $0.08/KWh which is intended to compete with the coal power plants, and it shows the temperature range with the Sunshot initiative and the current range of temperature for the systems operating today(3). Energy storage (ES) is the storing of some form of energy that can be drawn upon at a later time to perform some useful operation. A device that stores energy is sometimes called an accumulator. All forms of energy are potential energy (e.g. chemical or gravitational), kinetic energy, electrical energy, or thermal energy, and all these forms of energy could be stored with an appropriate method, system, or technology. This means that every form of energy has itself an accumulator (4).

Thermal energy storage (TES) systems have the potential of increasing the effective use of thermal energy equipment and of facilitating large-scale switching. They are normally useful for correcting the mismatch between the supply and demand of energy. There are mainly two types of TES systems, sensible storage systems and latent storage systems. As the temperature of a substance increases, its energy content also increases. The energy released (or absorbed) by a material as its temperature is reduced (or increased) is called sensible heat. On the other hand, the energy required to convert a solid material into a liquid material or a liquid material into a gas (phase change of a material) is called heat of fusion at the melting point (solid to liquid) and heat of vaporization (liquid to gas), respectively. Latent heat is associated with these changes of phase. The other category of storing heat is through the use of reversible endothermic chemical reactions. Chemical heat is associated to these reversible chemical reactions where heat is needed to dissociate a chemical product. All this heat (or almost all) will be recuperated later, when synthesis reaction takes place. A complete storage process involves at least three steps: charging, storing and discharging. In practical systems, some of the steps may occur simultaneously, and each step

can happen more than once in each storage cycle(4). Thermal energy can be stored nearly isothermally in some substances as the latent heat of phase changes, that is, as the heat of fusion (solid-liquid transition), heat of vaporization (liquid-vapor), or heat of solid-solid crystalline phase transformation occurs(5).

Sensible heat storage is thermal energy that can be stored in the change of temperatures of substances that experience a change in internal energy. Besides the density and the specific heat of the storage material, other properties are important for sensible heat storage: operational temperatures, thermal conductivity and diffusivity, vapor pressure, compatibility among materials stability, heat loss coefficient as a function of the surface areas to volume ratio, and cost(5). Sensible TES consists of a storage medium, a container (commonly tank), and inlet/outlet devices. Tanks must both retain the storage material and prevent losses of thermal energy. The existence of a thermal gradient across storage is desirable. Sensible heat storage can be made by solid media or liquid media(4). The energy stored as sensible heat can be calculated by the product of its mass, the average specific heat, and the temperature change.

Latent heat storage media can be cited as thermal energy that can be stored nearly isothermally in some substances as the latent heat of phase change, as heat of fusion (solid–liquid transition) or heat of vaporization (liquid–vapor transition). Today, mainly the solid–liquid transition is used, and substances used under this technology are called PCM. Storage systems utilizing PCM can be reduced in size compared to single-phase sensible heating systems. However, heat transfer design and media selection are more difficult and experience with low temperature salts has shown that the performance of the materials can degrade after a moderate number of freeze–melt cycles. Phase change materials allow large amounts of energy to be stored in relatively small volumes, resulting in some of the lowest storage media costs of any storage concepts(4). Phase change materials (PCMs) are proper candidates to increase stored energy density; PCMs enthalpies can be matched to sensible HTFs and to water or steam.

TES makes CSP capable and allows CSP to participate in intermediate and base loads markets which will need cost reduction in collector components and learning in economies of

scale(3). Thermal energy storage allows solar electricity to meet utility peak demands or even to enable solar energy to become a baseload power source. Thermal energy storage is the cheapest form of electrical energy storage and also one of the most efficient (6). One advantage of the thermal energy storage is that it can be collected at a different hours of it usage than the one that can be used or it can even be consumed during peak hours; this helps electric generation plants meet their goals and achieve efficiency targets. Solar generation without thermal energy storage will not be a continuous supply of energy. For CSP, it is always good to have in mind the amount of water consumption so having an air cooling and wet/dry hybrid cooling system offers highly viable alternatives that could reduce the total water usage of steam-generating CSP plants by 80% to 90% at a penalty in electricity cost in the neighborhood of 2% to 10%, depending on plant location and other assumptions(7).

1.1 Concentrated Solar Power (CSP) Technologies examples

CSP has different technologies and the following can be mentioned as the main ones or more common, parabolic trough, dish systems, and tower.

1.1.1 Tower

The tower CSP technology has mirrors or heliostats arranged around a tower with receivers located at the top of the tower. The sun light is reflected onto the receiver at the top of the tower. The receiver collects the sun light so the energy can be absorbed by the heat transfer fluid (HTF) which can be oil or molten salts. HTF should be of the purest grade from the onset, and must be kept free of organic impurities to avoid reactions(8). The DOE Concentrating Solar Power Program has developed detailed baseline costs and performance data for the power tower technology. In addition, detailed technology Research and Development (R&D) plans specify how these technologies are expected to change over time. The DOE also has established assumed plant deployment forecasts over time(9). The major risk for tower solar plants to reach market acceptance (competitiveness) is the incentives that will allow the plant to be competitive with

current non-renewable cost of generating power. Assuming incentives are provided, the risk for achieving cost reduction over the next 10–20 years is low to average (9). Solar plant and power plant scale-ups provide the largest cost reduction opportunity for power tower technologies(9).

1.1.2 Parabolic Trough

The parabolic trough uses long U-shaped mirrors with a tube located where the sunlight is reflected and collected with the HTF which can be oil or molten salts. Parabolic Trough can use steam generation system, a Rankin steam turbine/generator cycle, and optional thermal storage and/or fossil-fired backup systems (10). The existing parabolic trough plants have been designed to use solar energy as the primary energy source to produce electricity. Given sufficient solar input, the plants can operate at full-rated power using solar energy alone. During summer months, the plants typically operate for 10–12 hours a day on solar energy at full-rated electric output(10). The cost, performance, and risk of parabolic trough technology are fairly well established by the experience of the existing operating parabolic trough plants. Based on the data available, the analysis bounds the future potential cost of parabolic trough power(9). Assuming that technology improvements are limited to current demonstrated or tested improvements and a deployment of 2.8 GWe of installed capacity by the year 2020 and successful development of a thermal storage system, trough costs should drop to approximately 6.2¢/kWh(9). The major risk for parabolic trough solar plants to reach market acceptance (competitiveness) is the incentives that will allow the plant to be competitive with current non-renewable cost of generating power. Assuming incentives are provided the risk for achieving cost reduction over the next 10 – 20 years is low to average (9).

1.1.3 Dish Systems

Dish reflects the sun light or the energy to a focus point where the receiver will heat the working fluid; the working fluid can be hydrogen which will drive the turbine or Stirling engine.

The dish has some advantages like easy installation in rough or steep lands over other systems. Also the amount of energy generated is a function of the size of the parabolic dish system and the amount of dishes installed in a particular application. Conceptually, the dish Stirling system is the simplest of all thermal solar technologies, but the Stirling motor that converts the heat is a sophisticated closed-cycle motor that is highly specialized for this application. Stirling motors are not found in many applications. They are used as an ultra-quiet motor in attack submarines and for small power generation units (gen-sets). Dish engines are a primarily intermittent energy source, having only a pedestal as footprint, can be built within days, comes in small sizes (1-25 kW) and are thus modular(11). However, market penetration of Stirling gen-sets is marginal due to the dominance of the combustion motor (diesel gen-sets)(12).

Chapter 2: Background and Literature review

Research is needed on materials that can be used for thermal energy storage with higher efficiencies, for this competitive market of energy demand, improve efficiencies in the materials that are being used in the current Concentrated Solar Power (CSP) applications or in the market. Concentrated solar power technologies represent a good source of significant utility-scale renewable electricity generation for some regions in America, Europe and Africa(13). For CSP systems currently it has been used molten salts in the thermal energy storage phase. Charging a solar salt unit can be accomplished by taking the dry salt and melting it in a tank heated electrically or by steam, oil, or gas (14). In solar applications, thermal storages are usually taken as integrated parts of the solar utility system to overcome the operational problems related to the intermittent nature of solar energy(15). DOE estimates that a 6¢/kWh installed CSP energy system, without subsidies, would make solar energy competitive with the wholesale rate of electricity without additional subsidies, nearly everywhere in the U.S., with adequate direct normal irradiance (DNI). Achieving 6¢/kWh installed systems by 2020 represents a significantly more challenging goal than current "Business As Usual" projections of reaching 9¢/kWh for utility scale systems by 2020, and would enable large scale deployment of solar energy without subsidies(16). Taking in consideration the current technology, a concentrated solar power (CSP) plant in general has higher energy conversion efficiency and relatively low cost compared to other systems of energy generation like photovoltaic panels (17).

The melter has the capability to melt and bring the melt temperature up to 288 degree Celsius and then to pump the molten salt to the heat traced and insulated cold storage tank(14). Protective heating systems for the solar field are necessary for start-up, maintenance, or to recover from a frozen condition brought about by an unexpected equipment outage(18). Nowadays there is a big interest in developing sustainable and cheaper systems to generate and store energy due to self-sufficiency needs, high energy demand and the particular interests of different countries around the world. For this study, the main purpose is to search for materials and perform

programing simulations to select materials that can work at higher temperatures than the ones that are currently being used as molten salts.

The goal of this work is to complete the research on materials with small sizes; in the rage of 0.01 mm and 0.001 mm that can store energy at temperatures between 700°C and 1000°C. Some of the main characteristics that are being contemplated and reviewed for the new materials are heat capacity (Cp), thermal conductivity (k), density and cost. Heat transfer in a system has to be with the process from one equilibrium state to another and the amount of energy that is gain or lost in a system. Total energy is the sum of all forms of energy of a system and it consists of internal, kinetic, and potential energies. The sensible and latent forms of internal energy can be transferred from one medium to another as a result of a temperature difference, and are referred to as heat or thermal energy(19).

Regarding the amount of acreage or land needed for a CSP facility depends partly on the type of technology deployed. More importantly, though, land use is dependent on thermal storage hours and a location's solar insolation. Common practice is to state land requirements in terms of acres per MW. The range normally provided is 4–8 acres in a location with solar insolation similar to what is found in the U.S. Southwest desert (SNL 2009). The low end of the range is possible when greater self-shading of reflectors is allowed, although this results in reduced electricity output. The high end represents the additional land needed for energy storage, with energy storage resulting in higher capacity factor. Because of such variation, when considering land needs, it can be more useful to provide a number in terms of acres per MWh. When this is done, a comparison among CSP technology types can more easily be made. The general trend at this stage of technology development is that power towers require approximately 20% more land per MWh than troughs(20). Commercial dish-engine facilities have not yet been built, so a comparison of land requirements for this technology with other CSP technologies has not yet been made(20).

The resurgent interest in CSP has been driven by renewable portfolio standards in southwestern states and renewable energy feed-in tariffs in Spain. CSP has cost advantages over solar photovoltaic systems for large, centralized power plants. Certain CSP systems, in particular

parabolic troughs and power towers, are also amenable to the incorporation of thermal energy storage. Thermal energy storage is much less expensive than electric storage and allows CSP plants to increase the capacity factor and dispatch power as needed, for example to cover an evening demand peak(21).

However, CSP costs are still higher than conventional fossil fired generation. Costs are expected to fall as manufacturing scale and deployment increase. Further improvements in system efficiency are also necessary to improve the economics. Linear Fresnel and power towers are less mature than parabolic troughs and operating experience is needed to prove system reliability and cost. For these three CSP technologies, an improvement in the thermo physical properties of the heat transfer fluid (HTF) is one avenue for increased system efficiency(21).

Concentrated solar power systems need a storage subsystem or maintain a minimal temperature in order to have continuous operation. These subsystems can operate with an external source of energy, this means that mainly the outside source will be needed at the start of the operation or when the solar source is diminish or suspended for a longer period than the time than the HTF can deliver its energy stored(22).

2.1 Applications for concentrated solar power

Thermal energy storage is has been used in generation of energy on Concentrated Solar Power systems, concentrated solar power systems operates with parabolic trough, tower or dish. A tool that can be used to analyze the CSP systems is the solar advisor model (SAM) that can be used to evaluate and show the levelized cost of energy (LCOE), SAM is a helpful tool because it incorporates the financing, costing, and performance of systems, and makes it possible to apply consistent financing and cost assumptions across all solar technologies(23). SAM can be used also to compare cost and efficiencies with non-solar technologies(24). CSP has a good potential for electricity and chemical fuel applications(25)(9). Storage is valuable and has a trend that can be viable economically(25).

For solar power generation using CSP, the annual average amount of solar energy reaching the ground needs to be 6.0 kilowatt-hours per square meter per day (kWh/m2/day) or higher. This is the case in many regions of the West(12). The levelized cost of electricity for parabolic trough and tower systems is predicted to drop below 11 cents/kWh, making these technologies competitive in the market place(24)(26).

In premium solar resource areas, the average annual solar radiation exceeds 7.0kWh/m2/day. Using the most efficient solar generating technology (dish Stirling), an area the size of an NBA basketball court located in a premium solar resource would generate 60,740 kWh of electricity a year(12).

2.1.1 Parabolic trough

The parabolic trough system operates with a reflective surface with a parabolic shape defined by the formula $Y=x^2/4f$ where the distance f represents the location of the focal point of the parabola, which is basically the distance of the focal line of the parabola from its vertex. The area on the trough shaped parabola is cover with reflective material to concentrate the solar energy into the focal tube. In order for this to happen the symmetry plane or optical axis of the parabola arrangement needs to be directed toward the incoming light from the sun. The solar field is modular in nature and comprises many parallel rows of solar collectors, normally aligned on a north-south horizontal axis. Each solar collector has a linear parabolic-shaped reflector that focuses the sun's direct beam radiation on a linear receiver located at the focus of the parabola. The collectors track the sun from east to west during the day to ensure that the sun is continuously focused on the linear receiver. A heat transfer fluid is heated up as high as 393°C as it circulates through the receiver and returns to a series of heat exchangers in the power block, where the fluid is used to generate high-pressure superheated steam (100 bar, 371°C). The superheated steam is then fed to a conventional reheat steam turbine/generator to produce electricity(27).

Parabolic trough solar collectors

The parabolic trough solar collector can be arrange and form solar fields that can be used to generate electricity and store energy for later use.

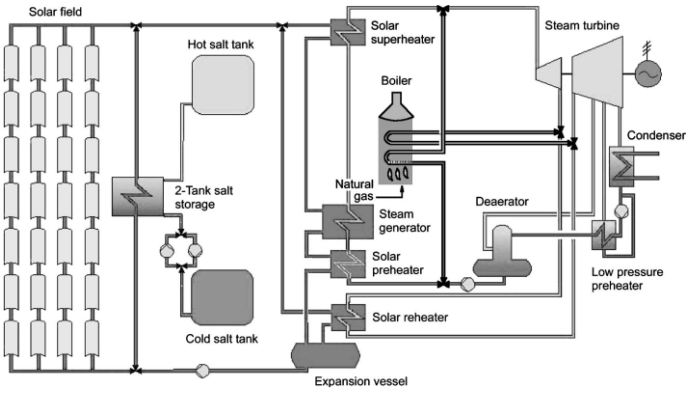

Figure 2.1 Process flow schematic of large-scale parabolic trough solar power plant. (Flabeg Solar International)

2.1.2 Power tower systems

The power tower system uses arrangements of numerous flat mirrors called heliostats tracking the sun, reflecting the sun light with its focus in to a receiver that is located on the top of a tower. This receiver collects the energy and a heat transfer fluid (HTF) is heated in order to be used to generate vapor to run a turbine and generate electricity. The HTF can be used also to store energy for later use when the sun goes down and the energy is not available during the night hours. The energy can be stored in a two tank system with molten salt on it. Regarding power towers, there is some experience based on plants operating in California but still more work to do to and to get sufficient experience as the one on parabolic trough systems. A tower power system can be shown in figure 2.2

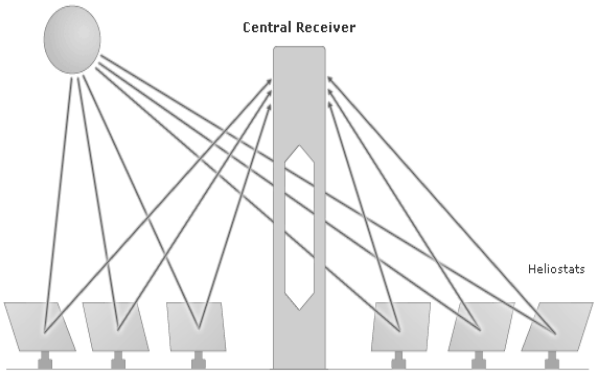

Figure 2.2 Tower power system

Power tower systems can use molten salt as HTF and be in the plant circuit for generating power. Also molten salt can store energy for the operation of the plant when the sun is not available at late or early hours of the day. Figure 4 shows a Molten-Salt power tower system

2.1.2 Solar Dish Systems

A solar dish system uses a dish with reflective material. The dish is similar to a satellite dish, the dish reflecting sun-light into a receiver which directs the energy to an engine generator. Commonly the engine used in this type of systems is a Stirling motor. This engine works based on a fluid expansion and contraction due to the different temperatures and pressures which produces mechanical work that can be used in the generator to produce electricity.

An individual solar parabolic dish - Stirling engine unit consists of a two axis tracking, parabolic dish reflector that focuses incoming sunlight onto a Stirling cycle engine/generator. The engine/generator uses the Stirling thermodynamic cycle to produce electricity without producing steam as an intermediate step. The parabolic dish reflector which moves to continuously face the sun can produce a high temperature (~1452°F) in the fluid located in the receiver(28). Figure 2.3 shows a solar dish with its receiver.

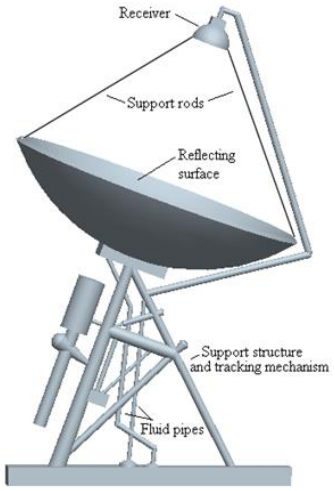

Figure 2.3 Solar parabolic Dish (Renewable energy source)

Big arrangements of parabolic dishes can be made in order to generate big amounts of electricity; depending on the size of the dish the electricity greeted by each can go from 3kw to 25kw.

The research for materials that will be used on CSP can take advantage of the Phase Change Material (PCM) on Thermal Energy Storage. Nanomaterials have the potential to dramatically improve thermal energy storage and heat transfer for concentrating solar power (CSP) plants. The goal of a two- to four-fold improvement in the thermal energy storage (TES) density, at an acceptable cost, for CSP plants is realistic. For TES, this requires exploring new metallic, polymetallic, or alloy, and inorganic salt nanoparticles coupled with innovative encapsulation strategies (nano phase-change materials [nano PCMs]).

There are ample data from experiments that show that the phase-change behavior of Nano scale metals and salts can be different from that of bulk materials(29). The advantages include increased heat transfer, increased thermal conductivity, and lower sedimentation for submicron particles.

Cost-cutting is still an important issue to be addressed. One of the important aspects of cost-cutting is the extended operation of the power generation system. Compared to a regular fossil

fuel power plant, the power generation system in a CSP plant only operates for less than 12 hours a day. Extended operation time will obviously maximize the operational capacity of a power generation system and reduce the cost, allowing the dispatch of energy during times when electricity is in the highest demand.

2.2 Phase Change Material (PCM)

Encapsulated phase change materials (PCM) can be used in thermal energy storage. Latent heat storage material has the advantage of performing the storage function at nearly constant temperature, which enables solar collectors to operate at higher efficiencies, and has a large specific storage capacity(30). However, there are some inherent drawbacks when PCM are used in the thermal storage system. Thermal energy storage using a fluidize bed with material that has better and the right properties like density, heat capacity, heat conductivity and low cost can bring a big benefit to the renewable energy field(30). The continuous effort to find the right material by performing simulation can lead to lowering the cost of energy considerably according to the actual cost. PCM can be evaluated with the following calculation. Illustration 2.1 shows the stages when temperature and heat varies on the process for the material that will store the energy by changing phase. When change in phase is mentioned it means that state can change from solid to liquid.

Regarding PCM, a number of studies (Lane et al., 1975, 1976; Heine and Abhat, 1978; Telkes, 1980; Fellchenfeld and Sarig, 1985) have been performed to find the most promising phase change materials (PCM) for thermal energy storage (TES). At the time the studies were performed, the salts were the one of the most extensively studied phase change materials for solar energy storage because of its low price, suitable phase change temperature, high latent heat, and availability(31). For this study other materials like sand, silica, graphite, iron, limestone, and, alumina have been analyzed and studied.

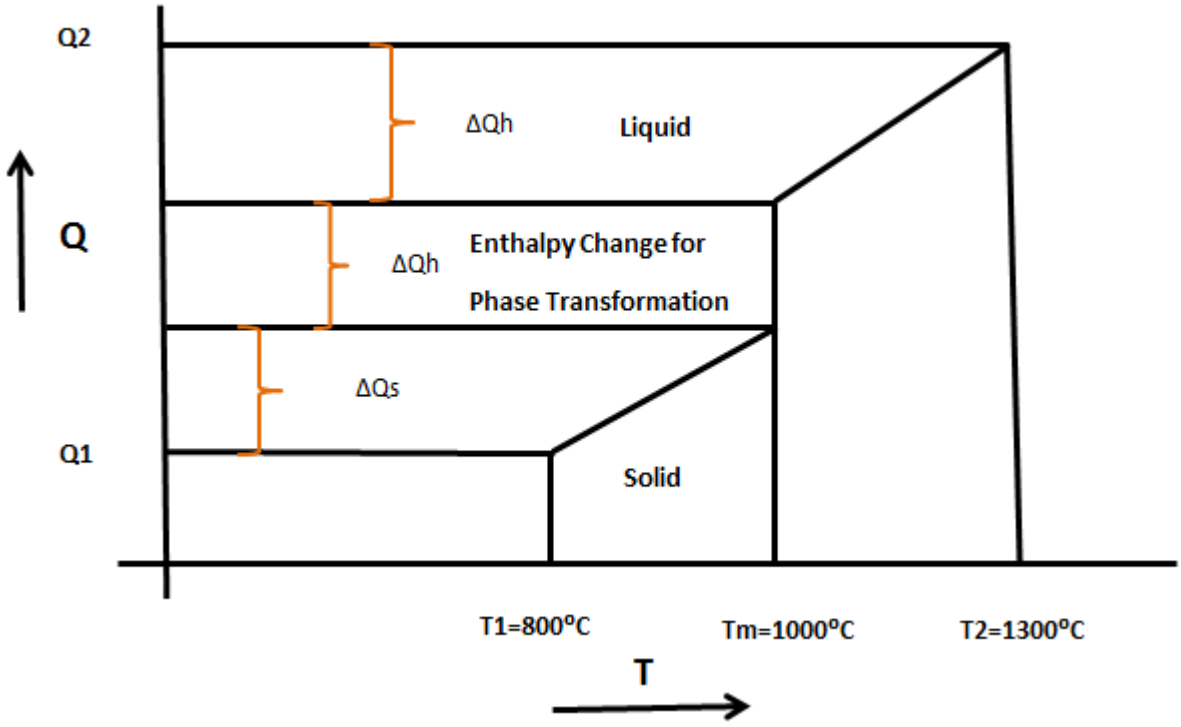

Illustration 2.1 shows that materials with a great PCM can help in the capacity and efficiency of materials in storage energy.

Phase-change materials behave like thermal greases after they reach their melt temperature. Their viscosity rapidly diminishes and they flow throughout the thermal joint to fill the gaps that were initially present. This process requires some compressive force, usually a few psi, to bring the two surfaces together and cause the material to flow(32).

2.3 Heat Transfer Fluid

One of the major challenges with the molten salt and similar salt mixtures is that they melt at a high temperature (200-400^{0}C). This implies that the HTF should be either kept in liquid stages when it's not being used to transfer heat from the receiver or should be heated to liquefy before operating the CSP plant. Both of these options add cost to the CSP plant. Advances in HTF go

with the hand with thermal storage developments because it can be found that a compatible fluid phase with appropriate stability will be required to carry the nanophase materials(33).

Here, we propose the solid particles as the HTF medium. These particles behave like fluid once it is in continuous motion and hence can be used for the HTF. Sandia National Laboratory has demonstrated the use of sand falling particle receiver(34). The solid particle receiver technology is expected to withstand higher temperature (1300^0C or more) and hence expected to improve performance and efficiency. Heat transfer salts have been used for many years in industrial circulation systems to provide heating for certain chemical reactions or processes(35).

For HTF needs, the requirements of solid particles are material compatibilities, i.e., minimal sintering and agglomeration and corrosion resistance to air and other transporting medium. They are also required to possess better thermal transport needs such as higher heat capacity (1.5 J/g-K or more), better conductivity, high solar absorptance, and low thermal emittance. Lower cost and abundance can make them practically feasible. According to our material search, most material that is stable for up to 1300^0C falls in the metal category. Metals have high thermal conductivity and meet the minimum needs for heat conductivity requirements. However, they have very low heat capacities (<1.5 J/g-K), which does not make them suitable for HTF needs in the standard form.

The proposed system uses a transporting fluid (e.g., air, Ar or even liquid metal) to carry the encapsulated solid particles. Transport gas proposed is used as a transport medium via fluidization or other transport mechanism. Using a stable material for coating that does not react with the transport medium at high temperatures can allow us to achieve high temperatures. The increase in thermal energy storage capacity is achieved by sensible heat in the thermal storage material and extracting latent heat during the PCM phase transition. These systems eliminate heat tracing and avoid parasitic-electricity losses compared to the molten salt storage design.

A framework for the encapsulated solid particle HTF is shown. Examples of high temperature efficient power-cycles include the air-Brayton supercritical CO2 cycles. The proposed HTF can employ a heat-exchanger to transfer heat from the solar receivers to transfer the thermal

energy to operate the power cycles(36). The heat-exchangers to operate the power-plant are not shown. TES systems have been evaluated and tested in order to use results for the industry and universities in order to make more efficient and competitive CSP systems(37).

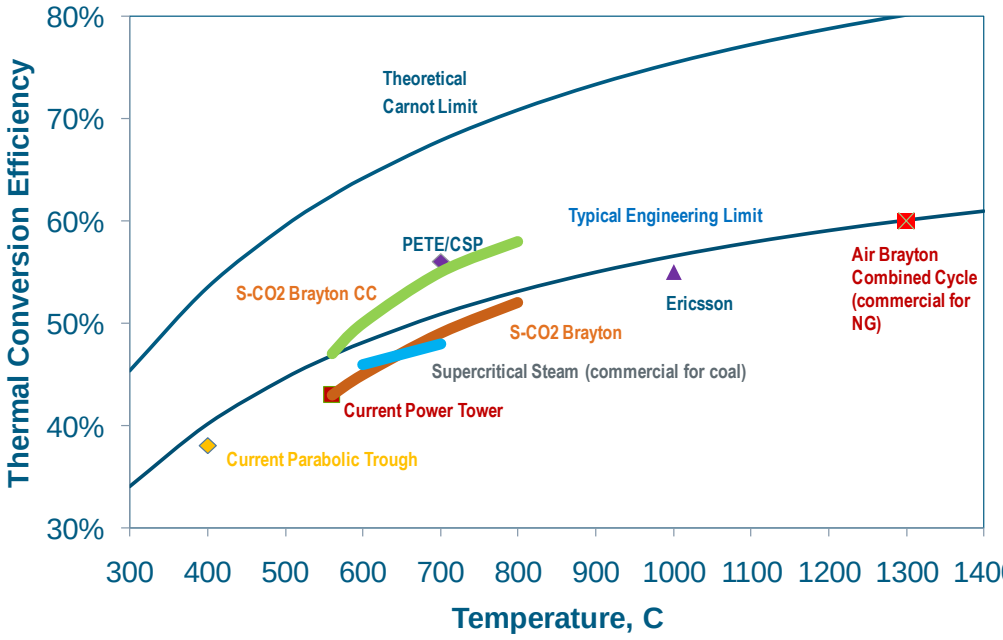

Figure 2.4 Thermal conversion efficiencies for different thermal systems (Source: U.S. DOE Golden field)(16)

2.3.1 Calculation of the effective thermal properties of the HTF systems

The principal modes of heat transfer in the solid particle system are usually conduction and convection. At high temperature (at 1000^0C for example, as is the case in our system), the radiative heat transfer plays an equally important role. Additionally, the contribution of each of these modes to the overall heat transfer may not be linearly additive for the solid particle system (38)(39) and the effects are more pronounced in the temperature gradient caused by changing phases in the encapsulated particle. The mutual interaction effects of the particles going through phase change must be accounted for. One of the best ways to transfer energy is to use encapsulated PCM as storage material and a packed bed as a heat exchange(30). Therefore, encapsulated PCM will be

greatly different from the traditional PCM, making the heat storage system more effective and simpler(30).

The effective thermal conductivity will determine how quickly the thermal energy gets transported and what should be the residence time of the particles exposed to the receiver. The packed-bed or fluidized-bed solid particle heat transfer can be expressed by the concept of effective thermal conductivity. Effective conductivity is based on the continuum and homogenous approximation of the macro scale. In general, the wall-to-bed heat transfer coefficient increases with decreasing particle diameter or increases operating pressure due to better packing and higher heat conductive particles.

Several authors have carried out work to evaluate the particle-to-fluid heat transfer coefficient via experiments (empirical) or theoretical estimates for idealized conditions and usually without accounting for radiation and with steady-state approximation such as heat transfer calculation from a single particle in a fluid medium and particle-to-fluid Nusselt number-heat transfer dependence calculation using mathematical treatment of conduction from a sphere (Fourier law) in the absence of convection and/or radiation or by adding the convective contribution to the overall heat transfer(40)(34)(41).

Effective thermal conductivity for the solid particles in a transporting fluid with maximum packing in cubic arrangement and with one-dimensional approximation for the spherical particles is given by

$$k_e = 1.57\, k \left(\frac{k_s}{k_s+k}\right)^2 \left(\ln\frac{k}{k} - \frac{k_s-k}{k_s}\right) + 0.21 \qquad (3)$$

where k_e is the effective conductivity of the system(42). Several other effective thermal conductivity calculation methods at various arrangements and packing level have been described in the review article(43).

Effective heat transfer is estimated using the total energy needed from heating the mixtures from temperature TL to TH. Assuming that the mixture melts at Tm, which lies between TL and TH and the heat of enthalpy at the melting point is h (in J/g), the effective specific heat is given by

$$C_{Peff} = \frac{\Delta H_{tot}}{T_H - T_L} \quad (4)$$

This calculation only incorporates the PCM and ignores the effects of particle interactions.

Improvements in the heat-transfer fluid (HTF) are necessary to bring down the LCOE for CSP. This can be accomplished by lowering the melting points and increasing the vapor pressure of these substances. Dow Chemical's and Solutia synthetic mineral oils have been used widely as the HTF in trough systems. The problem with these synthetic oils is that they break down at higher temperatures, preventing the power block from operating at higher, more efficient temperatures. Molten salts can withstand higher temperatures than the currently available synthetic oils and are being considered as an HTF. The downside is that they freeze at a higher temperature than the synthetic oils, which means a drop in temperature during the night may solidify the substance. This, in turn, can damage the equipment when the salt expands and puts pressure on the receivers. Corrosion of the receivers is another potential concern when salts are introduced. Nonetheless, research is being conducted to use this substance as both an HTF and TES medium. If this can be accomplished, costly heat exchangers would not be needed, thus helping reduce the LCOE(20).

Nanostructured materials have created numerous opportunities for many industrial areas(44). A variety of nanoparticles with unique physical properties, including optical, magnetic, electronic, chemical, and mechanical ones, have been used either alone or as functional additives to improve performance of materials(44). The structure, composition, and surface property, as well as the assembly of nanoparticles, can be tuned with high level of precision to allow bottom-up construction of novel materials(44). Owing to their small sizes and large surface to volume ratios, nanoparticles have been added into solid or liquid media to form homogeneous mixtures with intimate contacts(44). Nanostructured material have been looked up and seen as an important source to be use in the TES for CSP systems.

Nanoparticle synthesis and encapsulation are closely related topics. Bare nanoparticles are rarely stable because they have very high surface areas and are prone to agglomeration or sintering into larger particles and can also be reactive chemically. That is why encapsulation is a viable process when handling the material or HTF to work on a CSP system(33).

2.4 Environmental and Hedging Benefits

CSP plants provide environmental benefits by generating power without producing criteria and CO2 air emissions. In addition, the use of fixed cost renewable energy generation, such as CSP or wind, can decrease fossil fuel use and provide a hedge against fossil fuel price increases. While CSP plants may have environmental benefits due to emission reductions, they do require significant land area. A 100 MW CSP plant is estimated to cover approximately 800 acres (comprised mostly of the solar field) while a 500 MW combined cycle plant would occupy about 20 acres(45).

Chapter 3: Methodology

3.1 High temperature materials

Heat capacity, thermal conductivity, density, availability and cost to mention some of the characteristic of material to be selected and be used as thermal energy storage materials. Conduction, convection and radiation were looked up as well for the analysis and selection of materials. For thermal conductivity the Fourier's law is as shown

$$Q = kA\,{}^{dT}/_{dx} \tag{5}$$

Where Q is the conductive heat transfer, k thermal conductivity of the material, dT is the temperature difference across the material and dx is the material thickness. Also we can mention that the heat supplied or gained by a substance is as shown

$$Q = mCp\Delta T \tag{6}$$

Where m is the mass of the substance, Cp specific heat capacity and ΔT is the temperature rise or the temperature change. The radiation heat can be transfer between two surfaces at different temperatures without the necessity of any physical substance between them.

$$Q_{rad} = \sigma A T^4 \tag{7}$$

Where σ is the Stefan-Boltzmann constant, A is the radiating surface and T is the change in temperature. Regarding the particles, the shape is an important characteristic to review and for this study some typical sphericity of particles are shown in the following list.

3.2 Thermal properties, selection and methodology

The Factsage data base 6.2 version was selected and use because it has one of the largest data base for chemical thermodynamics, with the support of Factsage we evaluated phase diagrams, reactions and several other information regarding to different components and compositions. One of the advantages is that the data bases are integrated and link for faster and useful results gathering information for pure substances, compounds, liquid and solid oxide solutions, mattes, molten and solid salt solutions, alloys, metals, etc. The idea was that with the help of the software we could try so many different combinations of material and elements and get to the objectives planned. Also we took advantage of the modeling provided to validate with information search and found in the research community.

With the software also is possible to calculate multiphase conditions, multicomponent equilibrium with a wide variety of tabular and graphical output modes, getting the ability to process alloy design, metal treatments, how the liquid and solid stages of a certain alloy behaves with the change in composition and temperature in ternary and binary allows. By changing composition in weigh percent and looking at the change in the stage due also to the different temperature it was valuable information for the selection of the alloys and composition. Regarding viscosity variation in the program was a great tool to use because it relates to the viscosity of the structure of the melt and the structure of the components and it is calculated from the thermodynamic description of the melt.

The approach of looking at the phase diagrams was that we could calculate even edit binary, ternary and multicomponent phase diagram sections where the axes can be various combinations of temperature, pressure and volume composition, activity and chemical potential. Enthalpy of formation or phase transformation, as well enthalpies of mixing, heat contents and heat capacity measurements is some of the information utilized from the Factsage. Also for the selection of the materials the vapor pressure and density measurements were looked at. Some of the materials reviewed were the iron, silicon, aluminum to find out the changes on their thermodynamic properties.

3.3 Governing equations

For the simulation result show in the computational analysis section the following equations were taken out of the fluent program.

3.3.1 Modeling the Turbulent Viscosity

The turbulent viscosity, μt is computed from

$$\mu_t = \rho \tilde{v} f_{v1} \tag{8}$$

Where the viscous damping function, fv1, is given by

$$f_{v1} = \frac{x^3}{x^3 + C_{v1}^3} \tag{9}$$

And

$$X = \frac{\tilde{v}}{v} \tag{10}$$

The turbulent (or eddy) viscosity, μt, is computed by combining k and ϵ as follows:

$$\mu_t = = \rho C_\mu \frac{k^2}{\epsilon} \tag{11}$$

3.3.2 Realizable $k - \epsilon$ Model

The realizable k-ϵ model is a relatively recent development and differs from the standard k-ϵ model in two important ways:

• The realizable $k-\epsilon$ model contains a new formulation for the turbulent viscosity.

• A new transport equation for the dissipation rate ϵ has been derived from an exact equation for the transport of the mean-square vorticity fluctuation.

The term "realizable" means that the model satisfies certain mathematical constraints on the Reynolds stresses, consistent with the physics of turbulent flows. Neither the standard $k-\epsilon$ model nor the RNG $k-\epsilon$ model is realizable.

An immediate benefit of the realizable $k-\epsilon$ model is that it more accurately predicts the spreading rate of both planar and round jets. It is also likely to provide superior performance for flows involving rotation, boundary layers under strong adverse pressure gradients, separation, and recirculation.

$$\overline{u^2} = \frac{2}{3}k - 2v_t\frac{\partial U}{\partial x} \tag{12}$$

Using Equation 4.4-3 for, $v_t = \mu_t/\rho$ one obtains the result that the normal stress,u^2, which by definition is a positive quantity, becomes negative, i.e., "non-realizable", when the strain is large enough to satisfy

$$\frac{k}{\epsilon}\frac{\partial U}{\partial x} > \frac{1}{3C_\mu} \approx 3.7 \tag{13}$$

3.3.3 Transport Equations for the Realizable $k-\epsilon$ Model

The modeled transport equations for k and ϵ in the realizable k-ϵ model are

$$\frac{\partial}{\partial t}(\rho k) + \frac{\partial}{\partial x_j}(\rho k u_j) = \frac{\partial}{\partial x_j}\left[\left(\mu + \frac{\mu_t}{\sigma_k}\right)\frac{\partial k}{\partial x_j}\right] + G_k + G_b - \rho\epsilon - Y_M + S_k \tag{14}$$

and

$$\frac{\partial}{\partial t}(\rho\epsilon) + \frac{\partial}{\partial x_j}(\rho\epsilon u_j) = \frac{\partial}{\partial x_j}\left[\left(\mu + \frac{\mu_t}{\sigma_\epsilon}\right)\frac{\partial k}{\partial x_j}\right] + \rho C_1 S_\epsilon - \rho C_2 \frac{\epsilon^2}{k+\sqrt{v\epsilon}} + C_{1\epsilon}\frac{\epsilon}{k}C_{3\epsilon}G_b + S_\epsilon \qquad (15)$$

Where

$$C_1 = max\left[0.43\frac{n}{n+5}\right], \qquad \eta = S\frac{k}{\epsilon}, \qquad S = \sqrt{2S_{ij}S_{ij}} \qquad (16)$$

In these equations, Gk represents the generation of turbulence kinetic energy due to the mean velocity gradients.

3.3.4 Heat Transfer

The flow of thermal energy from matter occupying one region in space to matter occupying a different region in space is known as heat transfer. Heat transfer can occur by three main methods: conduction, convection, and radiation.

3.3.5 Natural Convection and Buoyancy-Driven Flows Theory

When heat is added to a fluid and the fluid density varies with temperature, a flow can be induced due to the force of gravity acting on the density variations. Such buoyancy-driven flows are termed natural-convection (or mixed-convection) flows and can be modeled by ANSYS FLUENT.
The importance of buoyancy forces in a mixed convection flow can be measured by the ratio of the Grashof and Reynolds numbers:

$$\frac{Gr}{Re^2} = \frac{g\beta\Delta TL}{v^2} \qquad (17)$$

When this number approaches or exceeds unity, you should expect strong buoyancy contributions to the flow. Conversely, if it is very small, buoyancy forces may be ignored in your simulation. In pure natural convection, the strength of the buoyancy-induced flow is measured by the Rayleigh number:

$$R_a = \frac{g\beta\Delta T L^3 \rho}{\mu\alpha} \tag{18}$$

Where β is the thermal expansion coefficient:

$$\beta = -\frac{1}{\rho}\left(\frac{\partial\rho}{\partial T}\right)_p \tag{19}$$

and α is the thermal diffusivity:

$$\alpha = \frac{k}{\rho C_p} \tag{20}$$

Rayleigh numbers less than 108 indicate a buoyancy-induced laminar flow, with transition to turbulence occurring over the range of 108 < Ra < 1010.

3.3.6 Discrete Ordinates (DO) Radiation Model Theory

The discrete ordinates (DO) radiation model solves the radiative transfer equation (RTE) for a finite number of discrete solid angles, each associated with a vector direction ~s fixed in the global Cartesian system (x, y, z). The fineness of the angular discretization is controlled by you, analogous to choosing the number of rays for the DTRM. Unlike the DTRM, however, the DO model does not perform ray tracing. Two implementations of the DO model are available in ANSYS FLUENT: uncoupled and (energy) coupled. The uncoupled implementation is sequential

in nature and uses a conservative variant of the DO model called the finite-volume scheme, and its extension to unstructured meshes. In the uncoupled case, the equations for the energy and radiation intensities are solved one by one, assuming prevailing values for other variables.

3.3.7 The DO Model Equations

The DO model considers the radiative transfer equation (RTE) in the direction $\rightarrow s$ as a field equation.

$$\nabla \cdot (I(\vec{r},\vec{s})\vec{s}) + (a+\sigma_s)I(\vec{r},\vec{s}) = an^2\frac{\sigma T^4}{\pi} + \frac{\sigma_s}{4\pi}\int_0^{4\pi} I(\vec{r},\vec{s}^1)\Phi(\vec{s},\vec{s}^1)d\Omega^1 \qquad (22)$$

ANSYS FLUENT also allows the modeling of non-gray radiation using a gray-band model. The RTE for the spectral intensity $I\lambda(\vec{r},\vec{s})$can be written as

$$\nabla \cdot (I\lambda(\vec{r},\vec{s})\vec{s}) + (a\lambda+\sigma_s)I\lambda(\vec{r},\vec{s}) = a\lambda n^2 I_{b\lambda} + \frac{\sigma_s}{4\pi}\int_0^{4\pi} I\lambda(\vec{r},\vec{s}^1)\Phi(\vec{s},\vec{s}^1)d\Omega^1 \qquad (23)$$

3.3.8 Discrete Phase

Equations of Motion for Particles. ANSYS FLUENT predicts the trajectory of a discrete phase particle (or droplet or bubble) by integrating the force balance on the particle, which is written in a Lagrangian reference frame. This force balance equates the particle inertia with the forces acting on the particle, and can be written (for the x direction in Cartesian coordinates) as

$$\frac{du_p}{dt} = F_D(u-u_p) + \frac{g_x(\rho_p-\rho)}{\rho_p} + F_x \qquad (24)$$

Where Fx is an additional acceleration (force/unit particle mass) term, FD (u−up) is the drag force per unit particle mass and

$$F_D = \frac{18_\mu}{\rho_p d^2{}_p} \frac{C_D R_e}{24} \tag{25}$$

Here, u is the fluid phase velocity, u_p is the particle velocity, μ is the molecular viscosity of the fluid, ρ is the fluid density, ρ_p is the density of the particle, and d_p is the particle diameter. Re is the relative Reynolds number, which is defined as

$$R_e \equiv \frac{\rho d_p |u_p - u|}{\mu} \tag{26}$$

3.3.9 Laws for Drag Coefficients

Several laws for drag coefficients, CD, are available for the Euler-Lagrange Model. The drag coefficient, CD, for smooth particles can be taken from

$$C_D = a_1 + \frac{a^2}{R_e} + \frac{a_3}{R_e{}^2} \tag{27}$$

3.3.10 Laws for Heat and Mass Exchange

Using ANSYS FLUENT's discrete phase modeling capability, reacting particles or droplets can be modeled and their impact on the continuous phase can be examined. Several heat and mass transfer relationships, termed "laws", are available in ANSYS FLUENT and the physical models employed in these laws are described in this section.

3.3.11 Inert Heating or Cooling (Law 1/Law 6)

The inert heating or cooling laws (Laws 1 and 6) are applied when the particle temperature is less than the vaporization temperature that you define, T_{vap}, and after the volatile fraction, $f_{v,0}$, of a particle has been consumed.

These conditions may be written as

$$Law\ 1: \qquad T_p < T_{vap} \tag{28}$$

$$Law\ 6: \qquad m_p \leq \left(1 - f_{v,0}\right) m_{p,0} \tag{29}$$

When using Law 1 or Law 6, ANSYS FLUENT uses a simple heat balance to relate the particle temperature, T_p (t), to the convective heat transfer and the absorption/emission of radiation at the particle surface:

$$m_p C_p \frac{dT_p}{dt} = hA_p\left(T_\infty - T_p\right) + \epsilon_p A_p \sigma\left({\theta^4}_R - {T^4}_p\right) \tag{30}$$

where m_p is mass of the particle in Kg, C_p is the heat capacity of the particle in J/Kg-K, A_p is the surface area of the particle in m2, T_∞ is the local temperature of the continuous phase in K, h is the convective heat transfer coefficient in W/m^2-K, ϵ_p is the particle emissivity with no dimensions, σ is the Sefan-Boltzman constant in 5.67 x 10^{-8} W/m^2-K^4 and θ_R is the radiation temperature $\left(\frac{G}{4\pi}\right)^{1/4}$

Equation 15.4-3 assumes that there is negligible internal resistance to heat transfer, i.e., the particle is at uniform temperature throughout.

G is the incident radiation in W/m2:

$$G = \int_{\Omega=4\pi} \mathrm{I} d\Omega \tag{31}$$

For the analysis the following characteristics and considerations have been reviewed.

C=ΔQ/mΔT	Heat capacity
ΔT= heat necessary/(mass)(S)	Thermal conductivity

$q = KA\, dt/dx$	Fourier's Law
$Q = KA\, \Delta T/d$	Heat transfer equation
$P = 6/dpSv$	Particle size and shape

There is a need to find materials than can store energy at higher temperatures than the ones are been used with current systems like molten salts. It has been found through research and analysis that shows that smaller size particles improves the heat exchange than larger particles. Silica may be considered as a TES material due to its cost but it still needs to be tested more broadly. Materials with target characteristics shown on table 1 need to be identify and tested in order to make energy more affordable and widely available to society. In the simulation it can be observed that the graphite which has a lower density can be a better TES material due to the easier movement on the fluidized bed and thermal conductivity. The nanofluids were found to have enhanced thermophysical properties (viscosity, specific heat capacity, thermal conductivity, and diffusivity)(46).

Chapter 4: Problem Definition

Our goal is to improve thermal energy storage with small particles by analyzing the effects of adding small particles with various material properties at high temperatures (700ºC-1000ºC). We will conduct our analysis by numerical simulation of the materials in a concentrating solar power system by optimizing the temperature distribution in the aperture zone of the solid particle receiver previously describe.

4.1 Problem approach

In order to have good thermal energy storage system that can work up to 1000°C the investigation and analysis of materials had to be made. A method to quantify the practical storage capacity of a thermal storage system could be to compare it to the amount of energy the storage media could hold if the entire inventory were at its upper temperature and discharge completely to the lower temperature. Thermo fluid analysis of engineered micro phase change materials with high temperature melting point and coating with material where they can be consider as encapsulated particles will be a sustainable part of the problem solution. The process to select materials needed to take in consideration key characteristics related to the thermal energy storage like heat capacity, thermal conductivity, melting point, density, cost, availability. The problem consists in finding materials that gain temperature within a starting point or charging stage; where the starting point will be analyzed through modeling the solid particle receiver (SPR) or a fluidized bed. The SPR consist of an arrangement of a vertical chamber with a rectangle shape with a supply on the top; the supply can be controlled with the size of the aperture. The aperture can make the material to fall in the form of a curtain where will receive the solar energy reflected from the heliostats at a certain height in the (SPR), this height will be recognized as the solar patch.

Accuracy of the entire receiver assembly is crucial for achieving proper concentration. Advance absorber materials is a key to achieving lower costs to increase the operating temperature, which increases power-cycle efficiency and reduces required storage size. But higher operating temperatures require an absorber coating on receivers with a lower thermal emittance. Silica sand

is one of the most common varieties of sand found in the world. It is used for a wide range of applications and it is very available since is used in variety of industrial processes to make glass, as fill and to create molds and castings. Sand is the general term for broken down granules of rocks or minerals.

Many of the thermochemical cycles require thermal energy to be input at a temperature in excess of 800°C. In addition, the ability to provide this heat input around-the-clock is advantageous from an operational perspective and necessitates the use of thermal storage. The solid particle receiver (SPR) is a direct absorption central receiver concept initially conceived in the 1980s. It utilizes a curtain of falling spherical ceramic particles that serve as both the heat transfer fluid (HTF) and thermal storage media. The principal advantages of the SPR are (1) potentially high receiver efficiency due to direct absorption, (2) operational temperatures in excess of1000°C, and (3) chemically benign, low-cost solid HTF and storage media(34).

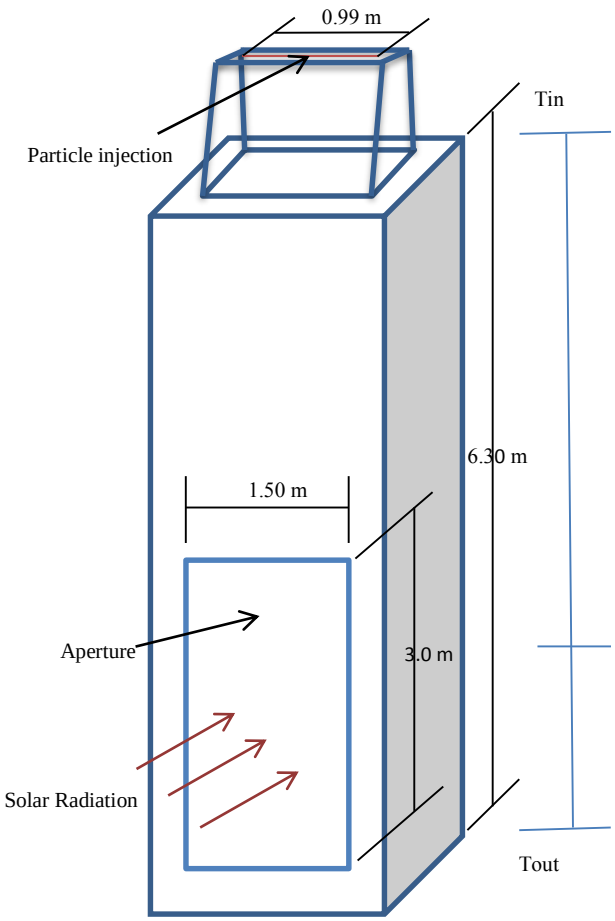

Figure 4.1 Solid Particle Receiver (SPR)

For the fluidized bed we used a simulation of 12 X 12 meter tank as the geometry with a 19-hole distributor at a velocity of 2 m/s, air was used as a the gas phase and graphite and silica were used as solid phase with a 2 meter height for the solid bed and particles with a of 0.01 mm.

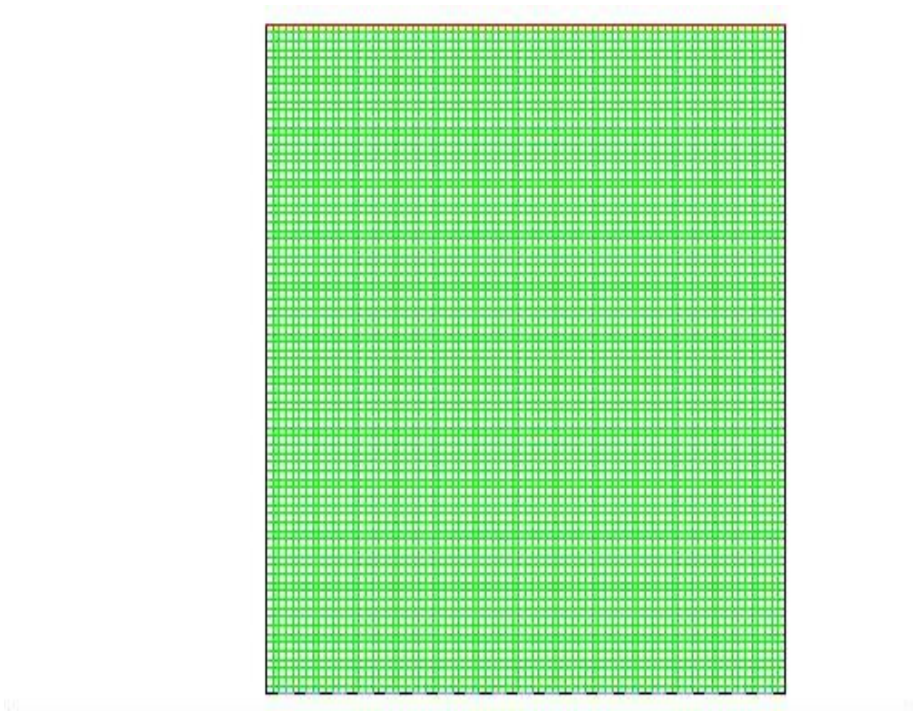

Figure 4.2 Tank geometry used in the simulation

Analysis section for the fluidized bed can considers the size, density and shape of the particles

$$\varphi = 6/dpSv \tag{32}$$

Where dp = diameter of the sphere having the same volume as a particle; Sv = volume ratio

Volume of a non-spherical particle Vp

$$Vp = \pi d^3 p/6 \tag{33}$$

Table 4.1 Sphericity of Materials

Materials	Sphericity
Sand (round)	0.92-0.98
Coal (crushed)	0.80-0.90
Milka flakes	0.28-0.30
Alumina	0.30-0.80
Catalysts	0.40-0.90
Limestone	0.50-0.90

Fluidize bed heat transfer

Conduction by Fourier's equation

$$q = -K\, dt/dx \tag{34}$$

K = thermal conductivity; dt/dx = temperature gradient in direction of the flow

Convection occurs only with liquids or gases and is dependent upon the movement of the elements of the fluid.

$$q = h(Tf - Ts) \tag{35}$$

h = heat transfer coefficient; Tf = fluid bulk temperature; Ts = surface temperature

Radiation heat can be transfer between two surfaces at a different temperature without the necessity of any physical substance between them.

$$q = \varepsilon\ell(T_1{}^4 - T_2{}^4) \tag{36}$$

Ɛ=exchange factor dependent on surface emissivity and geometrical arrangements; ℓ= Stefan-Boltzmann constant; $T_1{}^4$= temperature of the hotter surface; $T_2{}^4$)= temperature of the cooler surface

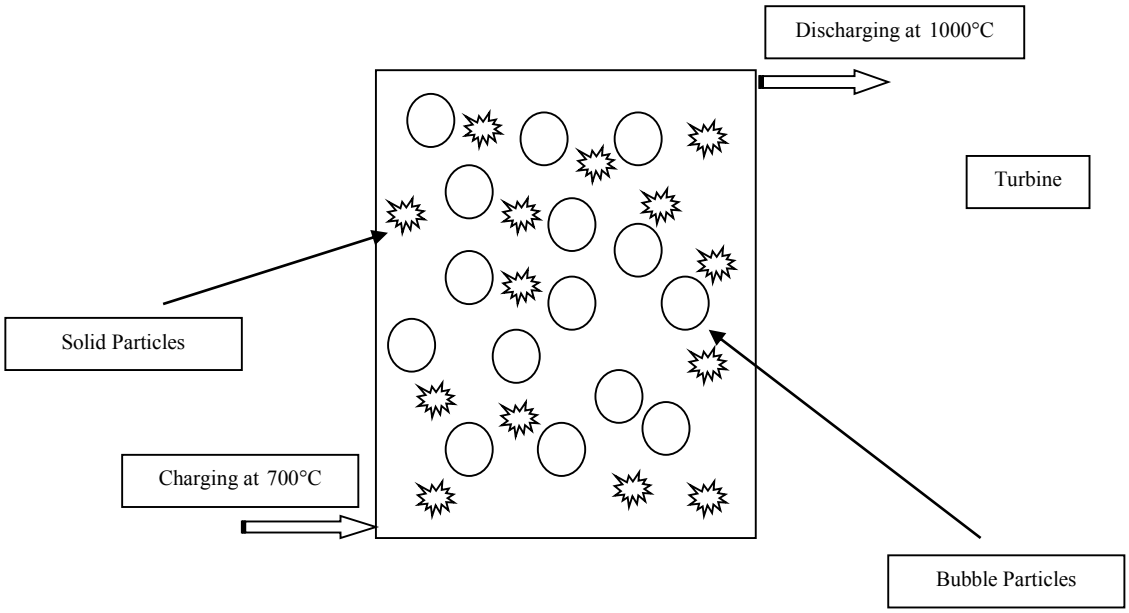

Figure 4.3 Fluidized bed

Fluidization is the process when solid particles are part of a fluid like state through the suspension in a gas or a liquid. Some of the advantages of using fluidized bed are heat and mass transfer rates between gas and particles are high when compared with other modes of contacting, it is suitable for large-scale operations and some of the disadvantages are erosion of pipes and vessels from abrasion by particles can be serious.

When a stationary closed system involves heat transfer only and no work interactions across its boundary, the energy balance relation reduces to

$$Q = mC_v\Delta T \tag{37}$$

Where Q is the amount of net heat transfer to or from the system.

Under steady conditions and in the absence of any work interactions, the conservation of energy relation for a control volume with one inlet and one exit with negligible changes in kinetic and potential energies can be expressed as

$$\dot{Q} = \dot{m} C_p \Delta T \tag{38}$$

Heat can be transferred in three different modes: conduction, convection, and radiation.

Conduction is the transfer of energy from the more energetic particles of a substance to the adjacent less energetic ones as a result of interactions between the particles, and is expressed by Fourier's law of heat conduction as

$$\dot{Q}_{cond} = -kA \frac{dT}{dx} \tag{39}$$

where k is the thermal conductivity of the material, A is the area normal to the direction of heat transfer, and $\frac{dT}{dx}$ is the temperature gradient.

Convection is the mode of heat transfer between a solid surface and the adjacent liquid or gas that is in motion, and involves the combined effects of conduction and fluid motion. The rate of convection heat transfer is expressed by Newton's law of cooling as

$$\dot{Q}_{conveccion} = hA_s(T_s - T_\infty) \tag{40}$$

where h is the convection heat transfer coefficient in $W/m^2 \cdot$℃ or $Btu/h \cdot ft2 \cdot °F$, A_s is the surface area through which convection heat transfer takes place, T_s is the surface temperature, and T_∞ is the temperature of the fluid sufficiently far from the surface.

Radiation is the energy emitted by matter in the form of electromagnetic waves (or photons) as a result of the changes in the electronic configurations of the atoms or molecules. The maximum rate of radiation that can be emitted from a surface at an absolute temperature T_s is given by the Stefan–Boltzmann law as $\dot{Q}_{\text{emit, max}} = \sigma A_s T_s^4$, where $\sigma = 5.67\,\text{X}10^{-8}\,W/m^2 \cdot K^4$ or

$0.1714\ X10^{-8}\ BTU/h \cdot ft^2 \cdot R^4$ is the Stefan–Boltzmann constant. When a surface of emissivity ε and surface area A_s at an absolute temperature T_s is completely enclosed by a much larger (or black) surface at absolute temperature T_{surr} separated by a gas (such as air) that does not intervene with radiation, the net rate of radiation heat transfer between these two surfaces is given by

$$\dot{Q}_{rad} = \varepsilon\sigma A_s(T_s^4 - T_{surr}^4) \quad (41)$$

In this case, the emissivity and the surface area of the surrounding surface do not have any effect on the net radiation heat transfer(19).

The objective of the fluent simulations is to understand how eulerian granular multiphase flow modeling (EGMF) works from the computational aspect of the problem. These types of flows use a fluidized bed, which is a combination of a fluid and a solid that has similar enough properties to a pure fluid that can be treated as such. It is important to conduct these simulations because of the purposes of TES, sodium nitrate has been used in these systems and will contain nano/micro-particles, in this case silica, which will enhance the sodium nitrate thermal properties. Thus the flow will consist of a liquid and a solid phase.

Chapter 5: Materials Characterization and Analysis

5.1 Characterization

For the analysis of the material we needed to take in consideration different characteristics like thermal conductivity, heat capacity, density, cost, availability and some others. For the analysis some software were used, including Factsage data base 6.2; which is a materials characteristics data base.

5.1.1 Feasibility studies of encapsulated particles

The feasibility of using liquid materials encapsulated in SiC particles was studied by using thermodynamic analysis and at temperatures ranging from 800 to 1300°C. Alloy melts of the Al-Si and Fe-Al-Si systems were considered for absorbing and desorbing energy for high temperature energy storage (TES) unit incorporated in a concentrating solar power scheme, and compared with the traditional NaNO3-KNO3 molten salt as a TES medium. Thermal energy storage (TES) provides the ability to extend the plant operating hours beyond that available from direct normal insulation(47). TES has always been associated closely with solar installations because solar energy availability is limited, and do not coincide with energy demand periods(48). In addition to determining the enthalpies for sensible heat and phase transformations, the phase equilibrium was determined for possible reactions at the liquid Al/SiC interfaces by calculating their thermodynamic stability. The transport of encapsulated SiC particles within a fluid and their effect on the thermal conductivity is discussed toward the efficacy of the thermal energy storage.

5.1.2 Heat transfer fluid with thermal energy storage.

Heat transfer fluid (HTF) with thermal energy storage (TES) for temperatures greater than 500°C can increase operating efficiencies with increasing temperatures as storage option for the Concentrating Solar Power CSP technology. Currently, molten salt (60wt.% NaNO3 - 40wt.% KNO3)(18) is widely used as the TES medium for a CSP plant. However, most molten salts are

unstable at high temperatures (800ºC-1300ºC), at which the electricity generation from a CSP power plant is expected to be more efficient and more cost competitive than with conventional source of power generation supplemented with a TES system. In addition, a CSP plant considered having a negligible carbon footprint would have natural energy resources when located in the southwestern states.

The purpose of the study was to determine the feasibility of using materials considering the enthalpy and thermal conductivity in the temperature range of 800ºC-1300ºC. In addition, the heat absorbing medium then encapsulated inside a hollow, spherical Si-C particle serving as the storage media can absorb heat during the charging phase from 800ºC to 1300ºC during the day time from sun radiation. The process is reversed during the discharging phase.

The storage media containing low-cost, highly stable materials in a fluid could behave similarly to a fluidized bed, porous media or even a packed bed depending on the flow velocity. For charging/discharging processes, air directly in contact with the storage media through fluidization that provides excellent heat transfer. At the storage mode, stagnant solid particles can be self-insulated to hold the heat. The synopsis presented here consists of the material systems selected for the heat absorbing mediums for comparisons and their thermodynamic analysis. Subsequently, the encapsulated particles (e.g., liquid Al encased in SiC) used for the heat transfer fluid system within the solar receiver are described with a discussion of possible chemical interactions among the material systems.

5.1.3 Selection and thermodynamic analysis of materials systems.

In considering materials for storage systems cycling between 800°C and 1300°C, the thermal conductivity and thermodynamic analysis (i.e., enthalpy and stability) were the primary criteria used for selection. Then the estimated cost also determined the possible materials. Gold was obviously eliminated because of its cost. In terms of the thermal conductivity, Al was favored over Cu because of the cost even though the thermal conductivity(49) of liquid Al (105W/m·K at

1000°C) was less than liquid Cu (166 W/m·K at 1083°C). To further minimize the cost, Al was alloyed with Fe and Si; their effect on enthalpy and phase equilibrium of the Al-Fe-Si system was examined.

Two forms of energy in a storage system involve sensible heat and any heat resulting from transformations (e.g., phase change or fusion). The thermodynamic concepts are summarized, here, though for further understanding, the authors refer to(50) for a thorough explanation of the equations for heat or enthalpy. Sensible heat (ΔH, kJ/kg) depends on the specific heat capacity (Cp, kJ/Kg·K) of the material (e.g., Al, KNO3 or B2O3) and the change in temperature of the material during heating or cooling, as determined by Eq. (42).

$$\Delta H = \int_{T_L}^{T_H} C_P \, dT \tag{42}$$

With any phase transformation, the enthalpies of transformation (ΔHtr) or the more specific transformation, melting (ΔHm), is added to Eq. (42) as shown in Eq. (43).

$$\Delta H_{tot} = \int_{T_L}^{T_{tr}} C_p \, dT + \Delta H_{tr} + \int_{T_{tr}}^{T_H} C_p \, dT \tag{43}$$

The units of enthalpy are usually denoted as kJ/kg, because comparison of the enthalpies for different materials will be discussed.

The sensible heats with enthalpies of transformation for Al, Si and a 56Al-44Si alloy (numbers indicate wt%) are shown in figure 5.1. The sensible heat of pure Al is consistently higher than pure Si, though the enthalpy of melting gives the curve an incremental change at 661°C. The sensible heat of 56Al-44Si alloy occurs between the Al and Si.

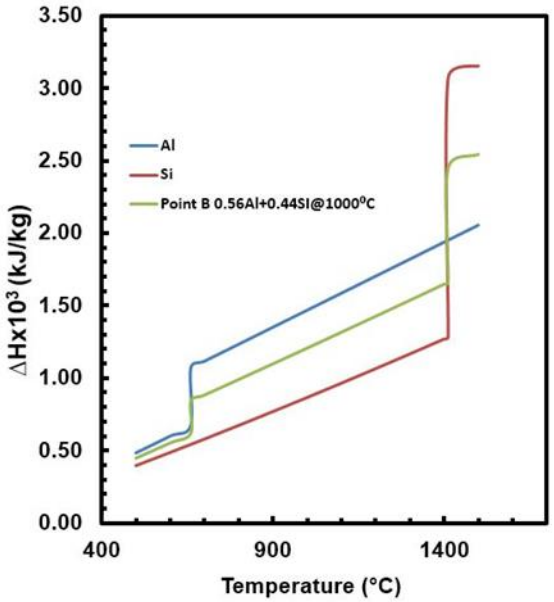

Figure 5.1 Enthalpies of transformation for Al, Si and a 56Al-44Si alloy (Source: Factsage)

A 56Al-44Si alloy was selected for analysis, because the Al-Si phase diagram easily depicts the precipitation of solid Si starting at approximately 1000°C upon cooling from 1300°C, as shown in figure 5.2. Further precipitation of solid Si occurs with decreasing temperatures to 800°C reaching a mixture about 25% solid-75% liquid. An Al-Si melt exists until the eutectic temperature of 577°C is reached though in the proposed system, the temperature would not decrease below 661°C.

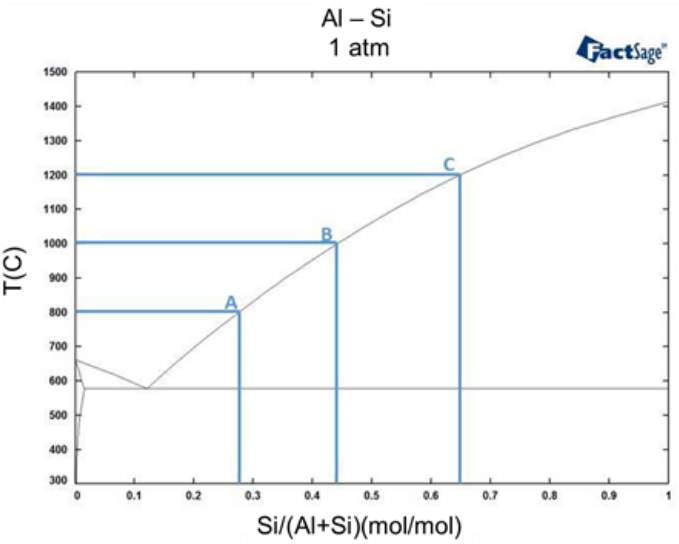

Figure 5.2 Al-Si Phase diagram showing the 56Al-44Si alloy as point B on the line (Source: Factsage)

5.1.4 Selection of alloy metal.

In order to select the material for an alloy some characteristics were consider like melting temperature, conductivity, latent heat of fusion, viscosity, availability, cost, reactivity, heat transfer, corrosion. For the case of aluminum the melting temperature is at 660°C with a latent heat of 95cal/g and for the silicon 1414°C with a latent heat of 430cal/g.

Two metals with different melting temperatures often form a eutectic mixture when melted together, which has a lower melting point for the metals by themselves. Sometimes these effects can significant lower the melting point in a range of materials that could be useful for metal alloy storage materials. The combination of the aluminum and silicon is a good alloy because of the results of the properties in this combination. For this particular alloy the eutectic structure of Al-Si occurs at 577°C, although increasing Si content the precipitation of solid Si increases from 577°C to 1411°C; melting temperature of Si shown in figure 5.1 . This is a wide range for the case of latent heat storage materials.

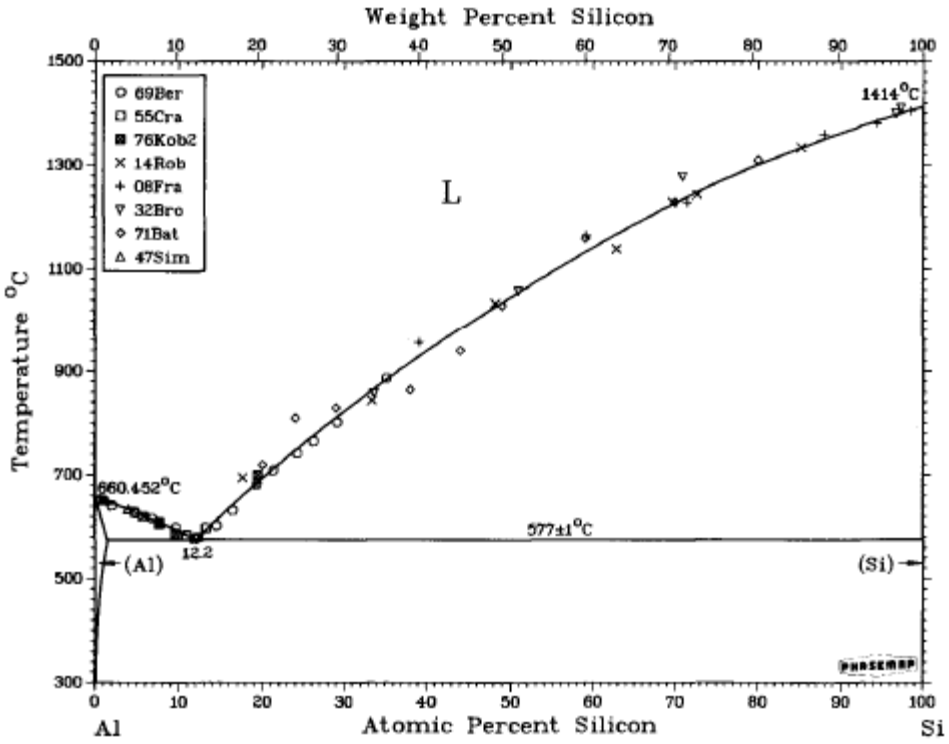

Figure 5.3 Al-Si Phase diagram with selected liquidus data(51)

For the aluminum and silicon alloy if we look at the latent heats of the metals that is 95 cal/g and 430 cal/g respectively and at a weight percent of 50-50 the melting point of the mixture is close to 1000°C and by interpolating the latent heats of both materials the result would be 263 cal/g which higher than some salts like sodium that have been used as heat storage medium. One good characteristic of this mixture is that is available and the cost is accessible in industrial quantities.

5.1.5 Binary and ternary alloys.

The Fe-Al-Si alloys were selected for consideration after examining the Fe-Si binary phase diagram as shown in figure 5.3 showing liquid existing at temperatures approximating 1200°C for

compositions near the Fe2Si and FeSi2 compounds. For the Fe2Si-Al and FeSi2-Al join, the liquids for the ternary occurs at approximately 1000°C at which ternary intermetallic (e.g., Fe2Al2Si) precipitates, as shown in figure 5.4. With the additions of Fe and Si to Al, the sensible heats of 42Fe-40Al-18Si and 38Fe-22Al-40Si are lower than for enthalpy of pure Al as shown in figure 5.5. However, the solidification does not give a significant enthalpy change in the sensible heat calculation, as shown in figure 5.5.

The interfacial silicide or carbide will depend on the formation of the oxycarbide (Al4CO4), which would then fix the oxygen potential and CO partial pressure within the precipitated Al4C3/Al4CO4 phases equilibrating with liquid Al, as shown in figure 5.6. For the stability between Al and SiC, a silicide and carbide phase can occur as shown in figure 5.7. If either a silicide or carbide phase develops at the Al/SiC interface, liquid Al would still exit and protected from further consumption.

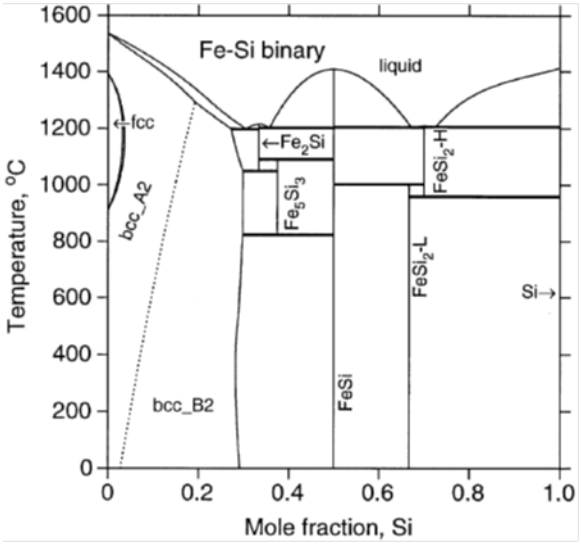

Figure 5.4 Calculated binary phase diagram of Fe-Si alloy(52)

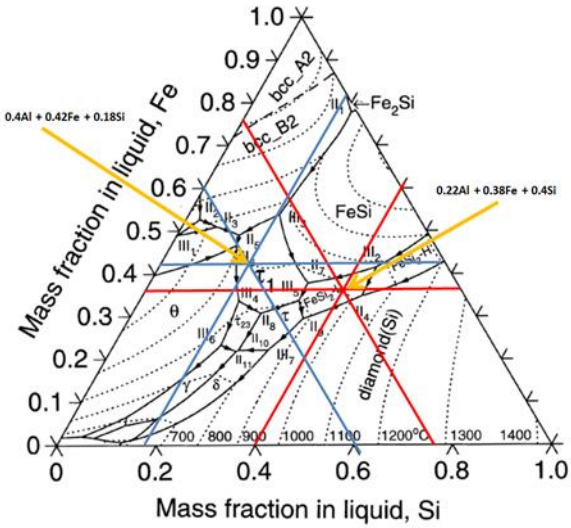

Figure 5.5 Ternary phase diagram of Al-Fe-Si showing the 2 compositions at 1273°K used for calculations(52)

The advantage of SiC is that SiO2 usually develops on the exterior of SiC protecting from further oxidation if air is used to carry the encapsulated Al in SiC.

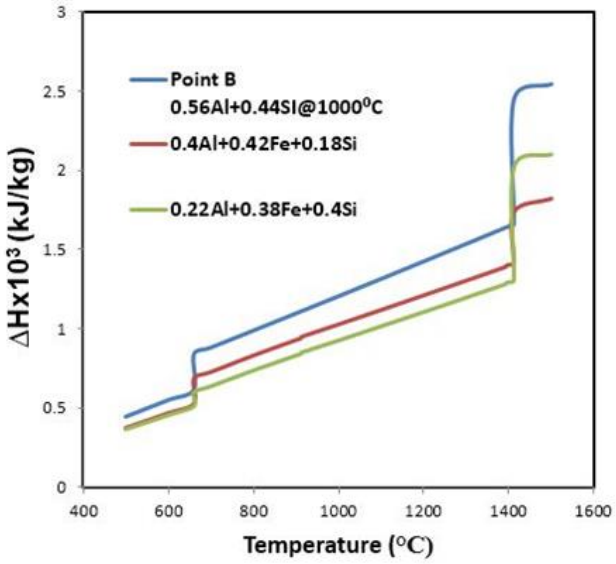

Figure 5.6 Sensible heat calculations comparing Al-Si binary and Al-Fe-Si ternary alloy at 1273°K (Source: Factsage)

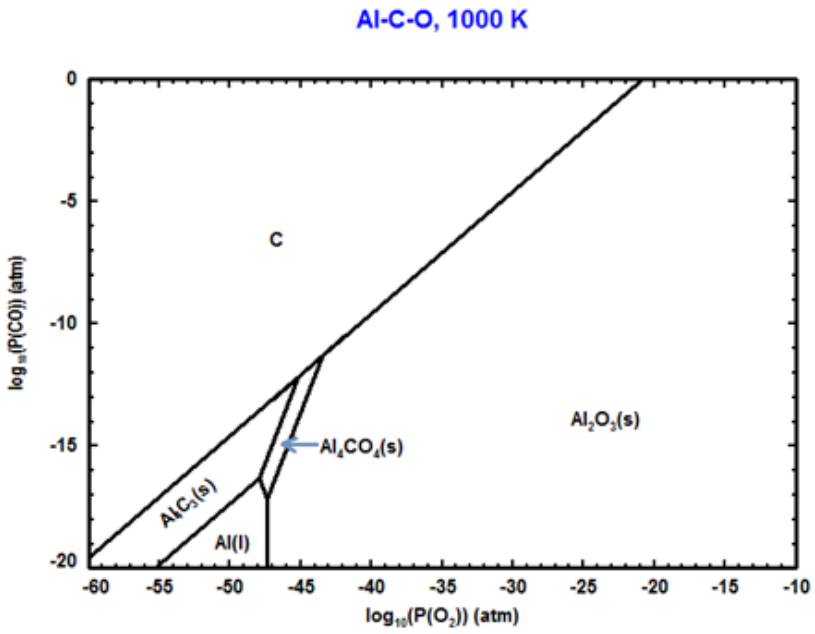

Figure 5.7 Stability Diagram Al-C-O @ 1000°K(53)

Al-Si provides higher sensible heats than NaNO3 or KNO3 with liquid Al having a comparable enthalpy, as shown in figure 5.8. The elements of Fe and Cu have lower sensible heats than Al and hence, the Fe and Si alloying with Al would lower its enthalpy.

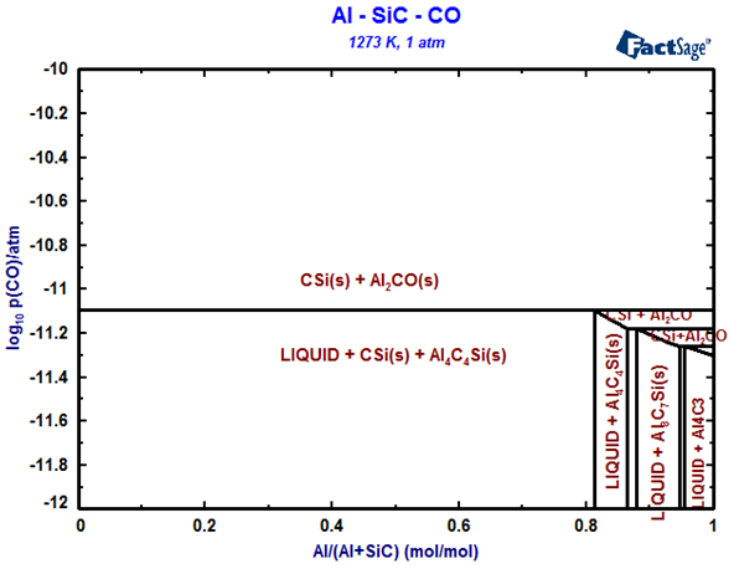

Figure 5.8 Phase Stability Diagram for Al-SiC-CO @ 1273°K (Source: Factsage)

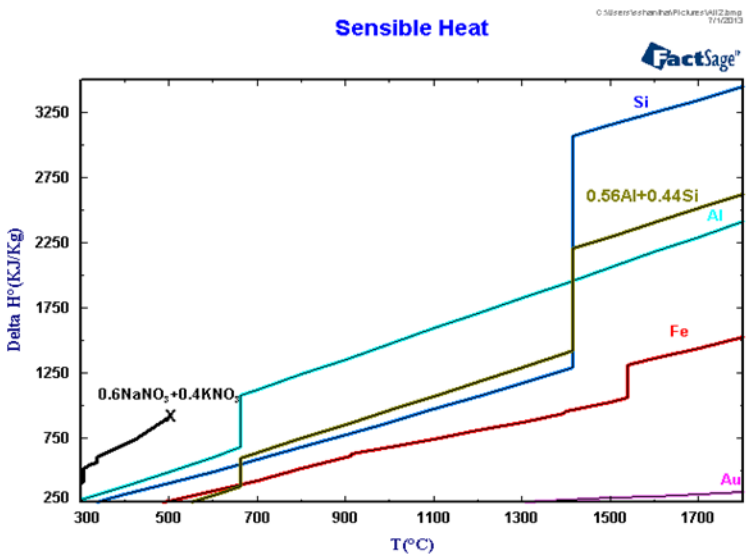

Figure 5.9 Sensible heats for comparing the difference between salts and metals (Source: HSC chemistry software)

Before perspective materials will be used in concrete commercial heat storage units, they should pass a long way of studying their physical, chemical properties(54).

5.2 Thermal characteristics

The nanofluids seemed to have enhanced thermophysical properties (viscosity, specific heat capacity, thermal conductivity, and diffusivity)(46). Understanding the nature of solid-liquid interfaces is important for many processes of technological interest, such as solidification, liquid-phase epitaxial growth, wetting, liquid-phase joining, crystal growth, and lubrication. Recent studies have reported on indirect evidence of density fluctuations at solid-liquid interfaces(55). Silica sand, quartzite rock, and taconite are compatible with nitrate salts, both in isothermal and cyclic conditions and can be used as filler material(56). In order to visualize the way CSP efficiency could be understand figure 5.10 shows characteristics that involves the energy collection, the system and the conversion at a different temperatures; minimizing collection losses enables efficient operation at higher temperature(57).

5.3 Materials Analysis

Table 5.1 Show materials characteristics evaluated for selection

Material	Cp – KJ/Kg·K	k – W/(m·K)@25°C	ρ – gr/cm³@293°K	$/Kg - dollars
Alumina ($Al2O_3$)	1.16	34.00	3.89	0.38
Graphite (Carbon C)	0.71	25.00	2.26	1.30
Iron (Fe)	0.45	80.00	7.87	0.60
Limestone	0.91	1.50	1.55	0.08
Sand	0.84	0.20	1.60	0.06
Silica (SiO_2)	0.84	0.04	2.64	0.10
Aluminum (Al)	0.90	237	2.70	1.54
Gold (Au)	0.13	310	19.3	45000
Cooper (Cu)	0.38	410	8.96	7.40

The science of heat transfer not only attempts to explain how heat energy may be transferred but is also used to predict the rate at which it will be transferred at certain specified conditions. Key elements in determining heat transfer include: a sample cross-sectional area, sample length, change in temperature across the sample, and a value of thermal conductivity. As one of the most meaningful values, thermal conductivity is a measure of how well heat energy travels through a material. Materials with lower values of thermal conductivity, k, such as silica, air, or wood, are considered insulators, as higher values of k, such as diamond, silver, and copper are conductors(19) (58).

If materials with PCM operating temperatures in the range between 700°C-1000°C are not selected in the near future due to their behavior or conditions that may not be the appropriate for a fluidized bed environment, other options like encapsulated materials can be used for evaluation

having the main material with the range PCM target and cover or encapsulated with a higher melting point material.

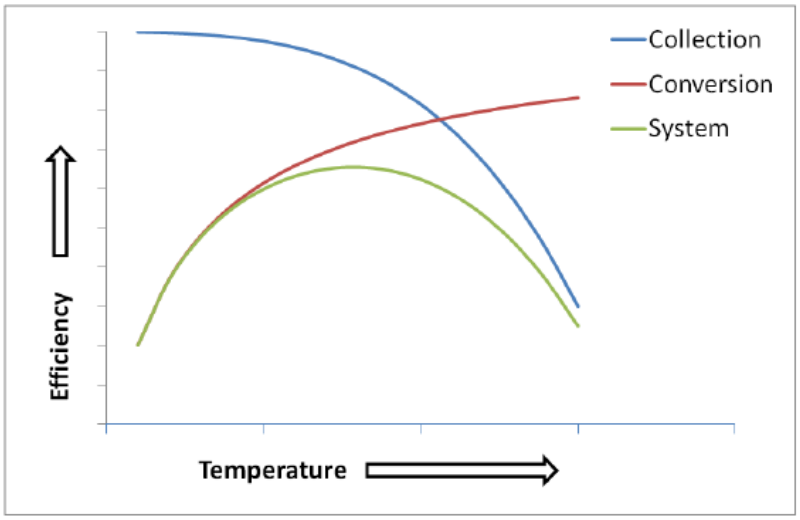

Figure 5.10 Efficiency tradeoff (57)

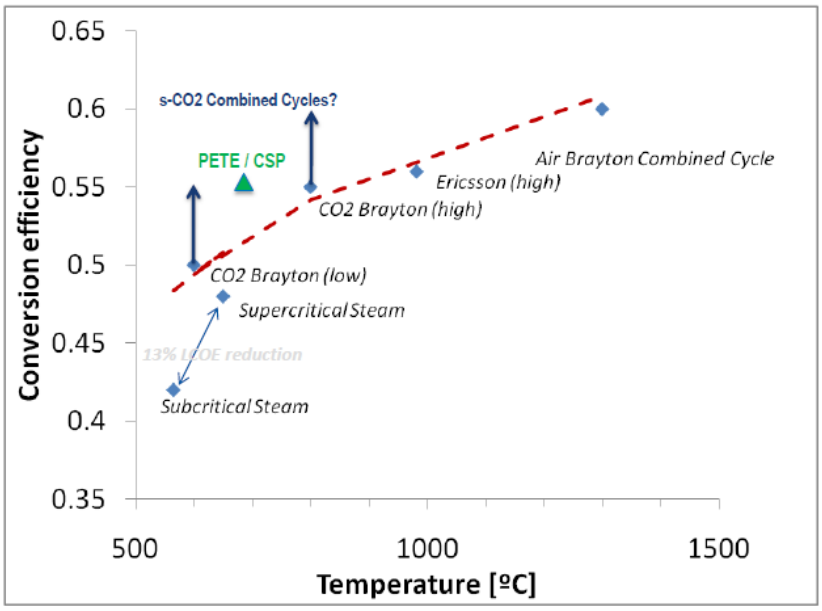

Figure 5.11 Power cycle comparison (57)

Subcritical steam (Baseline technology) 565°C, 42% efficiency, Supercritical steam >650°C, 48% efficiency, Supercritical CO2 Brayton 600°C-800°C, 50-55% efficiency, Ericsson 600°C-1000°C, 50-56% efficiency, Combined cycle: Air Brayton and Steam 1300°C, 60% efficiency, Combined cycle: CO2 Brayton and Steam 800°C, > 55% efficiency, PETE (PV) / CSP Hybrid 700°C, 55% efficiency(57)

In the present study, a feasibility studies to develop engineered high temperature heat transfer fluids (HTFs) for concentrating solar power system was performed. The study involved thermodynamic analysis for several binary and ternary alloys and their composition mixture that melts at high temperature (800ºC-1000ºC) and possess high enthalpy of fusion. The engineered HTFs are achieved by encapsulating alloys inside solid particles capable of operating at temperatures >1300°C. From our studies, we conclude that the 56%Al-44%Si alloy encapsulated in SiC particles possess desired melting point and possess high heat capacity. We also found that Fe-Al-Si encapsulated in SiC particles is also a potential candidate for high temperature HTFs.

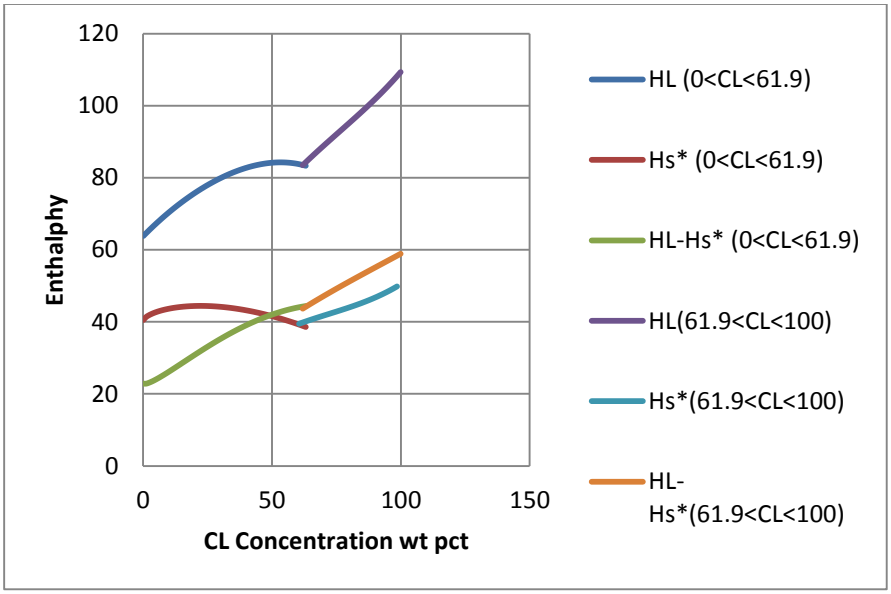

Figure 5.12 The enthalpies of interdendritic liquid and the solid in equilibrium with the liquid.

For the case were we can review enthalpies of a binary alloy during solidification I have analyzed thin and lead and base on the work of D.R. Poirier and P. Nandapurkar the previous graph is the result of analyzing the enthalpy of the interface of the dendritic solid, this is denoted Hs. This is computed by recognizing that for each value of CL (the composition of the interdendritic liquid) there is a corresponding value of Cs (the composition of the interfacial solid)(59).

Chapter 6: Computational Analysis

6.1 Introduction

Computer simulations have been run to obtain volume and mass fraction, changing time and velocity in order to have comparison between different parameters. For graphite and silica some computational simulations have been performed in a fluidized bed with the following parameters and results.

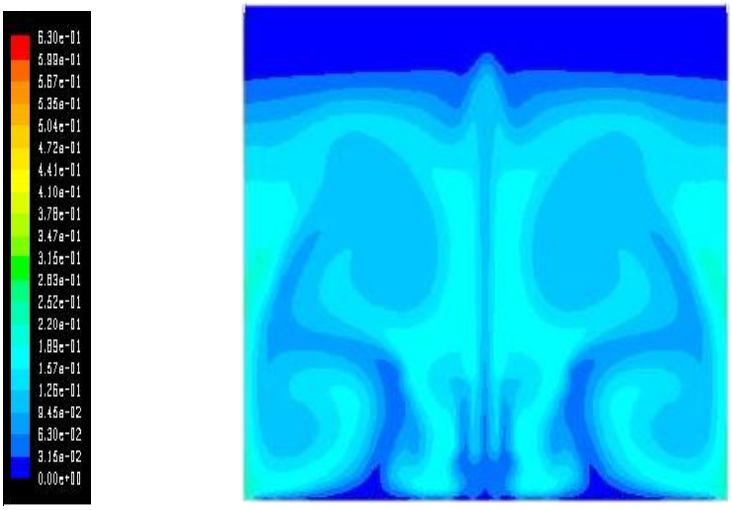

Figure 6.1 Volume fraction of Graphite at 7 seconds and a size particle of 0.01 mm.

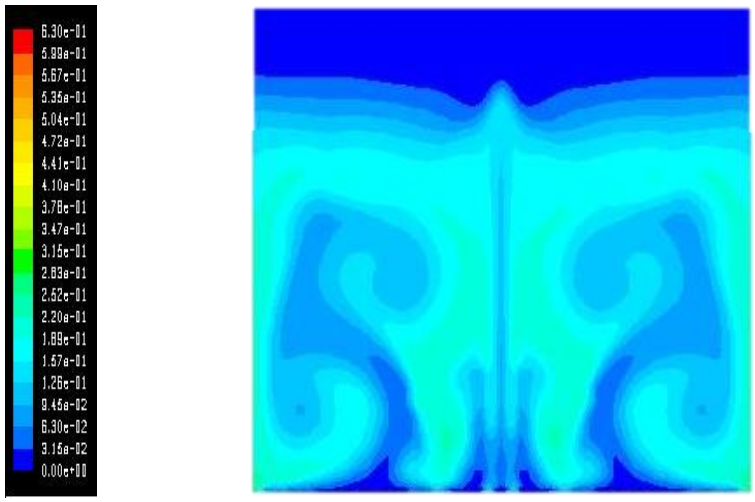

Figure 6.2 Volume fraction of Silica at 7 seconds and a size particle of 0.01 mm.

With the analysis performed it has been found that the size of the particle and density are key elements in a fluidized bed. The science of heat transfer not only attempts to explain how heat energy may be transferred but is also used to predict the rate at which it will be transferred at certain specified conditions. Key elements in determining heat transfer include: a sample cross-sectional area, sample length, change in temperature across the sample, and a value of thermal conductivity(19)(17). As one of the most meaningful values, thermal conductivity is a measure of how well heat energy travels through a material. Materials with lower values of thermal conductivity, k, such as silica, air, or wood, are considered insulators, as higher values of k, such as diamond, silver, and copper are conductors(60)(61)(62). If materials with PCM operating temperatures in the range between 700ºC-1000ºC are not selected in the near future due to their behavior or conditions that may not be the appropriate for a fluidized bed environment, other options like encapsulated materials can be used for evaluation having the main material with the range PCM target and cover or encapsulated with a higher melting point material(63)(1).

Through the use of software like Fluent simulation of heat in materials can be performed for analysis and better understanding. Hydraulic models are usually scaled according to laws based on traditional dimensionless parameters, for example, Reynolds number, Froude number, and length scales. It is never possible to ensure full similitude in a hydraulic model; in other words it is never possible to have simultaneous equality of all dimensionless parameters. Therefore, it is essential that the dominant processes and forces are modeled(64). Computational fluid dynamics (CFD) is the analysis of systems involving fluid flow, heat transfer and associated phenomena such as chemical reactions by means of computer-based simulation(65).

6.2 Computational model

A computational fluid dynamics (CFD) model was developed using FLUENT to simulate the gas-particle flow along with the heat transfer involved throughout the SPR. For this computational analysis first the model was generated followed by the mesh; for this step a total of ten meshes with a variation of 1% were generated with the purpose to find out which one was the ideal. Sensitivity studies were

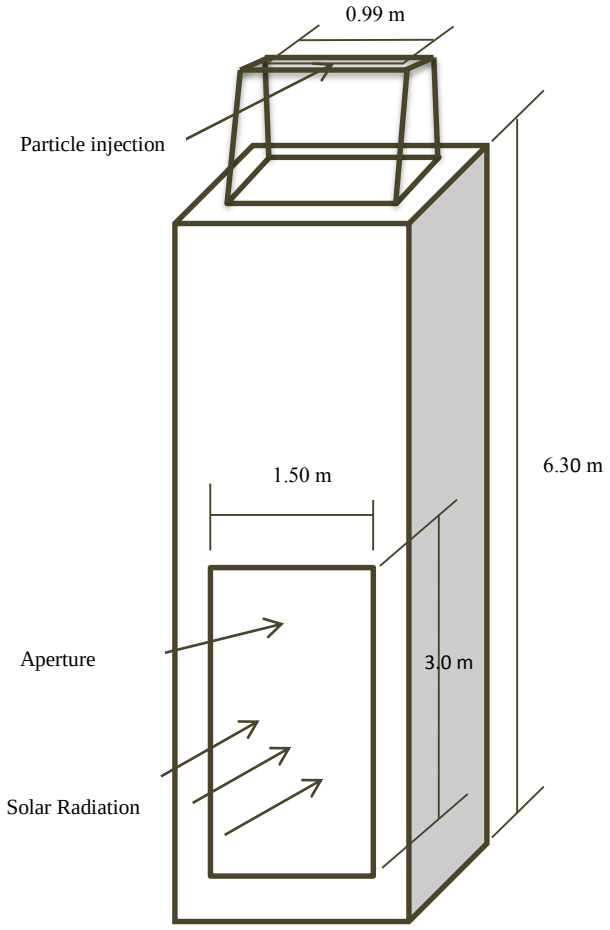

Figure 6.3 Geometry of the SPR model used for the simulations

performed using a wide number of hexahedral elements (up to approximate 900,000 cells), was analyzed and it was found that a grid with aproximate160,000 cells provided grid independence, as previously demonstrated by Siegel. Additional validation studies were performed taking into

consideration velocity of particles and position, also volume fraction and position. For this additional validation plots were performed and compared against previous work by Siegel.

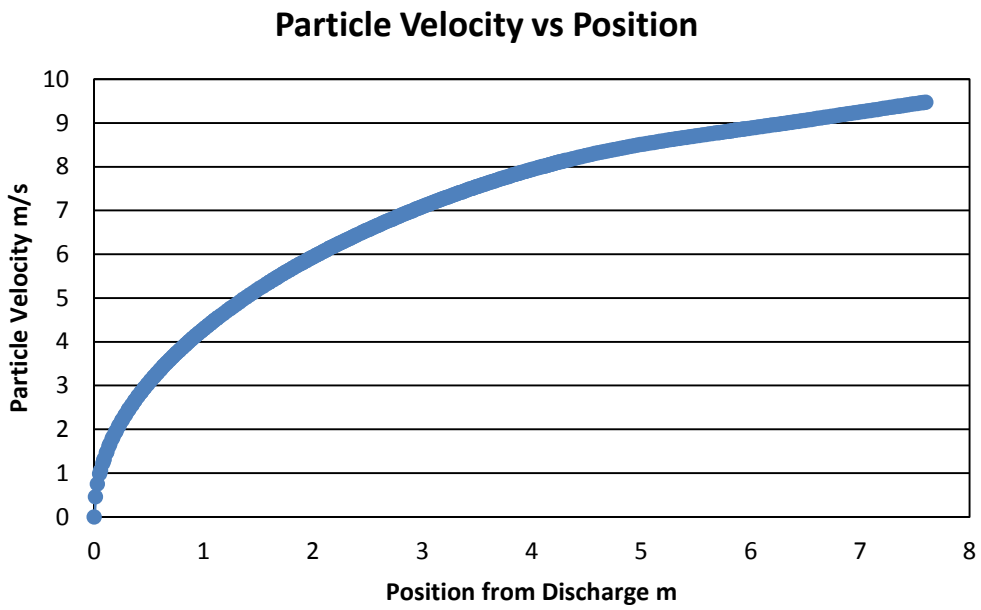

Figure 6.4 Simulated particle velocity versus position

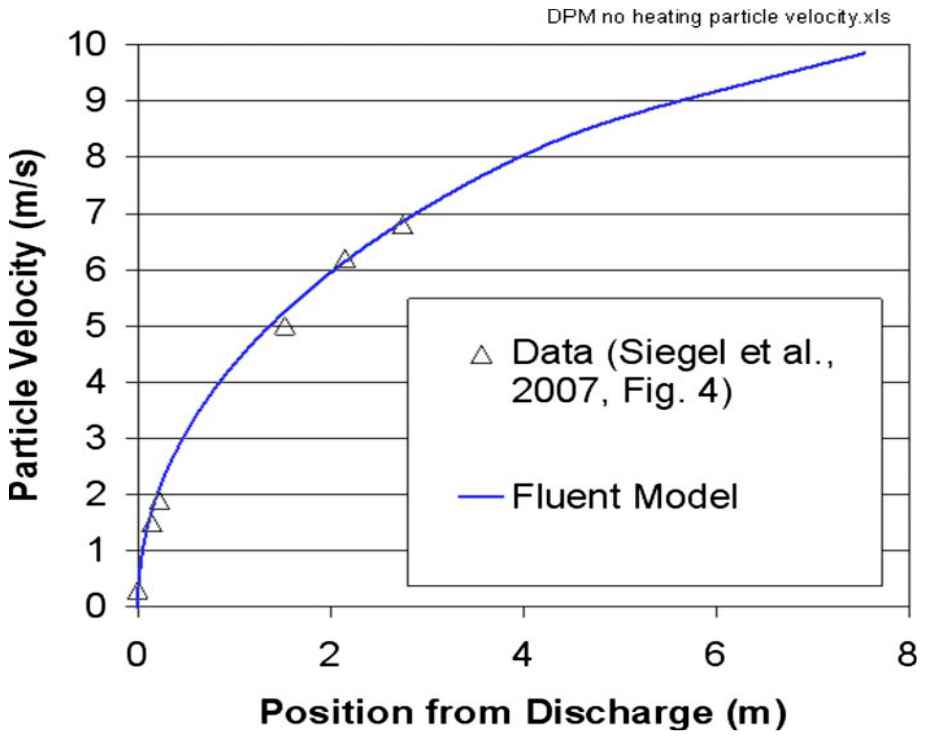

Figure 6.5 Simulated and measured particle velocity versus position (Siegel)

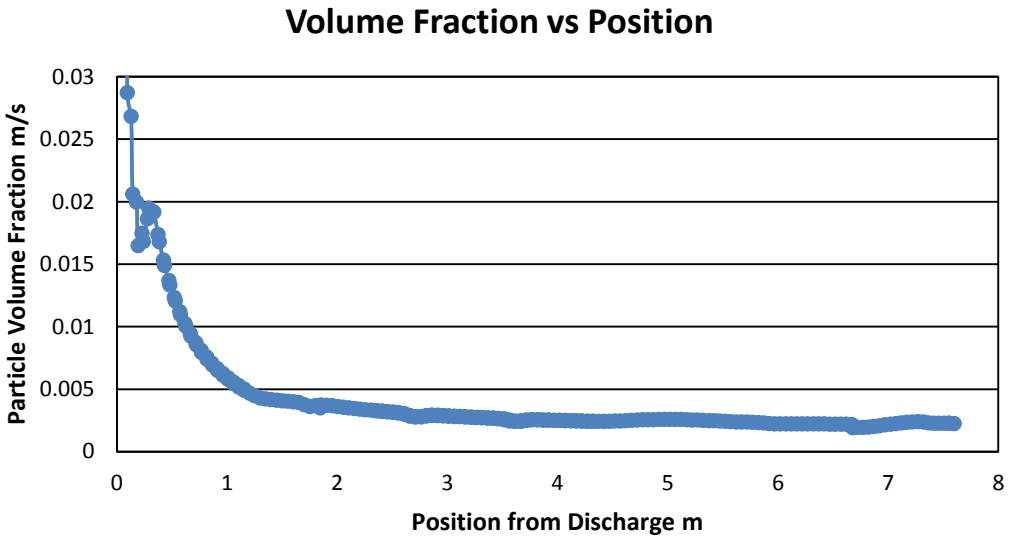

Figure 6.6 Simulated volume fraction versus position

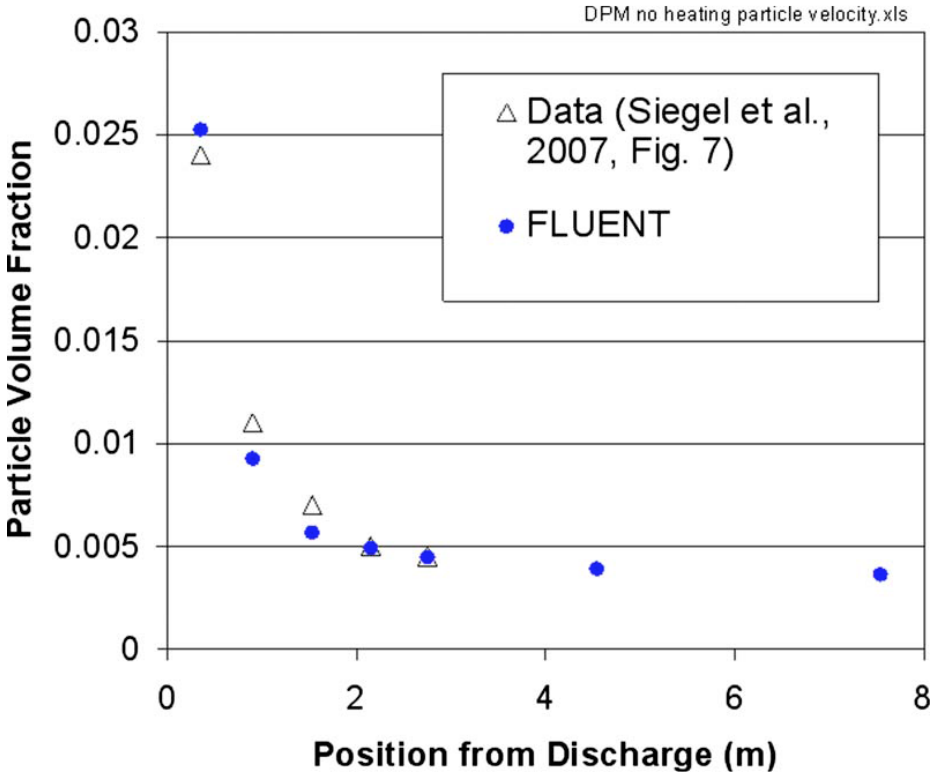

Figure 6.7 Simulated volume fraction versus position

For the validation the analysis was performed in steady state using models of energy with radiation (discrete ordinance), viscosity (turbulence) and discrete phase model. For the energy model two bands were used; one for light and the other one for heat. The model has to be with the emissivity and the absorptivity, the visible light relates to the light emitted and the infrared light refers to the heat. For the angular analysis in the model there are eight octants with theta and phi direction.

For the second model which is the viscosity (turbulence) it was taken in consideration the Reynolds-Averaged Navier-Stokes (RANS) equations and relates to the continuity and momentum equations. Also for the viscosity model characteristic k-ε realizable which always keeps the positive terms were also considered. For the analysis of the particles the mass flow rate of the curtain was made of three rows with one hundred particles each with a total of three hundred particles, with this configuration there was a buoyancy effect which I identity as the air friction channels. In order to continue with the model for the simulation the material properties were added and a consideration made was to have the Cp in function of time; this means that with the Cp was changing as the time was also changing.

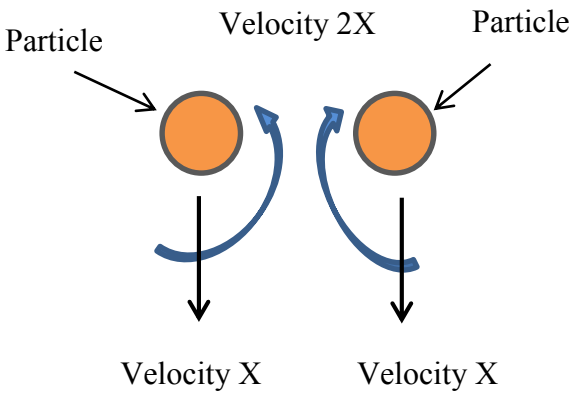

Figure 6.8 Buoyancy effect

Regarding the boundary conditions the top of the solid particle receiver (SPR) was consider as the inlet, the bottom as the output, and in the middle of the SPR where the aperture is, the solar patch is located.

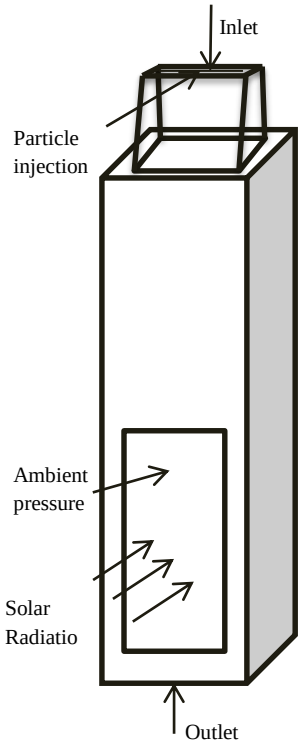

Figure 6.9 Boundary conditions

Particles once loaded on the top of the SPR the particles start falling through the top opening to the body of the receiver where lower in the SPR will be exposed to the solar energy through the aperture. The governing equations for the gas-phase conservation of mass, momentum and energy are solved by Fluent. Turbulent flow was modeled using the realizable k-ε turbulence model (using default values) with the standard wall function. The effects of buoyancy are included in the turbulence model. The realizable k-ε model has been validated for a wide range of flows including jets, mixing layers, channel and boundary layer flows, and separated flows making it a desirable

model for this study. The frontal aperture and bottom outlet of the receiver were specified as fixed pressure boundaries where air could enter and exit the domain.

The motion of the particles falling through the receiver is governed in FLUENT by a time-integrated force balance on each particle that relates particle acceleration, drag, and gravity in a Lagrangian reference frame. The formulation assumes that the interaction between particles is negligible, which is valid for particle volume fractions less than approximately 10%. Previous tests of falling particles have shown that the particle volume fraction is less than 5%. However, the particles do interact with the continuous gas phase and entrain air as they fall through the receiver. Two-way turbulence coupling was activated in FLUENT. The mass flow rate of the particles was also prescribed as per the on-sun test conditions, and this value was used in FLUENT to determine the rate of particle release (particles per second) based on the mass of each particle and the number of release points. Surfaces representing the bottom opening of the cavity, as well as the aperture in the front of the receiver, were defined as outlets where particles could escape. All other wall surfaces were defined as reflecting surfaces for the solid particles.

6.3 Radiation

Convection and radiative heat transfer discrete-ordinates radiation were also included in the discrete-phase particle model. The particles were assumed to be spherical, and the particle radiation scattering factor in FLUENT was assumed to be 0.3. The particles absorb, emit, and scatter irradiation, reducing the amount of solar flux that reaches the walls of the receiver. The mass flow rate of the particles, which impacts the particle concentration, also impacts the amount of irradiation received by the particles and cavity walls. Particles also emit thermal radiation.

With the use of nano particles the fluidization process can be utilized; fluidization is the operation by which a bed of solid particles can be contemplated as a fluid when is in contact with air. At the beginning the air flows slowly upward through a bed of solid particles, percolating through the void spaces between them; this condition is known as a fixed bed. As the air flow accelerates particles begin to move apart and may vibrate slightly(66).

6.4 Verification and validation

Particles of different materials were run for the temperature tracing within the solid particle receiver. Simulated results of alumina, graphite, iron, limestone, sand and silica particles at a different mass flow rates and heat fluxes on the solid particle receiver are investigated to examine the impact of heat flux, mass flow rate, and particle sizes on thermal efficiency for various materials.

Before carrying out the simulation, firstly mesh convergence analysis is performed (Figure 6.10). For this, six meshes are considered for the same size of the solar patch. The mesh refinement is continued until < 1% variation in the temperature gain is achieved. Steps followed to generate the meshes are:

- First, convert the 3 yellow faces into real faces, select the 4 edges and create face. They should be blue now. Two of them will remain yellow which are not needed.
- Second, split the small solar patch face from the big aperture face (only connected).
- Third, split the faces from the volume, (only connected).
- Fourth, set boundary conditions; top inlet wall, bottom outlet (pressure outlet), solar patch (wall), aperture (pressure inlet).
- Fifth, create volume mesh (mesh as hex submap), 10 meshes of interval sizes ranging from 50 to 25 (decrements of 5), and
- Sixth, save mesh file as "SPR 0.1m^2 50 mesh" by changing the last number according to the interval size.

Following the mesh convergence investigation, radiation convergence analysis is also carried out (Figure 6.11). Here, 10 meshes with the interval size obtained from the first study are considered and the size of solar patch is varied. The process is repeated until < 1% change in temperature difference from case to case is achieved.

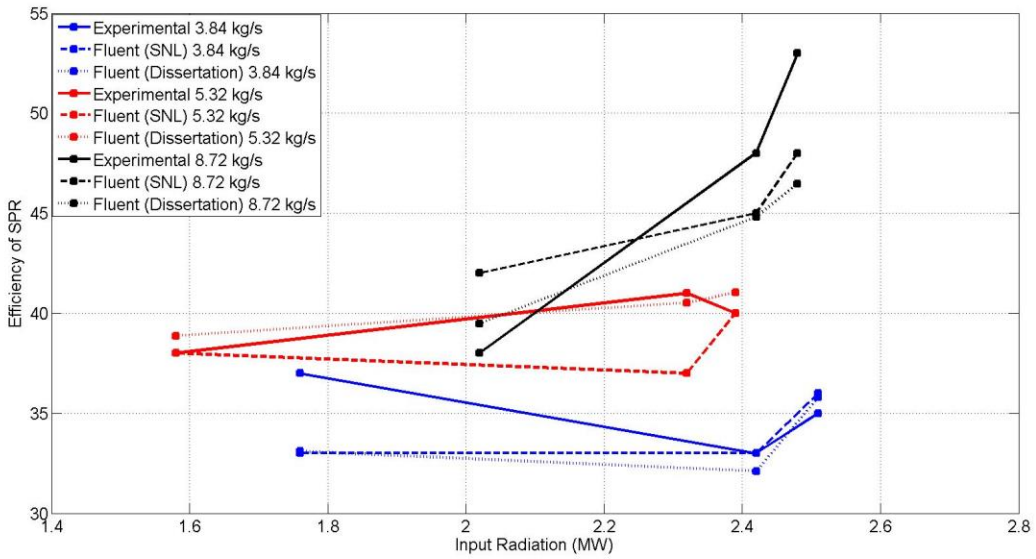

Figure 6.10 Efficiency of SPR depending on input radiation

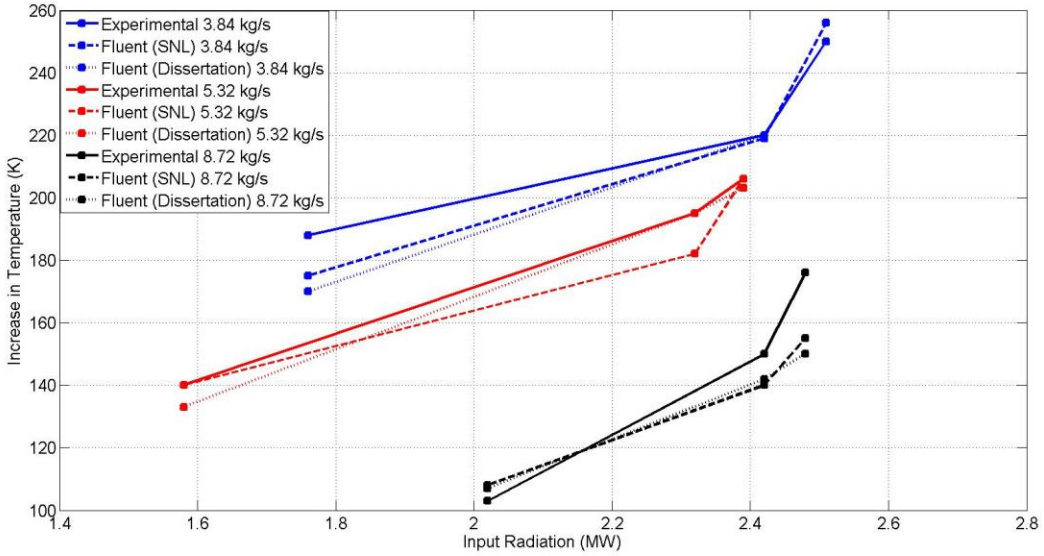

Figure 6.11 Effect on temperature increase in temperature of SPR

6.5 Simulation of heat gain in particles on solid particle receiver

For this simulations high temperature heat transfer fluids (HTFs) for concentrating solar power system were performed. The study involved thermodynamic analysis and their composition mixture that melts at high temperature and possess high enthalpy of fusion. For these simulation materials like alumina, alumina silicate, graphite, iron, limestone, sand and silica were run at a three different mass flow (3.84Kg/s,5.32Kg/s,8.72Kg/s) and heat flux. Results show that with the increase of mass flow rate the amount of heat stored in the particles increase but one of the disadvantages is that the volume in the material to handle is higher. The engineered HTFs are achieved by encapsulating alloys inside solid particles capable of operating at temperatures >1300°C. From the plots regarding the increase in particles temperature and solar particle receiver can be observed that the while the mass flow rate increases the temperature in the particle decreases and while the mass flow rate increases the efficiency of the solid particle increases.

The table 6.1 summarizes the cases that were simulated. A total six varying heat-flux cases and three mass flow rate cases for each of the heat-flux situation were considered. The heat flux cases were chosen based on realistic solar radiation situation for a solar tower system.

Table 6.1 Show materials characteristics evaluated for selection

Figure	Mass Flow Rate Kg/s	Heat Flux MW	Inlet Temperature °K	Observation on graph
6.12	3.84	1	573	Initially particles lose temperature.
6.13	3.84	2	573	Particles gain temperature at end of process.
6.14	3.84	4	573	Iron higher temp. due to the Cp.
6.15	3.84	6	555	Gain temperature since the beginning.
6.16	3.84	8	551	Particles start gaining temp. through the process.
6.17	3.84	10	528	The higher the heat the higher the gain.
6.18	5.32	1	573	Initially particles lose temperature.
6.19	5.32	2	566	Through the process particles gain temperature.
6.20	5.32	4	555	Initially the particles gain temperature.
6.21	5.32	6	555	Initially the particles gain temperature.
6.22	5.32	8	551	Particles start gaining temp. through the process.
6.23	5.32	10	566	Through the process particles gain temperature.
6.24	8.72	1	573	Particles initially lose temperature.
6.25	8.72	2	556	Initially the particles gain temperature.
6.26	8.72	4	574	Particles initially gain temperature.
6.27	8.72	6	555	Gain in temperature is observed initially.
6.28	8.72	8	551	Through the process particles gain temperature.
6.29	8.72	10	573	The higher the heat the higher the gain.

Temperature distribution of a 3.84 kg/s solid particle curtain mass flow rate is reported in the Figures 6.12 through 6.17. In the results reported in the Figure 6.12, the inlet temperature is 573°K (300°C) while the applied heat is 1MW. In this case it can be observed that trough out the process, initially the particles lose temperature and they exit at a much lower temperature because the irradiance is low. In the results reported in the Figure 6.13, the inlet temperature is 573°K (300°C) while the applied heat is 2MW. In this case it can be observed that trough out the process, initially the particles lose energy, but once they pass through the opening, they regain temperature and they exit at a higher temperature. In the results reported in the Figure 6.14, the inlet temperature is 573°K (300°C) while the applied heat is 4MW. In this case it can be observed that trough out the process, initially the particles lose energy, but once they pass through the opening, they regain temperature and they exit at a higher temperature. Iron particles have a much lower Cp therefore; the outlet temperature is higher than the rest. In the results reported in the Figure 6.15, the inlet temperature is 551°K (278°C) while the applied heat is 6MW. In this case it can be observed that trough out the process; initially the particles gain temperature increasing the temperature while the particles go through the solid particle receiver. In the results reported in the Figure 6.16, the inlet temperature is 555°K (282°C) while the applied heat is 8MW. In this case it can be observed that trough out the process; initially the particles gain temperature in most of the cases just a low variance can be seen in the limestone. In the results reported in the Figure 6.17, he inlet temperature is 528°K (255°C) while the applied heat is 10MW. In this case it can be observed very clearly that trough out the process, initially the particles gain temperature while traveling down the solid particle receiver, with this we confirm that with the higher the heat applied the heat gain is also higher.

Temperature distribution of a 5.32 kg/s solid particle curtain mass flow rate is reported in the Figures 6.18-23. In the results reported in the Figure 6.18, the inlet temperature is 573°K (300°C) while the applied heat is 1MW. In this case it can be observed that trough out the process; initially most of the particles lose temperature. In the results reported in the Figure 6.19, the inlet temperature is 566°K (293°C) while the applied heat is 2MW. In this case it can be observed that

trough out the process, initially the particles gain temperature; which is a different behavior compared with the previous. In the results reported in the Figure 6.20, the inlet temperature is 555°K (282°C) while the applied heat is 4MW. In this case it can be observed that trough out the process; initially the particles gain temperature for all of the materials including limestone. In the results reported in the Figure 6.21, the inlet temperature is 555°K (282 C) while the applied heat is 6MW. In this case it can be observed that trough out the process, initially the particles gain temperature as they travel through the solid particle receiver. In the results reported in the Figure 6.22, the inlet temperature is 551°K (278°C) while the applied heat is 8MW. In this case it can be observed that trough out the process; the tendency is that from the beginning the particles gain temperature. In the results reported in the Figure 6.23, the inlet temperature is 566°K (293°C) while the applied heat is 10MW. For this case it can be observed very clearly that trough out the process, initially the particles gain temperature and continues until reaches its higher point in the solar path in the opening.

Temperature distribution of a 8.72 kg/s solid particle curtain mass flow rate cases are reported in the Figures 6.24 through 6.29. In the results reported in the Figure 6.24, the inlet temperature is 573°K (300°C) while the applied heat is 1MW. In this case it can be observed that trough out the process; initially the particles lose temperature due to the low heat applied. In the results reported in the Figure 6.25, the inlet temperature is 556°K (283°C) while the applied heat is 2MW. In this case it can be observed that trough out the process; initially the particles gain temperature; for this case you can see the change in tendency from the previous one. In the results reported in the Figure 6.26, the inlet temperature is 574°K (301°C) while the applied heat is 4MW. In this case it can be observed that trough out the process, initially the particles gain temperature as they travel in the solid particle receiver. In the results reported in the Figure 6.27, the inlet temperature is 555°K (282°C) while the applied heat is 6MW. In this case it can be observed that trough out the process; initially the particles present the tendency to gain temperature. In the results reported in the Figure 6.28, the inlet temperature is 551°K (278°C) while the applied heat is 8MW. Also in this case it can be observed that the tendency trough out the process, initially the particles

gain temperature and increase it in the aperture of the solid particle receiver. In the results reported in the Figure 6.29, the inlet temperature is 573°K (300°C) while the applied heat is 10MW. In this case it can be observed very clearly that trough out the process; initially the particles gain temperature and increase the temperature while they travel down.

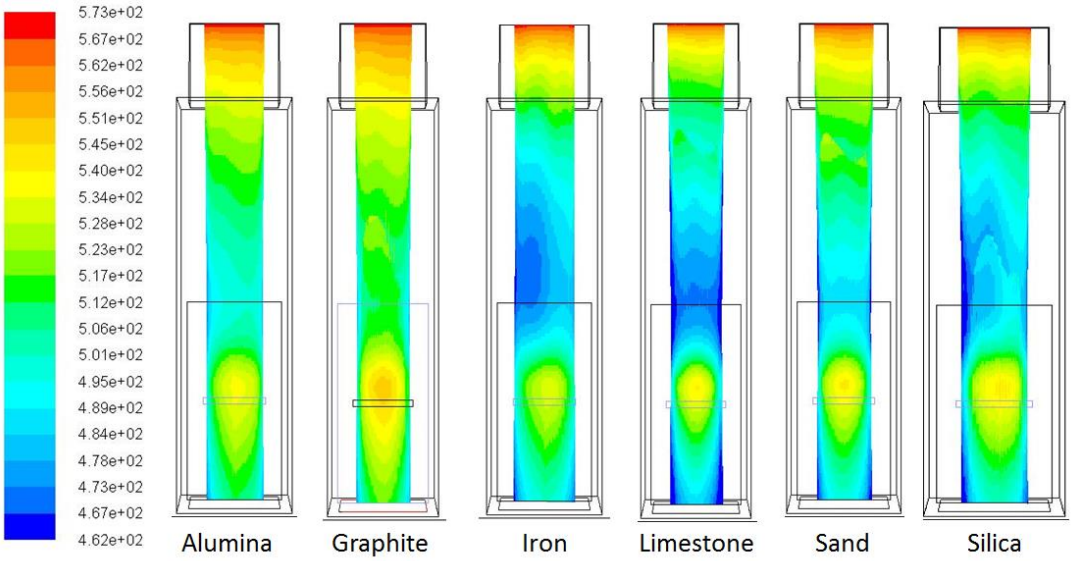

Figure 6.12 Mass flow rate at 3.84 Kg/s and Heat Flux at 1MW

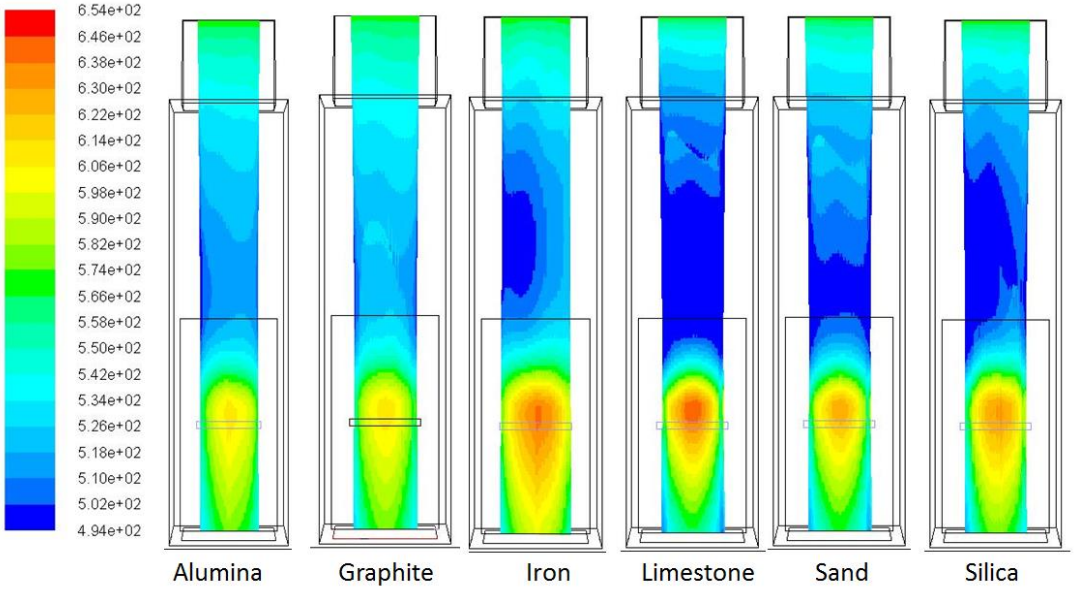

Figure 6.13 Mass flow rate at 3.84 Kg/s and Heat Flux at 2MW

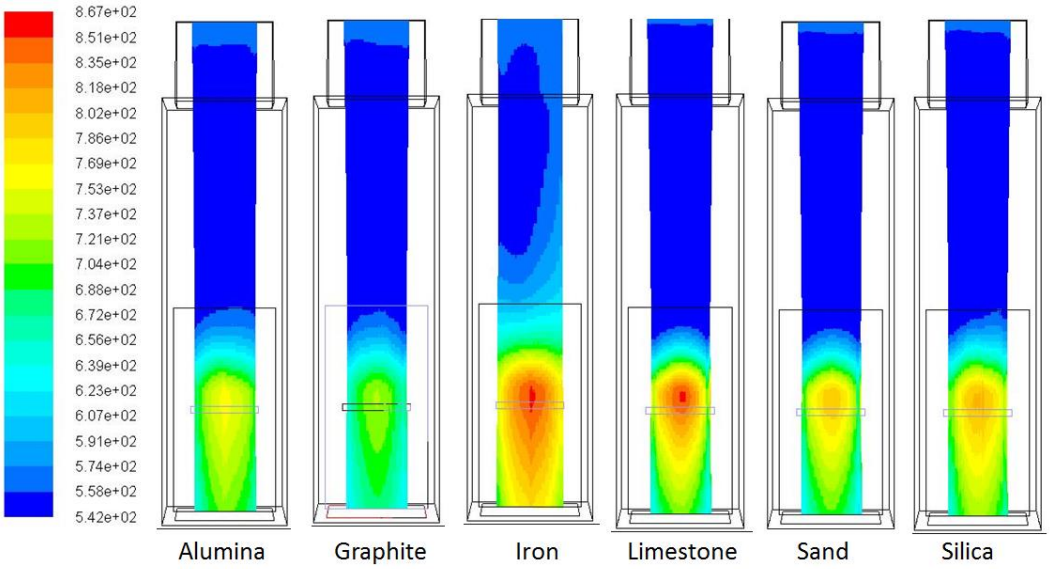

Figure 6.14 Mass flow rate at 3.84 Kg/s and Heat Flux at 4MW

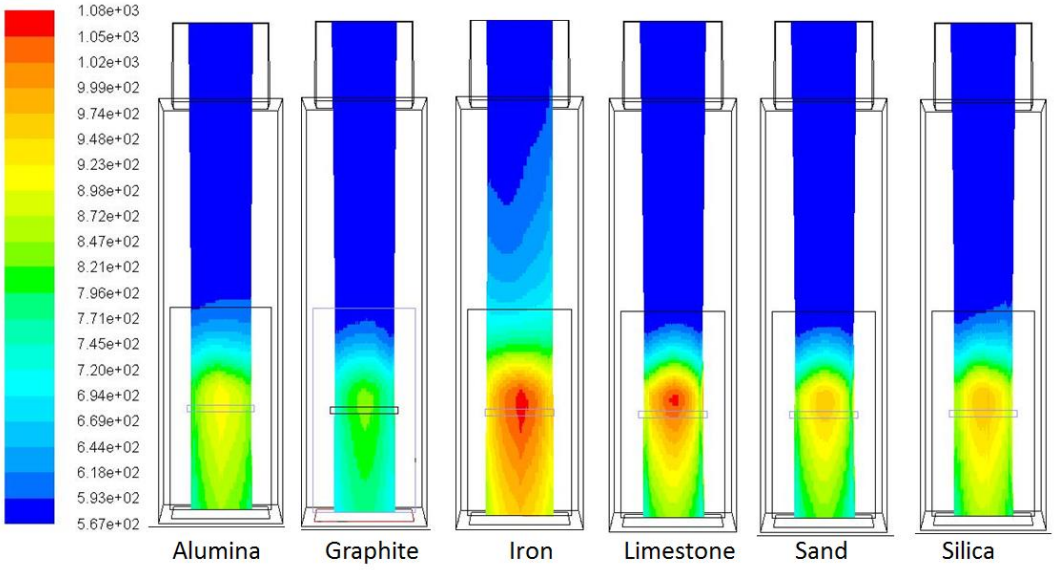

Figure 6.15 Mass flow rate at 3.84 Kg/s and Heat Flux at 6MW

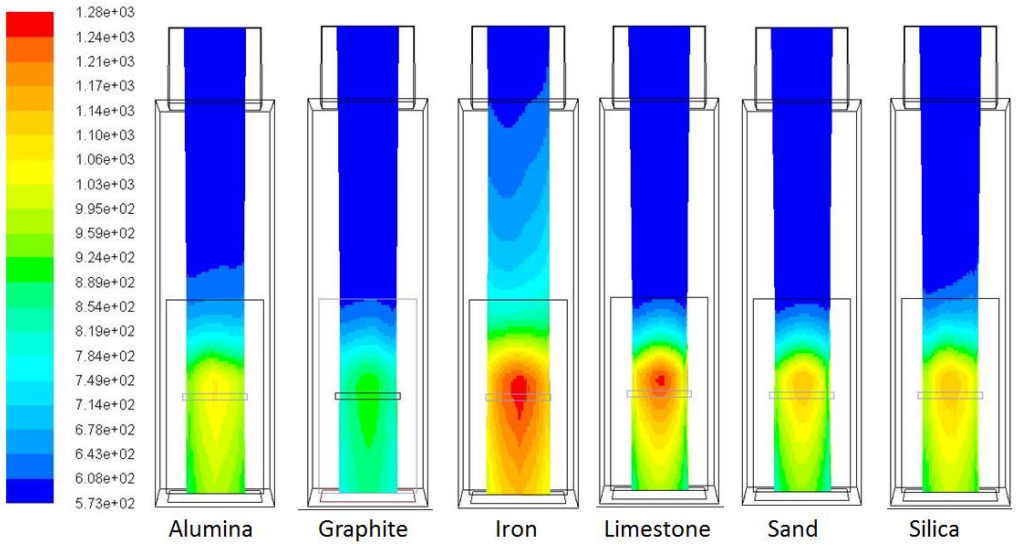

Figure 6.16 Mass flow rate at 3.84 Kg/s and Heat Flux at 8MW

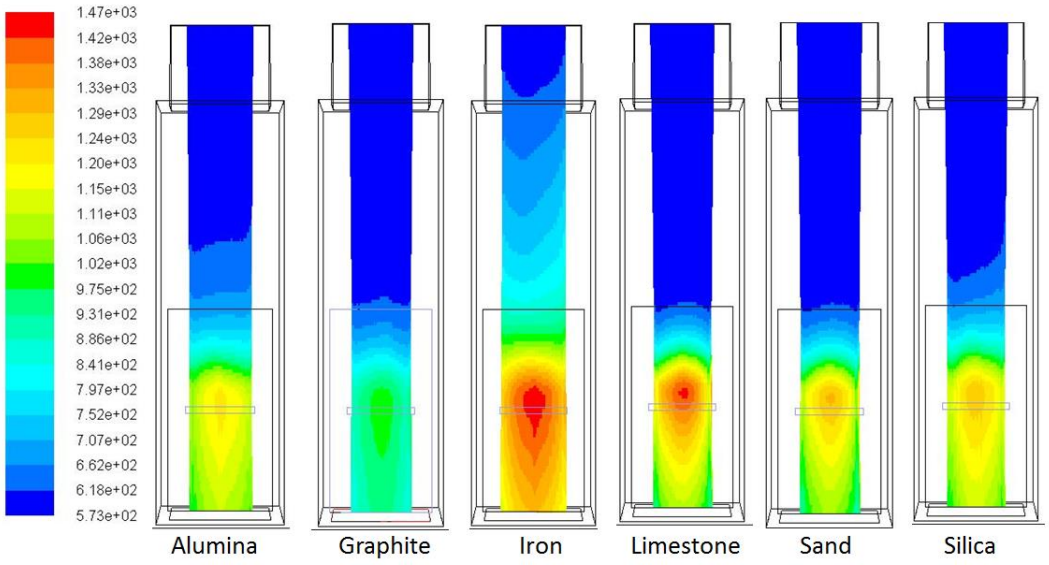

Figure 6.17 Mass flow rate at 3.84 Kg/s and Heat Flux at 10MW

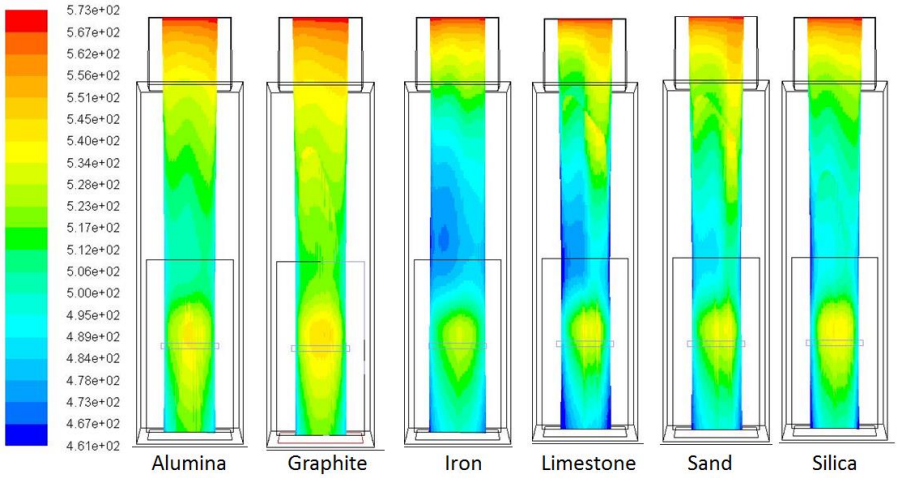

Figure 6.18 Mass flow rate at 5.32 Kg/s and Heat Flux at 1MW

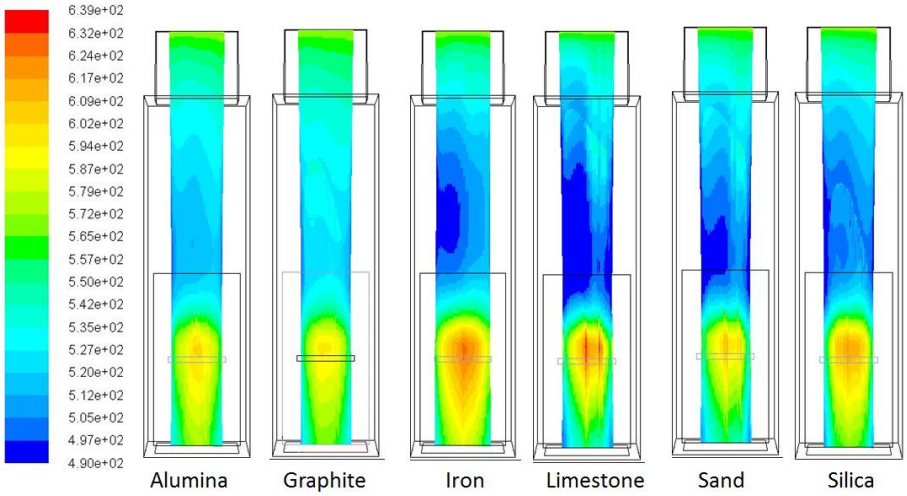

Figure 6.19 Mass flow rate at 5.32 Kg/s and Heat Flux at 2MW

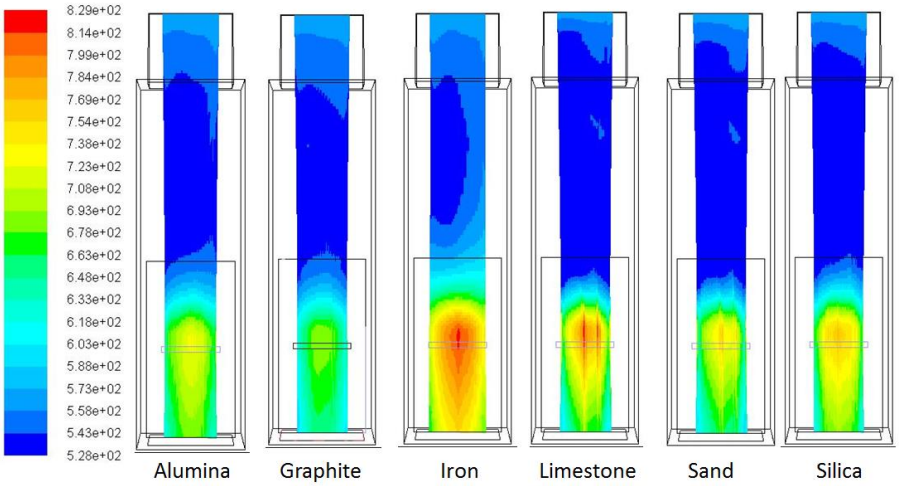

Figure 6.20 Mass flow rate at 5.32 Kg/s and Heat Flux at 4MW

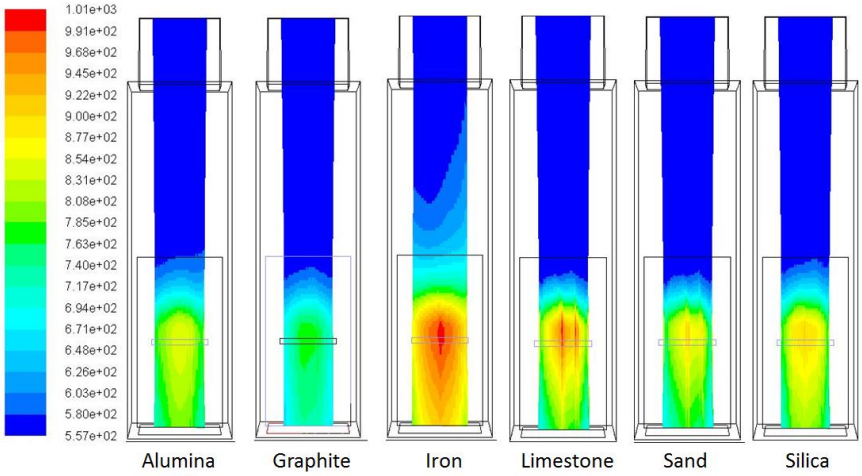

Figure 6.21 Mass flow rate at 5.32 Kg/s and Heat Flux at 6MW

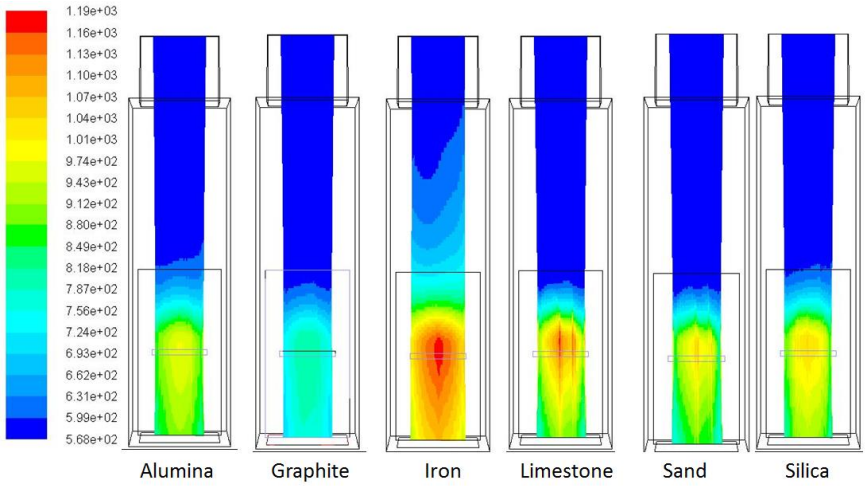

Figure 6.22 Mass flow rate at 5.32 Kg/s and Heat Flux at 8MW

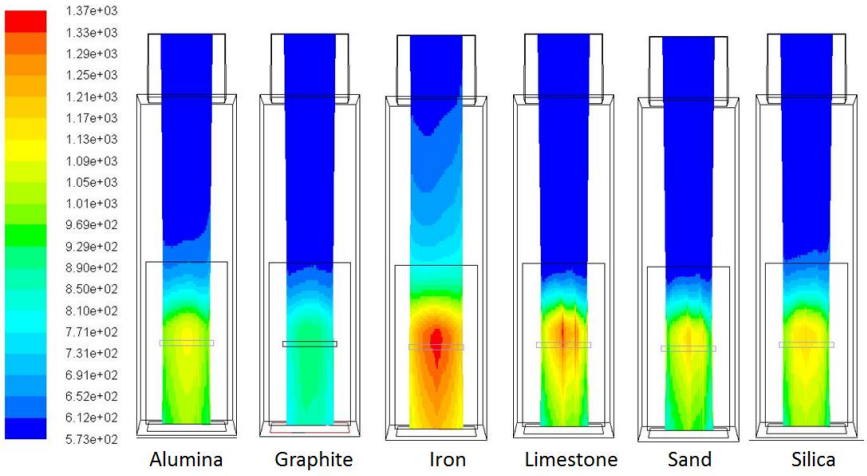

Figure 6.23 Mass flow rate at 5.32 Kg/s and Heat Flux at 10MW

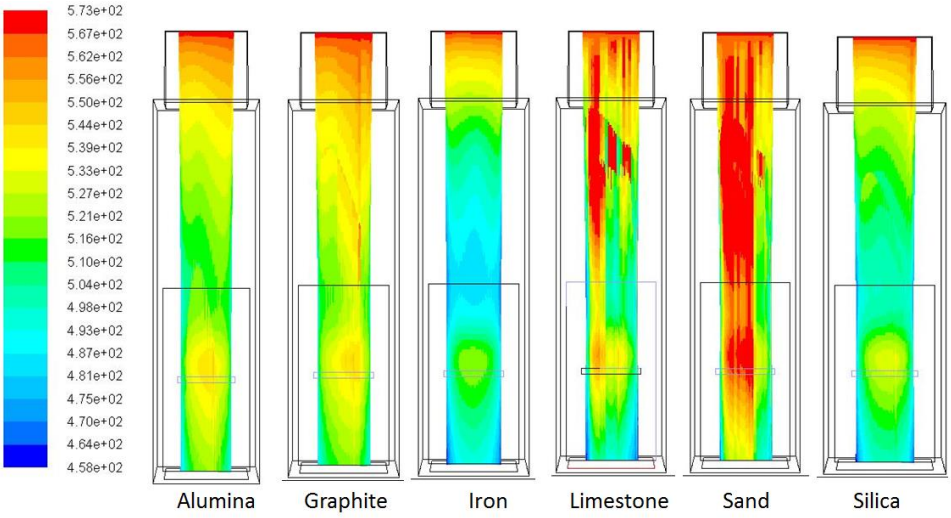

Figure 6.24 Mass flow rate at 8.72 Kg/s and Heat Flux at 1MW

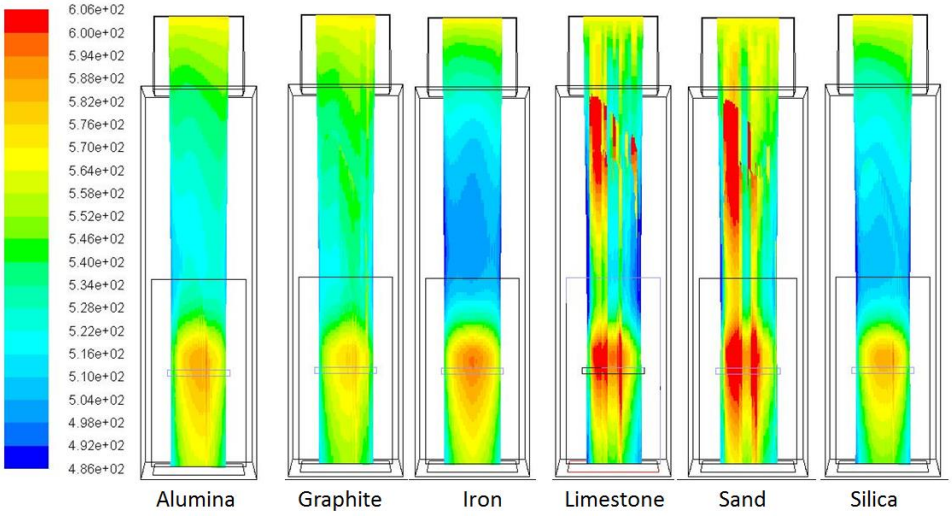

Figure 6.25 Mass flow rate at 8.72 Kg/s and Heat Flux at 2MW

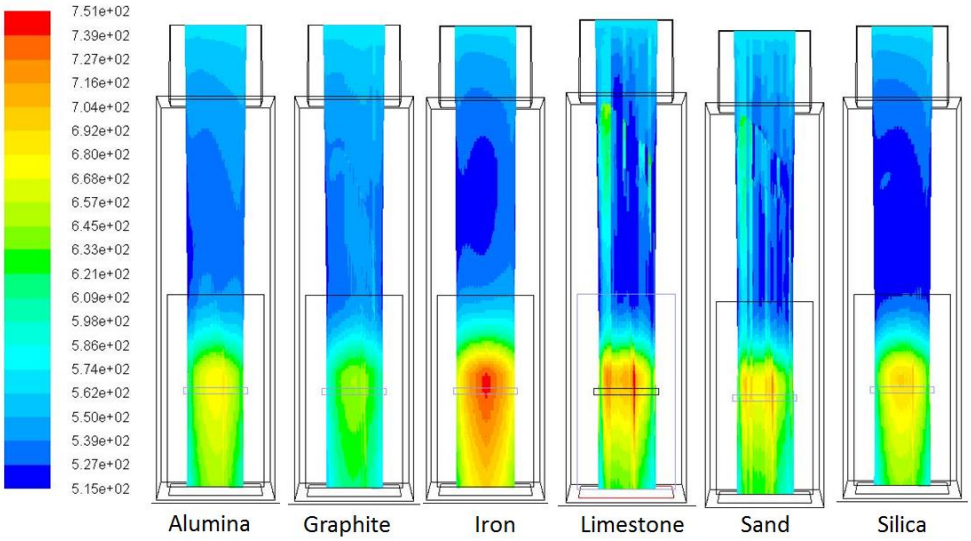

Figure 6.26 Mass flow rate at 8.72 Kg/s and Heat Flux at 4MW

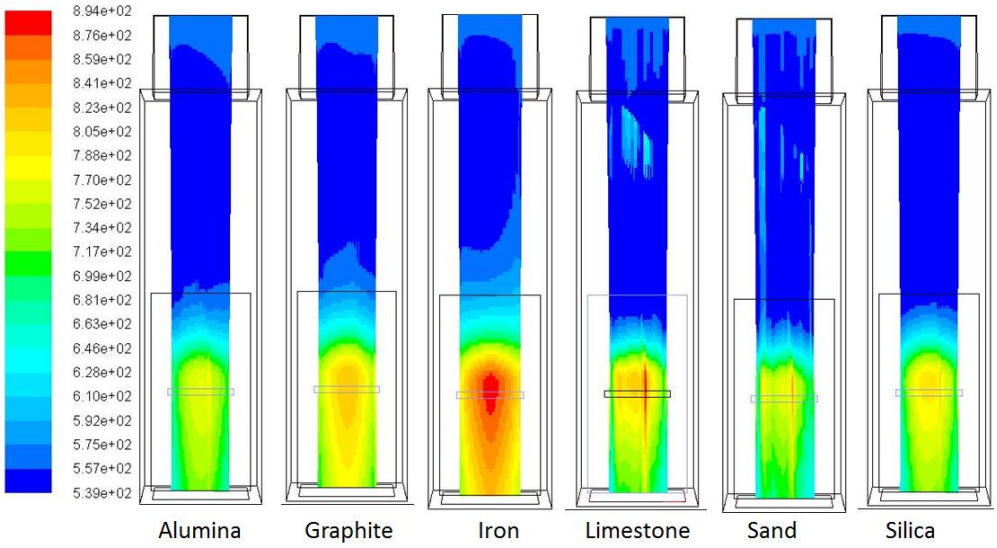

Figure 6.27 Mass flow rate at 8.72 Kg/s and Heat Flux at 6MW

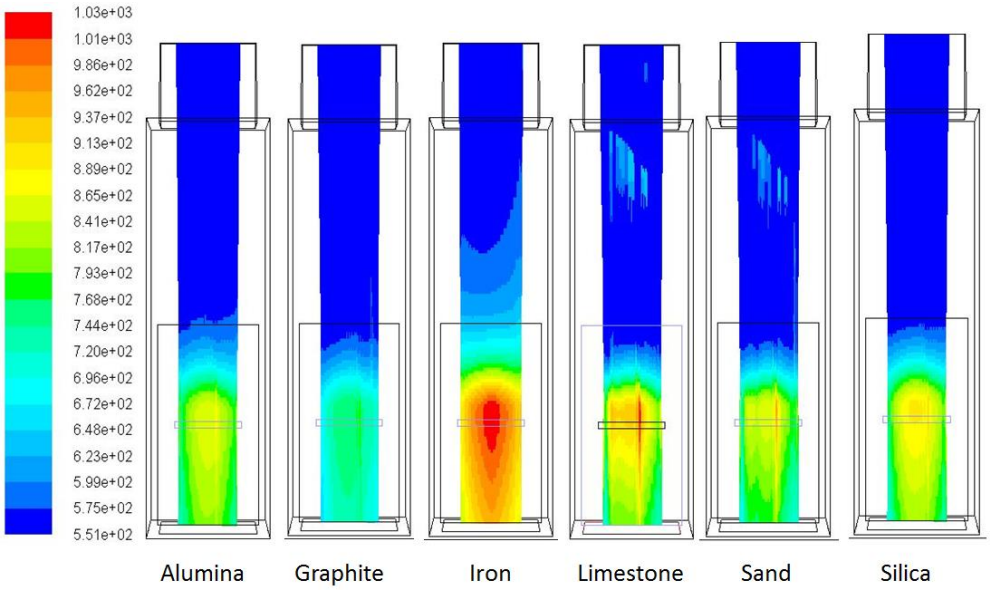

Figure 6.28 Mass flow rate at 8.72 Kg/s and Heat Flux at 8MW

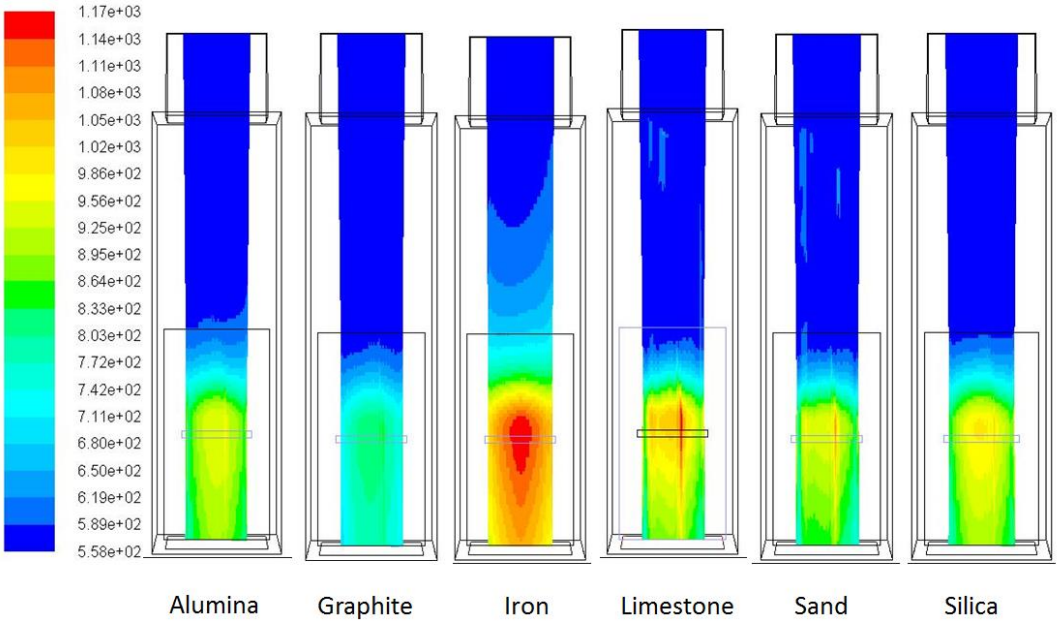

Figure 6.29 Mass flow rate at 8.72 Kg/s and Heat Flux at 10MW

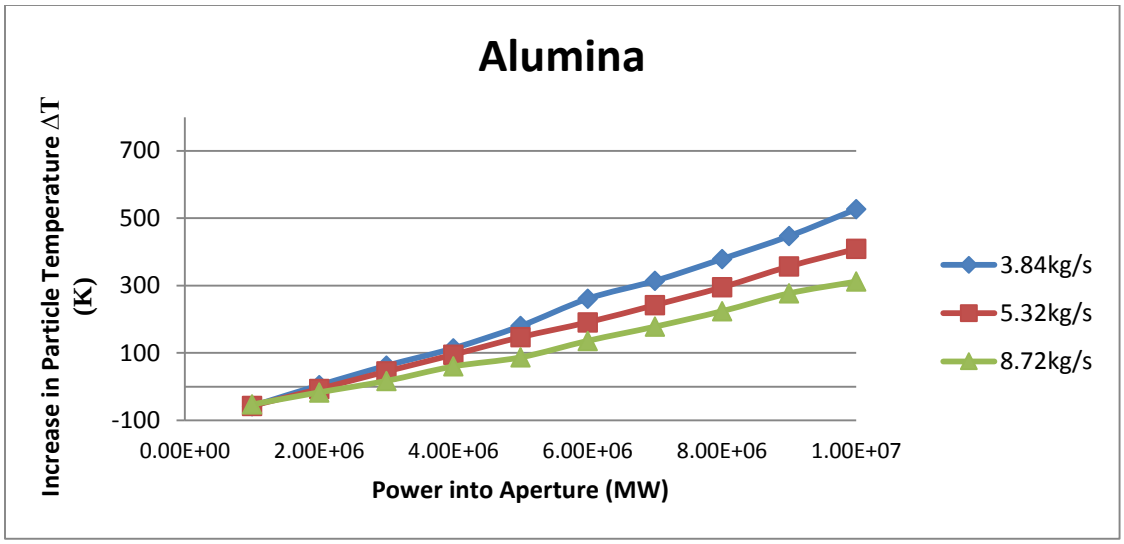

Figure 6.32 Increase in particle temperature

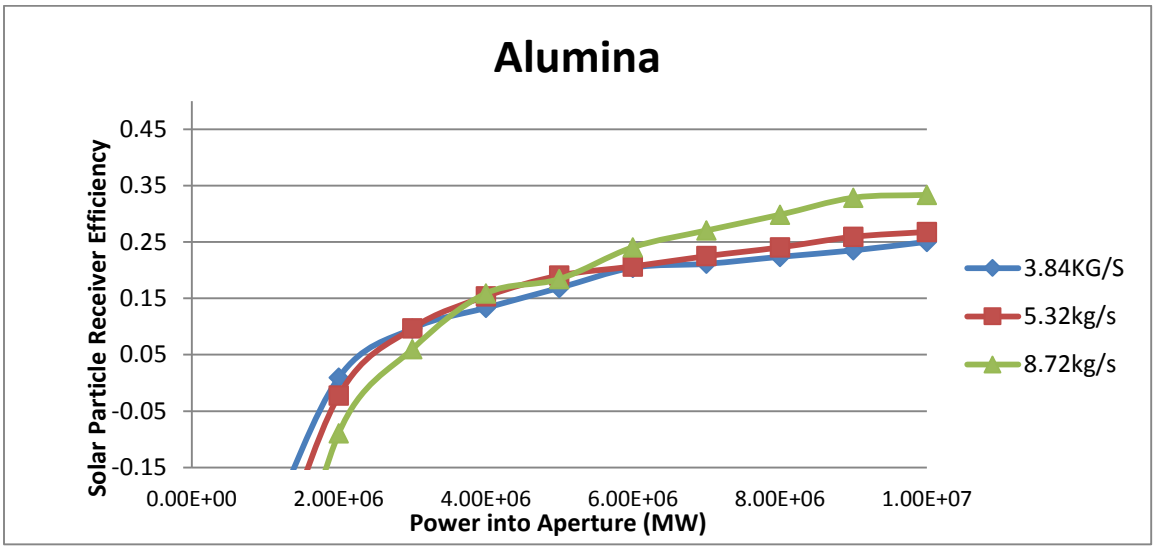

Figure 6.33 Solar particle receiver efficiency

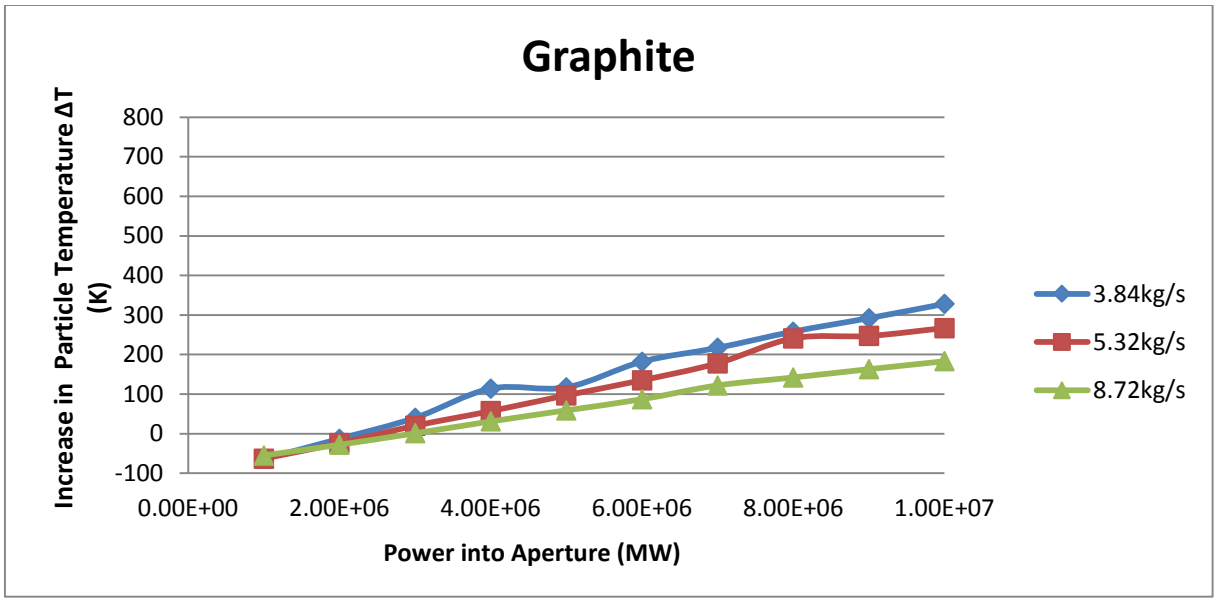

Figure 6.34 Increase in particle temperature

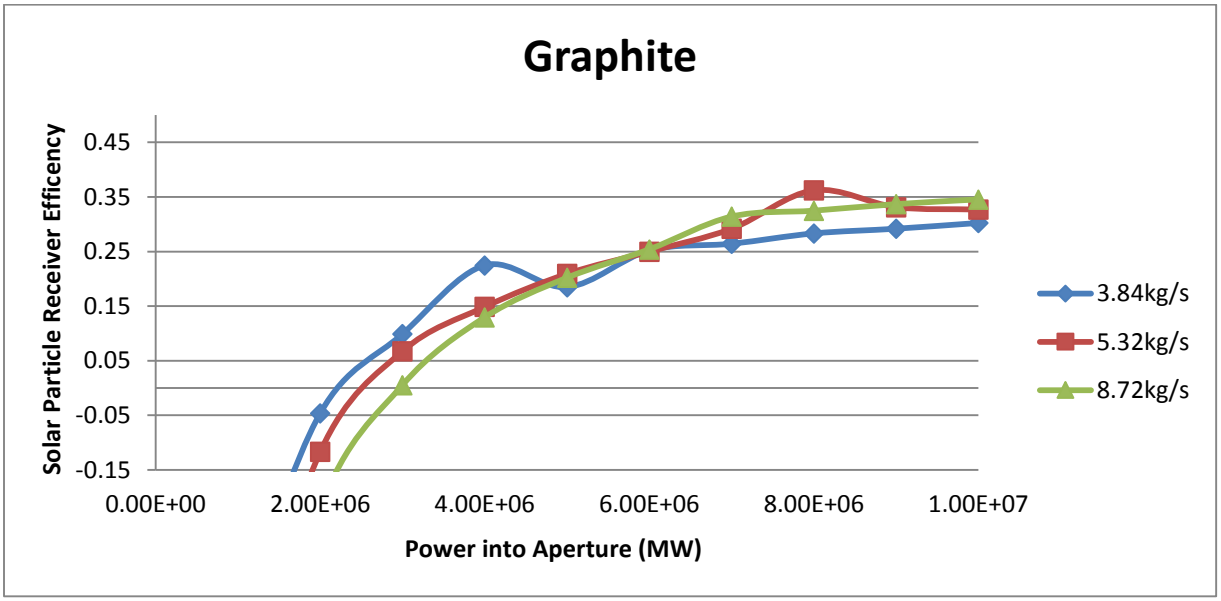

Figure 6.35 Solar particle receiver efficiency

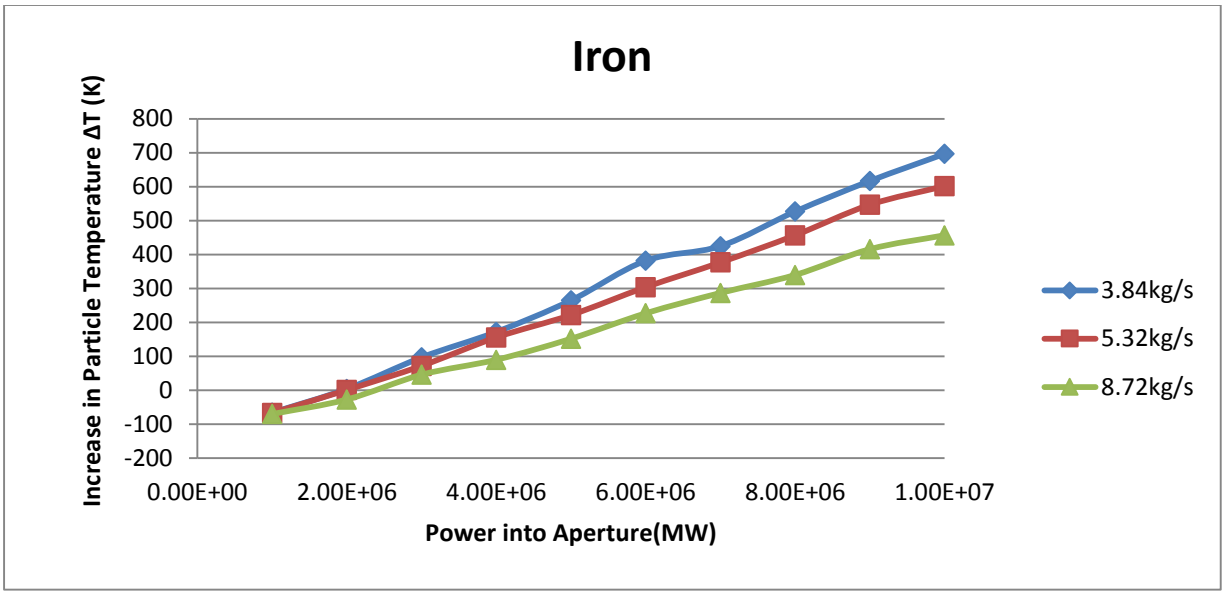

Figure 6.36 Increase in particle temperature

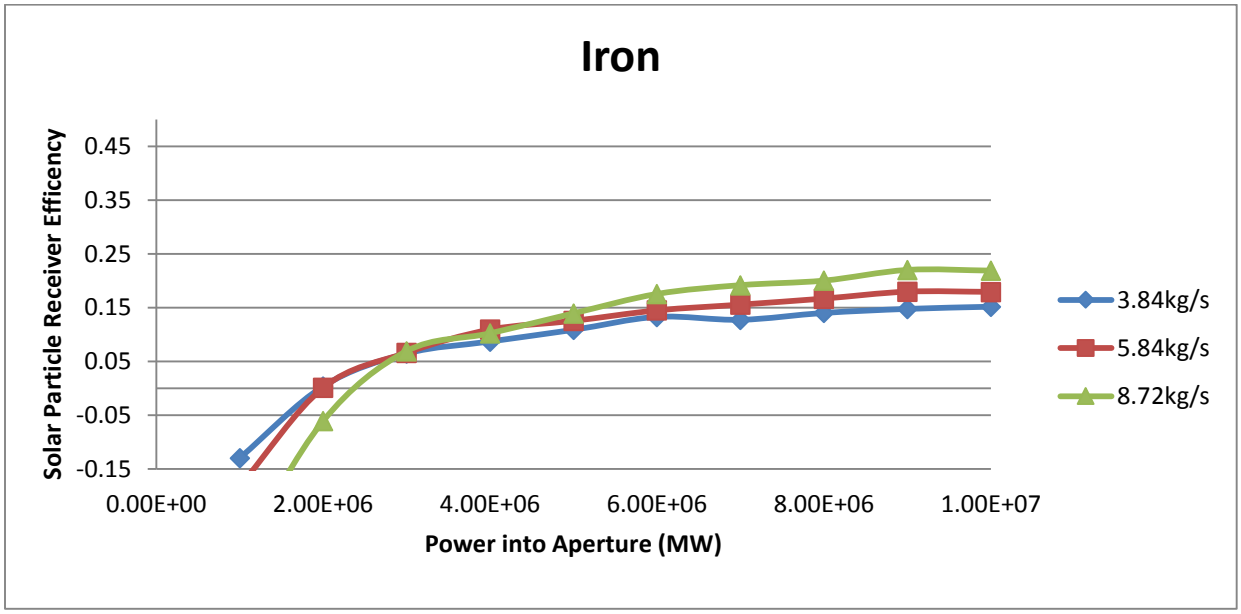

Figure 6.37 Solar particle receiver efficiency

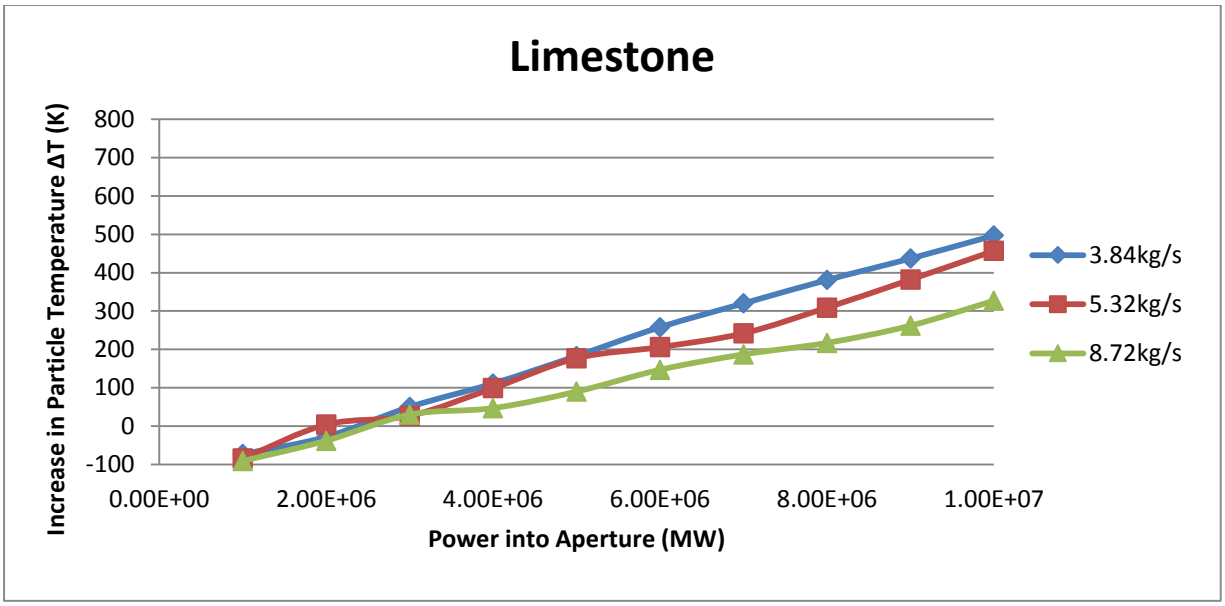

Figure 6.38 Increase in particle temperature

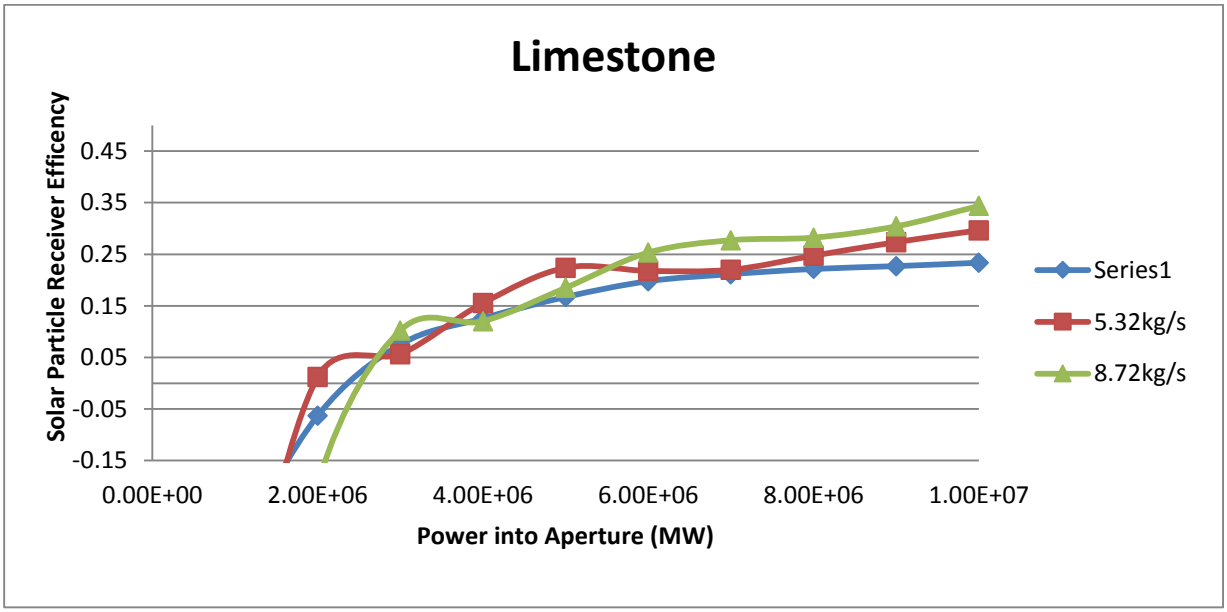

Figure 6.39 Solar particle receiver efficiency

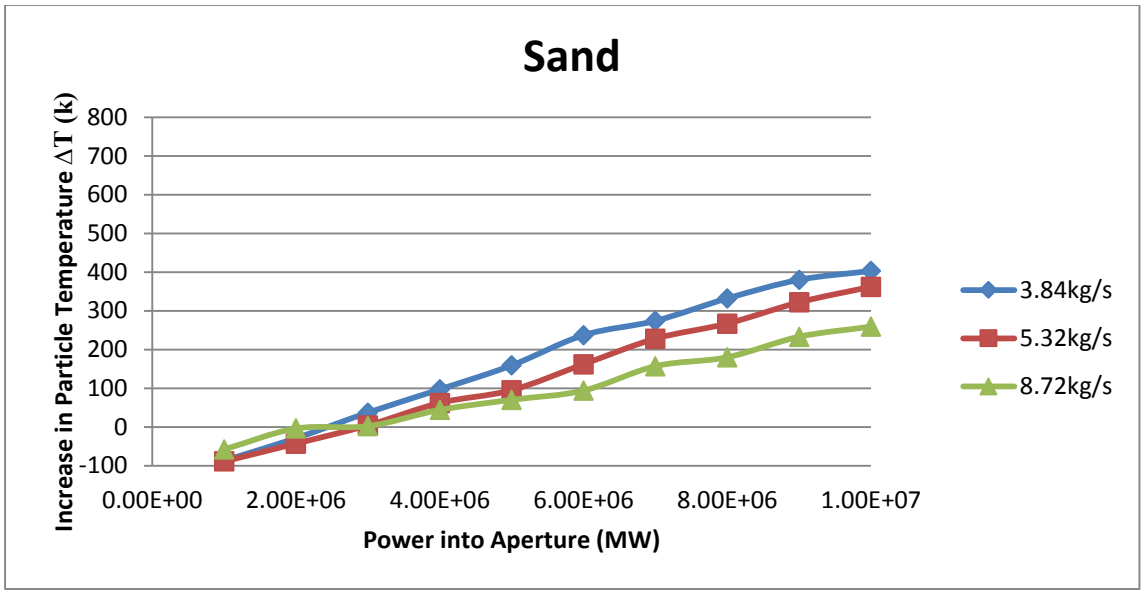

Figure 6.40 Increase in particle temperature

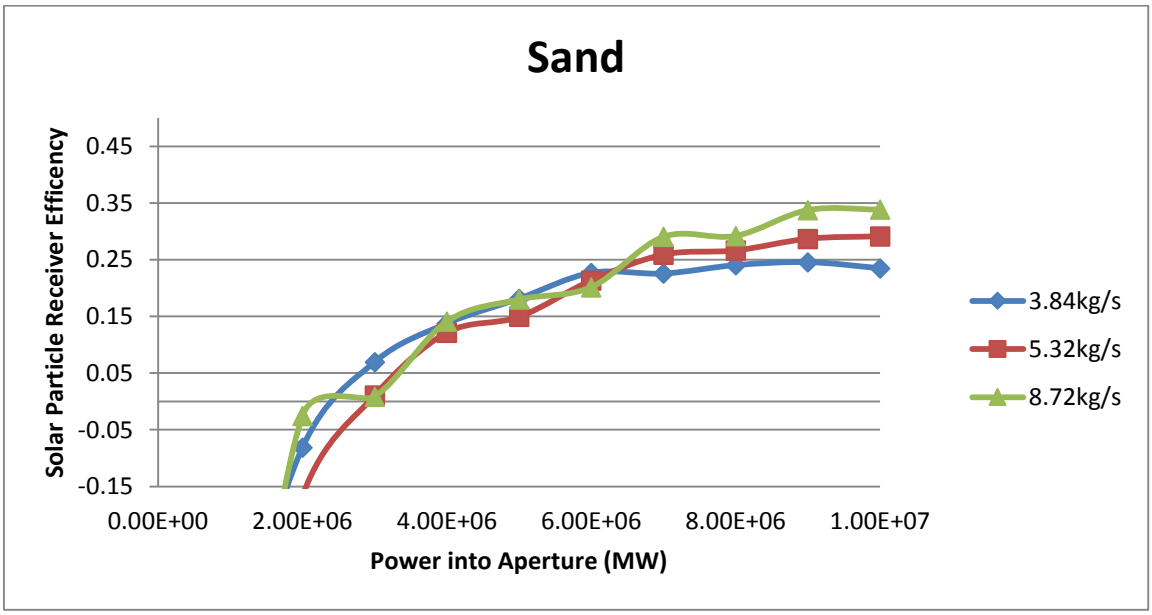

Figure 6.41 Solar particle receiver efficiency

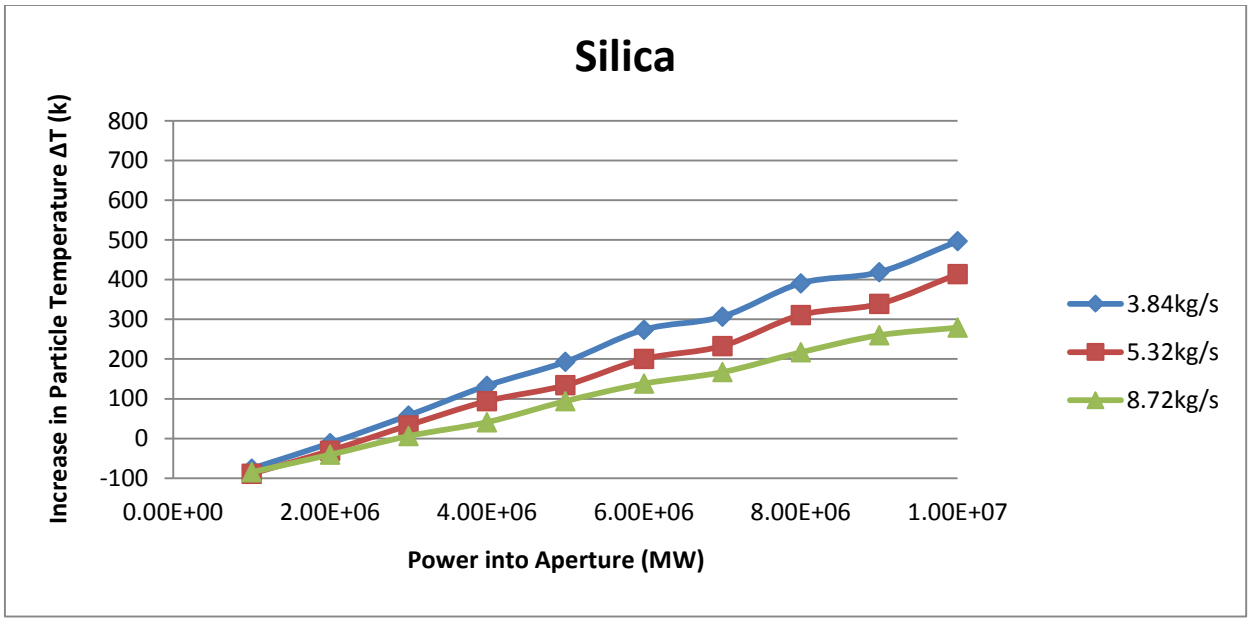

Figure 6.42 Increase in particle temperature

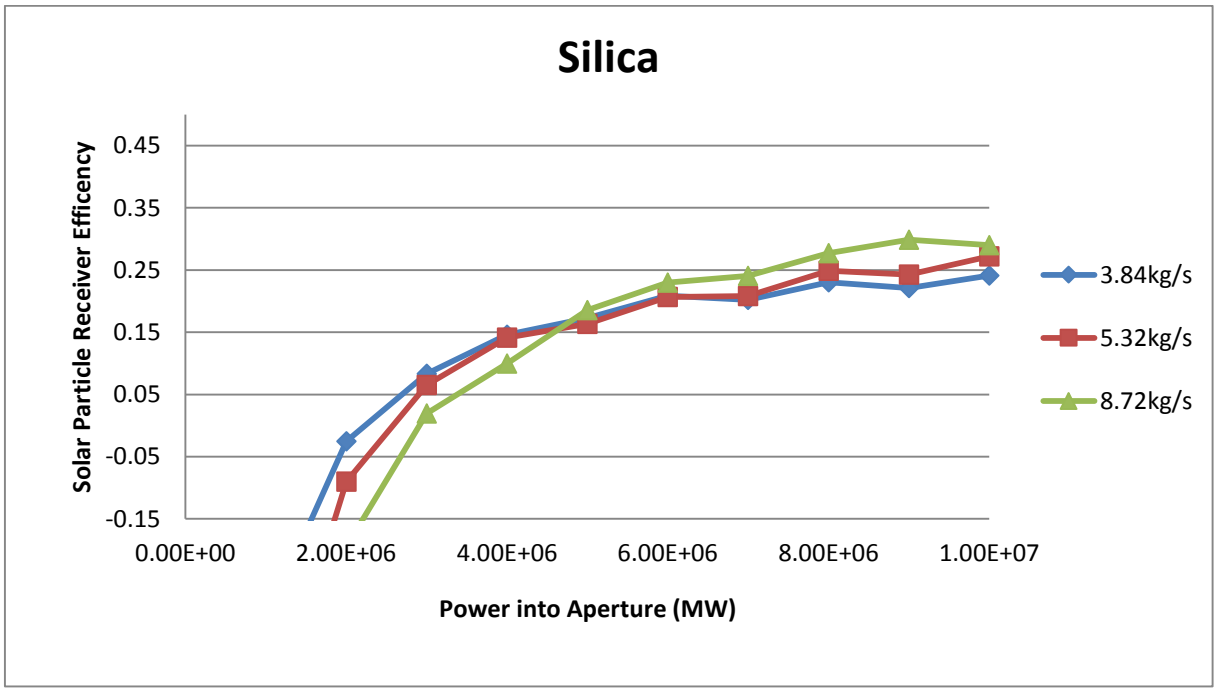

Figure 6.43 Solar particle receiver efficiency

Conclusions

In order to make thermal energy storage more efficient there is a need to find materials than can store energy at higher temperatures than the ones that has been used with current systems like molten salt. This is also back up by all the initiatives from DOE, several universities and some other interests in the concentrated solar power area in order to reduce the electric energy production or the LCOE. According to several publications refer in this study an because of the thermal characteristics of the materials it has been found through research that shows that smaller size particles improve the heat exchange.

It is important to point out that some of the key elements in determining heat transfer include: sample length, change in temperature across the sample, and a value of thermal conductivity.

Through the use of software like Fluent, simulation of heat in materials can be performed for analysis and better understanding of how material behave under different circumstances.

The study involved thermodynamic analysis for several binary and ternary alloys and their composition mixture that melts at high temperature and possess high enthalpy of fusion; so for experimental studies AlSi can be used as an alloy with promising results, due to availability, reasonable price as well as its thermodynamic characteristics.

References

1. Blake DM. Nanomaterials for heat transfer fluid and and thermal storage. 2009;(Lxl).

2. Yang Z, Garimella S V. Thermal analysis of solar thermal energy storage in a molten-salt thermocline. Sol Energy. Elsevier Ltd; 2010 Jun;84(6):974–85.

3. Glatzmaier G. Future Trends for CSP Thermal Energy Storage p Seminar. 2011;

4. Gil A, Medrano M, Martorell I, Lázaro A, Dolado P, Zalba B, et al. State of the art on high temperature thermal energy storage for power generation. Part 1—Concepts, materials and modellization. Renew Sustain Energy Rev. 2010 Jan;14(1):31–55.

5. Herrmann U, Kearney DW. Survey of Thermal Energy Storage for Parabolic Trough Power Plants. J Sol Energy Eng. 2002;124(2):145.

6. Price H, Brosseau D, Kearney D, Kelly B. DOE Advanced Thermal Energy Storage Development Plan For Parabolic Trough Technology. 2007.

7. Solar C, Electricity P. Concentrating Solar Power Commercial Application Study : Reducing Water Consumption of Concentrating Solar Power Electricity Generation Report to Congress. 2001;2001.

8. Moens L, Blake DM, Blake M. MECHANISM OF HYDROGEN FORMATION IN SOLAR PARABOLIC. :1–15.

9. Llc L, Group C. Executive Summary : Assessment of Parabolic Trough and Power Tower Solar Technology Cost and Performance Forecasts Executive Summary : Assessment of Parabolic Trough and Power Tower Solar Technology Cost and Performance Forecasts. 2003;(October).

10. Herrmann U, Kelly B, Price H. Two-tank molten salt storage for parabolic trough solar power plants. Energy. 2004 Apr;29(5-6):883–93.

11. Leitner A, Owens B. Brighter than a Hundred Suns : Solar Power for the Southwest Period of Performance : November 20 , 2001 to October 31 , 2002 Period of Performance : 2003;(January).

12. Leitner A. Fuel From the Sky : Natl Renew Energy Lab. 2002;

13. Concentrating Solar Power (CSP) Milestone Report. (March 2010).

14. Information P, Properties T. Hitec ® Solar Salt. :8787–9.

15. Megahed IE. EXPERIMENTAL TESTING OF FLUIDIZED. 1988;5(l):15–25.

16. Office GF. FINANCIAL ASSISTANCE FUNDING OPPORTUNITY ANNOUNCEMENT High Operating Temperature Fluids Funding Opportunity Announcement Number : DE-FOA-0000567 Announcement Type : Initial Issue Date : Application Due Date : 2012;1–51.

17. Van Lew JT, Li P, Chan CL, Karaki W, Stephens J. Analysis of Heat Storage and Delivery of a Thermocline Tank Having Solid Filler Material. J Sol Energy Eng. 2011;133(2):021003.

18. Kearney D, Kelly B, Herrmann U, Cable R, Pacheco J, Mahoney R, et al. Engineering aspects of a molten salt heat transfer fluid in a trough solar field. Energy. 2004 Apr;29(5-6):861–70.

19. Cengel YA. A Practical Approach.

20. Efficiency E. 2008 SOLAR TECHNOLOGIES MARKET REPORT. US Dep Energy Energy Effic Renew Energy [Internet]. 2010;(January):131. Available from: http://escholarship.org/uc/item/5f24h660.pdf

21. Glatzmaier GC, Turchi CS. Proceedings of ES2009 Energy Sustainability 2009 July 19-23, 2009, San Francisco, California USA. 2009;2–5.

22. Wang & Kreith - Sensible Heat Storage Options 1985.pdf.

23. Blair N, Mehos M, Christensen C, Cameron C. Modeling Photovoltaic and Concentrating Solar Power Trough Performance , Cost , and Financing with the Solar Advisor Model Preprint. Solar Energy. 2008.

24. Turchi C, Mehos M, Ho CK, Kolb GJ. Current and Future Costs for Parabolic Trough and Power Tower Systems in the US Market Preprint. 2010;(October).

25. Jones S. Concentrating Solar Power : The “ Other ” Solar … A Systems Perspective Concentrating Solar Power - Tower. 2004;

26. Copy of SAM Parabolic Trough Cost Model w indexing.

27. Price H, Lüpfert E, Kearney D, Zarza E, Cohen G, Gee R, et al. Advances in Parabolic Trough Solar Power Technology. J Sol Energy Eng. 2002;124(2):109.

28. Bengtson H. Concentrating Solar Power Technologies 2: Parabolic Dish Stirling Engine Systems. 2010.

29. FP depression by nanoparticles 43237.pdf.

30. Hawlader MN a., Uddin MS, Zhu HJ. Encapsulated phase change materials for thermal energy storage: Experiments and simulation. Int J Energy Res. 2002 Feb;26(2):159–71.

31. Sozen ZZ, Grace JR, Pinder KL. Thermal energy storage by agitated capsules of phase change material. 1. Pilot scale experiments. Ind Eng Chem Res. 1988 Apr;27(4):679–84.

32. Peterson GP. Heat Transfer Fundamentals. 2009 Jan;818–69.

33. blake_nanomaterials.

34. Siegel NP, Ho CK, Khalsa SS, Kolb GJ. Development and Evaluation of a Prototype Solid Particle Receiver: On-Sun Testing and Model Validation. J Sol Energy Eng. 2010;132(2):021008.

35. Survey of TES Salts ORNLTM5682.pdf.

36. Wright SA, Radel RF, Vernon ME, Rochau GE, Pickard PS. Operation and Analysis of a Supercritical CO 2 Brayton Cycle. 2010;(September).

37. Specification for Thermal Storage Process & Components Integration Laboratory. 2012;(43064).

38. Flamant G, Lu JD, Variot B. Towards a generalized model for vertical walls to gas—solid fluidized beds heat transfer—II. Radiative transfer and temperature effects. Chemical Engineering Science. 1993. p. 2493–503.

39. Lu JD, Flamant G, Variot B. Theoretical study of combined conductive, convective and radiative heat transfer between plates and packed beds. Int J Heat Mass Transf. 1994 Mar;37(5):727–36.

40. Shent J, Kaguei S, Wakao N. Measurements of particle-to-gas heat transfer coefficients from one-shot thermal responses in packed beds. ELSEVIER. 1981;36(8):1283–6.

41. W. E. Ranz and W. R. Marshall J. Evaporation From Drops. 1952.

42. Kunii D, Smith JM. Heat transfer characteristics of porous rocks. AIChE J [Internet]. 1960;6(1):71–8. Available from: http://doi.wiley.com/10.1002/aic.690060115

43. Wakao, N., & Kaguei S. Heat and Mass Transfer in Packed Beds. New York: Gordon and Breach, Science Publishers.; 1982.

44. Hong Y, Ding S, Wu W, Hu J, Voevodin A a, Gschwender L, et al. Enhancing heat capacity of colloidal suspension using nanoscale encapsulated phase-change materials for heat transfer. ACS Appl Mater Interfaces. 2010 Jun;2(6):1685–91.

45. Stoddard L, Abiecunas J, Connell RO. Economic , Energy , and Environmental Benefits of Concentrating Solar Power in California Economic , Energy , and Environmental Benefits of Concentrating Solar Power in California. 2006;(April).

46. Nelson IC, Banerjee D, Ponnappan R. Flow Loop Experiments Using Polyalphaolefin Nanofluids. J Thermophys Heat Transf. 2009 Oct;23(4):752–61.

47. May D. Parabolic Trough Reference Plant for Cost Modeling with the Solar Advisor Model Summary. 2010;

48. Medrano M, Gil A, Martorell I, Potau X, Cabeza LF. State of the art on high-temperature thermal energy storage for power generation. Part 2—Case studies. Renew Sustain Energy Rev. 2010 Jan;14(1):56–72.

49. Gale, W. F., & Totemeier TC. Smithells Metals refercene book. Eighth Edi. ELSEVIER, editor. 2004.

50. Rao YK. Stoichiometry and Thermodynamics of Metallurgical processes. Cambridge University Press; 1985.

51. Diagram E. The AI-Si (Aluminum-Silicon) System 26.98154 28.0855. 1984;5(1):74–84.

52. Liu Z, Chang YA. Thermodynamic Assessment of the Al-Fe-Si System. 1999;30(April):1081–95.

53. Maheswaraiah N, Sandate A V., Bronson A. Reactive Processing of a ZrB 2 /ZrC/Zr-Si Ceramic Composite with a Controlled Oxygen Potential. Int J Appl Ceram Technol. 2013 Mar;10(2):234–44.

54. Kenisarin MM. High-temperature phase change materials for thermal energy storage. Renew Sustain Energy Rev. 2010 Apr;14(3):955–70.

55. Oh SH, Kauffmann Y, Scheu C, Kaplan WD, Rühle M. Ordered liquid aluminum at the interface with sapphire. Science. 2005 Oct;310(5748):661–3.

56. Pacheco JE, Showalter SK, Kolb WJ. DEVELOPMENT OF A MOLTEN-SALT THERMOCLINE THERMAL STORAGE SYSTEM FOR PARABOLIC TROUGH PLANTS. 2001;

57. Team CSP, February M. DOE ' s SunShot Initiative SunShot History. 2011;

58. 2 [16]. engineering tool box;

59. Poirier DR, Nandapurkar P. Enthalpies of a Binary Alloy during Solidification. 1988;19(December):3057–61.

60. Kunii D, Levenspiel O. Fluidization Engineering. Second edi. Butterworth-Heinemann, editor. 1991.

61. Noranzyk A, Nalysis ERA, Ssociated ERA, Ample WS, Dial LE. Thermal Conductivity Measurements of Graphite Samples Colorado School of Mines Energy ' s Science Undergraduate Laboratory Internship under the direction of Dr . Todd A . 2009;

62. Watano S, Nakamura H, Hamada K, Wakamatsu Y, Tanabe Y, Dave RN, et al. Fine particle coating by a novel rotating fluidized bed coater. Powder Technol. 2004 Mar;141(3):172–6.

63. Jaques BN, May T, Solar M. CSP storage options : Phase change materials. 2010;5–8.

64. Physical Modeling of Mixing in Water Storage Tanks.

65. An-Introduction-to-Computational-Fluid-Dynamics-Versteeg.pdf.

66. Glicksman Azzola Modlin JSEE 1988 fluidized_bed_solar_collector.pdf.

Appendix

Data to make graph on Figure 5.11 to analyze enthalpies of binary alloy during solidification, in this case was for Lead and Tin.

Formula Imput (0<CL<61.9)	
CL	0.1
Start	0
incremen	1

(0<CL<61.9)	
CL	0.1
Start	0
incremen	1

(0<CL<61.9)	
CL	0.1
Start	0
incremen	1

CL	HL (0<CL<61.9)
0.1	63.84492488
1.1	64.56639487
2.1	65.273871
3.1	65.96755793
4.1	66.64764897
5.1	67.314326
6.1	67.96775958
7.1	68.60810883
8.1	69.23552152
9.1	69.85013404
10.1	70.45207138
11.1	71.04144717
12.1	71.61836364
13.1	72.18291165
14.1	72.73517068
15.1	73.27520881
16.1	73.80308276
17.1	74.31883787
18.1	74.82250807
19.1	75.31411593
20.1	75.79367265
21.1	76.26117803
22.1	76.71662048
23.1	77.15997705
24.1	77.59121341
25.1	78.01028382
26.1	78.41713118
27.1	78.81168701
28.1	79.19387145
29.1	79.56359324
30.1	79.92074975
31.1	80.26522698

CL	Hs* (0<CL<61.9)
0.1	40.52332744
1.1	41.31576041
2.1	41.78017543
3.1	42.14586947
4.1	42.45350825
5.1	42.72002761
6.1	42.95455013
7.1	43.16271731
8.1	43.34833775
9.1	43.51414436
10.1	43.6621884
11.1	43.79406372
12.1	43.91104309
13.1	44.01416583
14.1	44.10429637
15.1	44.1821649
16.1	44.24839645
17.1	44.30353216
18.1	44.3480452
19.1	44.38235292
20.1	44.40682631
21.1	44.4217974
22.1	44.42756519
23.1	44.42440044
24.1	44.41254958
25.1	44.39223787
26.1	44.36367216
27.1	44.32704305
28.1	44.28252683
29.1	44.23028706
30.1	44.17047594
31.1	44.10323551

CL	HL-Hs* (0<CL<61.9)
0.1	22.86745821
1.1	22.83976024
2.1	23.05583716
3.1	23.35235572
4.1	23.69633134
5.1	24.07276954
6.1	24.47298209
7.1	24.89124549
8.1	25.32347411
9.1	25.76658642
10.1	26.21816324
11.1	26.67624667
12.1	27.13921388
13.1	27.60569373
14.1	28.07450932
15.1	28.54463712
16.1	29.01517706
17.1	29.48532998
18.1	29.95438051
19.1	30.42168361
20.1	30.88665394
21.1	31.34875735
22.1	31.80750395
23.1	32.26244237
24.1	32.71315507
25.1	33.15925433
26.1	33.60037895
27.1	34.03619135
28.1	34.46637516
29.1	34.89063309
30.1	35.30868514
31.1	35.72026695

Formula Imput (0<CL<61.9)	
CL	0.1
Start	0
incremen	1

(0<CL<61.9)	
CL	0.1
Start	0
incremen	1

(0<CL<61.9)	
CL	0.1
Start	0
incremen	1

CL	HL (0<CL<61.9)
32.1	80.59689954
33.1	80.91563063
34.1	81.22127213
35.1	81.51366447
36.1	81.79263676
37.1	82.05800667
38.1	82.30958055
39.1	82.54715331
40.1	82.77050853
41.1	82.97941836
42.1	83.17364361
43.1	83.35293368
44.1	83.5170266
45.1	83.66564903
46.1	83.79851622
47.1	83.91533206
48.1	84.01578906
49.1	84.09956833
50.1	84.16633962
51.1	84.21576129
52.1	84.24748031
53.1	84.26113227
54.1	84.2563414
55.1	84.23272052
56.1	84.18987109
57.1	84.12738318
58.1	84.04483546
59.1	83.94179526
60.1	83.81781849
61.1	83.67244969
62.1	83.50522204
63.1	83.31565731

CL	Hs* (0<CL<61.9)
32.1	44.02869866
33.1	43.94699004
34.1	43.85822679
35.1	43.76251927
36.1	43.65997164
37.1	43.55068238
38.1	43.43474478
39.1	43.31224734
40.1	43.18327418
41.1	43.04790534
42.1	42.90621709
43.1	42.75828222
44.1	42.60417028
45.1	42.44394778
46.1	42.27767844
47.1	42.10542334
48.1	41.92724108
49.1	41.74318797
50.1	41.55331815
51.1	41.35768374
52.1	41.1563349
53.1	40.94932003
54.1	40.7366858
55.1	40.51847729
56.1	40.29473803
57.1	40.06551013
58.1	39.83083434
59.1	39.59075008
60.1	39.34529557
61.1	39.09450785
62.1	38.83842285
63.1	38.57707542

CL	HL-Hs* (0<CL<61.9)
32.1	36.12512847
33.1	36.52303267
34.1	36.91375449
35.1	37.29707986
36.1	37.67280487
37.1	38.04073494
38.1	38.40068418
39.1	38.75247476
40.1	39.09593633
41.1	39.43090554
42.1	39.75722554
43.1	40.0747456
44.1	40.3833207
45.1	40.68281118
46.1	40.97308245
47.1	41.25400464
48.1	41.52545239
49.1	41.78730454
50.1	42.03944396
51.1	42.28175726
52.1	42.51413468
53.1	42.73646982
54.1	42.94865955
55.1	43.15060378
56.1	43.34220535
57.1	43.52336987
58.1	43.69400563
59.1	43.85402343
60.1	44.0033365
61.1	44.14186035
62.1	44.26951274
63.1	44.38621352

(61.9<CL<100)	
CL	61.9
Start	61.9
Incremen	1

CL	HL(61.9<CL<100)
61.9	83.47430757
62.9	84.1637501
63.9	84.8453757
64.9	85.51972147
65.9	86.18733284
66.9	86.84876357
67.9	87.50457574
68.9	88.15533978
69.9	88.80163442
70.9	89.44404675
71.9	90.08317215
72.9	90.71961437
73.9	91.35398546
74.9	91.98690581
75.9	92.61900413
76.9	93.25091748
77.9	93.88329121
78.9	94.51677903
79.9	95.15204298
80.9	95.78975341
81.9	96.430589
82.9	97.07523678
83.9	97.72439208
84.9	98.37875858
85.9	99.03904828
86.9	99.7059815
87.9	100.3802869
88.9	101.0627015
89.9	101.7539706
90.9	102.4548477
91.9	103.166095
92.9	103.8884827
93.9	104.6227894
94.9	105.3698021
95.9	106.1303161
96.9	106.905135
97.9	107.6950706
98.9	108.5009434
99.9	109.3235819

(61.9<CL<100)	
CL	60.5
Start	61.9
Incremen	1

CL	Hs*(61.9<CL<100)
60.5	39.46369655
61.5	39.72196702
62.5	39.97431055
63.5	40.22128619
64.5	40.46345304
65.5	40.70137016
66.5	40.93559663
67.5	41.16669152
68.5	41.3952139
69.5	41.62172285
70.5	41.84677744
71.5	42.07093676
72.5	42.29475986
73.5	42.51880583
74.5	42.74363373
75.5	42.96980265
76.5	43.19787166
77.5	43.42839983
78.5	43.66194623
79.5	43.89906994
80.5	44.14033004
81.5	44.38628559
82.5	44.63749567
83.5	44.89451936
84.5	45.15791573
85.5	45.42824385
86.5	45.70606279
87.5	45.99193164
88.5	46.28640946
89.5	46.59005534
90.5	46.90342833
91.5	47.22708752
92.5	47.56159198
93.5	47.90750079
94.5	48.26537302
95.5	48.63576774
96.5	49.01924403
97.5	49.41636095
98.5	49.8276776

(61.9<CL<100)	
CL	61.9
Start	61.9
Incremen	1

CL	HL-Hs*(61.9<CL<10
61.9	43.65776716
62.9	44.10052129
63.9	44.53955393
64.9	44.97498704
65.9	45.4069426
66.9	45.83554258
67.9	46.26090893
68.9	46.68316363
69.9	47.10242864
70.9	47.51882593
71.9	47.93247746
72.9	48.34350521
73.9	48.75203114
74.9	49.15817721
75.9	49.5620654
76.9	49.96381767
77.9	50.36355599
78.9	50.76140231
79.9	51.15747862
80.9	51.55190688
81.9	51.94480905
82.9	52.3363071
83.9	52.726523
84.9	53.11557872
85.9	53.50359621
86.9	53.89069746
87.9	54.27700442
88.9	54.66263906
89.9	55.04772334
90.9	55.43237925
91.9	55.81672874
92.9	56.20089377
93.9	56.58499632
94.9	56.96915835
95.9	57.35350184
96.9	57.73814874
97.9	58.12322102
98.9	58.50884065
99.9	58.8951296

Data to develop plots 6.24-6.37 for efficiency and change in temperature

Alumina							
Mass Flow (kg/s)	Radiation (W)	Inlet Temp (K)	Outlet Temp (K)	Cp (J/kg K)	Avg Energy	Delta T	Efficiency
3.84	1.00E+06	573	515	-70045.9736	-268977	-58	-0.26898
3.84	2.00E+06	573	577	4843.38	18598.58	4	0.009299
3.84	3.00E+06	573	635	75255.4264	288980.8	62	0.096327
3.84	4.00E+06	573	687	138674.616	532510.5	114	0.133128
3.84	5.00E+06	573	753	219564.612	843128.1	180	0.168626
3.84	6.00E+06	573	834	319444.7643	1226668	261	0.204445
3.84	7.00E+06	573	887	385159.936	1479014	314	0.211288
3.84	8.00E+06	573	952	466144.4175	1789995	379	0.223749
3.84	9.00E+06	573	1020	551326.9839	2117096	447	0.235233
3.84	1.00E+07	573	1100	652144.4239	2504235	527	0.250423
5.32	1.00E+06	573	516	-68841.1857	-366235	-57	-0.36624
5.32	2.00E+06	573	566	-8471.9957	-45071	-7	-0.02254
5.32	3.00E+06	573	618	54581.9355	290375.9	45	0.096792
5.32	4.00E+06	573	668	115470.3055	614302	95	0.153576
5.32	5.00E+06	573	720	179064.1839	952621.5	147	0.190524
5.32	6.00E+06	573	764	233089.3903	1240036	191	0.206673
5.32	7.00E+06	573	815	295956.1264	1574487	242	0.224927
5.32	8.00E+06	573	868	361568.7855	1923546	295	0.240443
5.32	9.00E+06	573	930	438686.1339	2333810	357	0.259312
5.32	1.00E+07	573	982	503666.9355	2679508	409	0.267951
8.72	1.00E+06	573	520	-64021.0161	-558263	-53	-0.55826
8.72	2.00E+06	573	556	-20566.1937	-179337	-17	-0.08967
8.72	3.00E+06	573	590	20595.6139	179593.8	17	0.059865
8.72	4.00E+06	573	633	72821.724	635005.4	60	0.158751
8.72	5.00E+06	573	660	105711.0639	921800.5	87	0.18436
8.72	6.00E+06	573	709	165588.6768	1443933	136	0.240656
8.72	7.00E+06	573	751	217106.8848	1893172	178	0.270453
8.72	8.00E+06	573	797	273737.632	2386992	224	0.298374
8.72	9.00E+06	573	850	339253.1739	2958288	277	0.328699
8.72	1.00E+07	573	885	382674.9264	3336925	312	0.333693

Graphite							
Mass Flow (kg/s)	Radiation (W)	Inlet Temp (K)	Outlet Temp (K)	Cp (J/kg K)	Avg Energy	Delta T	Efficiency
3.84	1.00E+06	573	509	-112941.55	-433695.55	-64	-0.4337
3.84	2.00E+06	573	560	-24016.97	-92225.163	-13	-0.04611
3.84	3.00E+06	573	613	77338.068	296978.181	40	0.098993
3.84	4.00E+06	573	687	234100.904	898947.471	114	0.224737
3.84	5.00E+06	573	690	240830.951	924790.853	117	0.184958
3.84	6.00E+06	573	755	393820.099	1512269.18	182	0.252045
3.84	7.00E+06	573	790	481877.621	1850410.07	217	0.264344
3.84	8.00E+06	573	831	590086.429	2265931.89	258	0.283241
3.84	9.00E+06	573	865	683957.936	2626398.48	292	0.291822
3.84	1.00E+07	573	901	787439.998	3023769.59	328	0.302377
5.32	1.00E+06	573	510	-111279.05	-592004.57	-63	-0.592
5.32	2.00E+06	573	549	-43910.681	-233604.82	-24	-0.1168
5.32	3.00E+06	573	593	38020.034	202266.581	20	0.067422
5.32	4.00E+06	573	630	111778.949	594664.011	57	0.148666
5.32	5.00E+06	573	670	196515.617	1045463.08	97	0.209093
5.32	6.00E+06	573	708	281824.542	1499306.56	135	0.249884
5.32	7.00E+06	573	751	384009.493	2042930.5	178	0.291847
5.32	8.00E+06	573	814	544557.382	2897045.27	241	0.362131
5.32	9.00E+06	573	820	560519.372	2981963.06	247	0.331329
5.32	1.00E+07	573	840	614569.706	3269510.84	267	0.326951
8.72	1.00E+06	573	518	-97862.281	-853359.09	-55	-0.85336
8.72	2.00E+06	573	545	-51047.408	-445133.39	-28	-0.22257
8.72	3.00E+06	573	574	1870.1742	16307.919	1	0.005436
8.72	4.00E+06	573	604	59484.3252	518703.316	31	0.129676
8.72	5.00E+06	573	632	115892.473	1010582.36	59	0.202116
8.72	6.00E+06	573	660	174844.7	1524645.79	87	0.254108
8.72	7.00E+06	573	695	252112.597	2198421.85	122	0.31406
8.72	8.00E+06	573	715	298050.431	2598999.76	142	0.324875
8.72	9.00E+06	573	736	347682.13	3031788.17	163	0.336865
8.72	1.00E+07	573	756	396280.864	3455569.13	183	0.345557

Iron							
Mass Flow (kg/s)	Radiation (W)	Inlet Temp (K)	Outlet Temp (K)	Cp (J/kg K)	Avg Energy	Delta T	Efficiency
3.84	1.00E+06	573	507	-33690.584	-129371.84	-66	-0.12937
3.84	2.00E+06	573	577	2062.813	7921.2019	4	0.003961
3.84	3.00E+06	573	670	50698.4822	194682.17	97	0.064894
3.84	4.00E+06	573	745	90863.9691	348917.64	172	0.087229
3.84	5.00E+06	573	838	141838.707	544660.64	265	0.108932
3.84	6.00E+06	573	955	207807.404	797980.43	382	0.132997
3.84	7.00E+06	573	998	232567.312	893058.48	425	0.12758
3.84	8.00E+06	573	1100	292407.223	1122843.7	527	0.140355
3.84	9.00E+06	573	1190	346500.638	1330562.5	617	0.14784
3.84	1.00E+07	573	1270	395601.702	1519110.5	697	0.151911
5.32	1.00E+06	573	506	-34196.033	-181922.89	-67	-0.18192
5.32	2.00E+06	573	574	515.478685	2742.3466	1	0.001371
5.32	3.00E+06	573	645	37497.1241	199484.7	72	0.066495
5.32	4.00E+06	573	729	82224.6688	437435.24	156	0.109359
5.32	5.00E+06	573	795	118108.804	628338.84	222	0.125668
5.32	6.00E+06	573	877	163600.564	870355	304	0.145059
5.32	7.00E+06	573	950	204946.31	1090314.4	377	0.155759
5.32	8.00E+06	573	1030	251172.942	1336240.1	457	0.16703
5.32	9.00E+06	573	1120	304323.185	1618999.3	547	0.179889
5.32	1.00E+07	573	1175	337400.857	1794972.6	602	0.179497
8.72	1.00E+06	573	503	-35711.479	-311404.09	-70	-0.3114
8.72	2.00E+06	573	546	-13861.334	-120870.83	-27	-0.06044
8.72	3.00E+06	573	619	23866.9694	208119.97	46	0.069373
8.72	4.00E+06	573	663	46992.6702	409776.08	90	0.102444
8.72	5.00E+06	573	725	80070.8321	698217.66	152	0.139644
8.72	6.00E+06	573	800	120853.873	1053845.8	227	0.175641
8.72	7.00E+06	573	860	154086.631	1343635.4	287	0.191948
8.72	8.00E+06	573	913	183890.54	1603525.5	340	0.200441
8.72	9.00E+06	573	989	227362.1	1982597.5	416	0.220289
8.72	1.00E+07	573	1030	251172.942	2190228.1	457	0.219023

				Sand			
Mass Flow (kg/s)	Radiation (W)	Inlet Temp (K)	Outlet Temp (K)	Cp (J/kg K)	Avg Energy	Delta T	Efficiency
3.84	1.00E+06	573	486	-126287.721	-484944.85	-87	-0.48494
3.84	2.00E+06	573	544	-42326.341	-162533.15	-29	-0.08127
3.84	3.00E+06	573	610	54337.127	208654.568	37	0.069552
3.84	4.00E+06	573	670	143248.727	550075.112	97	0.137519
3.84	5.00E+06	573	732	236160.315	906855.61	159	0.181371
3.84	6.00E+06	573	810	354545.127	1361453.29	237	0.226909
3.84	7.00E+06	573	847	411284.96	1579334.25	274	0.225619
3.84	8.00E+06	573	905	500983.352	1923776.07	332	0.240472
3.84	9.00E+06	573	953	575913.56	2211508.07	380	0.245723
3.84	1.00E+07	573	976	612041.339	2350238.74	403	0.235024
5.32	1.00E+06	573	484	-129166.501	-687165.79	-89	-0.68717
5.32	2.00E+06	573	530	-62677.273	-333443.09	-43	-0.16672
5.32	3.00E+06	573	577	5856.2	31154.984	4	0.010385
5.32	4.00E+06	573	635	91263.752	485523.161	62	0.121381
5.32	5.00E+06	573	668	140269.115	746231.692	95	0.149246
5.32	6.00E+06	573	735	240682.752	1280432.24	162	0.213405
5.32	7.00E+06	573	801	340800.264	1813057.4	228	0.259008
5.32	8.00E+06	573	840	400521.627	2130775.06	267	0.266347
5.32	9.00E+06	573	895	485452.352	2582606.51	322	0.286956
5.32	1.00E+07	573	935	547740.752	2913980.8	362	0.291398
8.72	1.00E+06	573	515	-84422.248	-736162	-58	-0.73616
8.72	2.00E+06	573	569	-5851.816	-51027.836	-4	-0.02551
8.72	3.00E+06	573	575	2927.552	25528.2534	2	0.008509
8.72	4.00E+06	573	617	64659.32	563829.27	44	0.140957
8.72	5.00E+06	573	643	103116.44	899175.357	70	0.179835
8.72	6.00E+06	573	667	138779.72	1210159.16	94	0.201693
8.72	7.00E+06	573	730	233146.727	2033039.46	157	0.290434
8.72	8.00E+06	573	753	267869.16	2335819.08	180	0.291977
8.72	9.00E+06	573	806	348433.559	3038340.63	233	0.337593
8.72	1.00E+07	573	832	388237.115	3385427.64	259	0.338543

Silica							
Mass Flow (kg/s)	Radiation (W)	Inlet Temp (K)	Outlet Temp (K)	Cp (J/kg K)	Avg Energy	Delta T	Efficiency
3.84	1.00E+06	573	497	-81849.15	-314300.74	-76	-0.3143
3.84	2.00E+06	573	561	-13171.729	-50579.44	-12	-0.02529
3.84	3.00E+06	573	631	64975.3468	249505.332	58	0.083168
3.84	4.00E+06	573	706	152218.613	584519.474	133	0.14613
3.84	5.00E+06	573	766	224630.741	862582.046	193	0.172516
3.84	6.00E+06	573	847	326077.81	1252138.79	274	0.20869
3.84	7.00E+06	573	880	368623.788	1415515.34	307	0.202216
3.84	8.00E+06	573	964	480098.558	1843578.46	391	0.230447
3.84	9.00E+06	573	992	518270.213	1990157.62	419	0.221129
3.84	1.00E+07	573	1070	627277.343	2408745	497	0.240874
5.32	1.00E+06	573	484	-95475.778	-507931.14	-89	-0.50793
5.32	2.00E+06	573	542	-33836.632	-180010.88	-31	-0.09001
5.32	3.00E+06	573	606	36702.1331	195255.348	33	0.065085
5.32	4.00E+06	573	667	106398.412	566039.552	94	0.14151
5.32	5.00E+06	573	707	153406.416	816122.133	134	0.163224
5.32	6.00E+06	573	773	233230.38	1240785.62	200	0.206798
5.32	7.00E+06	573	806	274198.093	1458733.86	233	0.208391
5.32	8.00E+06	573	884	373828.702	1988768.69	311	0.248596
5.32	9.00E+06	573	912	410552.645	2184140.07	339	0.242682
5.32	1.00E+07	573	987	511416.684	2720736.76	414	0.272074
8.72	1.00E+06	573	488	-91294.603	-796088.94	-85	-0.79609
8.72	2.00E+06	573	532	-44619.183	-389079.27	-41	-0.19454
8.72	3.00E+06	573	579	6620.7648	57733.0691	6	0.019244
8.72	4.00E+06	573	614	45705.6131	398552.946	41	0.099638
8.72	5.00E+06	573	667	106398.412	927794.153	94	0.185559
8.72	6.00E+06	573	711	158164.091	1379190.87	138	0.229865
8.72	7.00E+06	573	740	192966.488	1682667.77	167	0.240381
8.72	8.00E+06	573	790	254247.063	2217034.39	217	0.277129
8.72	9.00E+06	573	833	308240.634	2687858.33	260	0.298651
8.72	1.00E+07	573	852	332478.929	2899216.26	279	0.289922

y (m)	v (m/s)		y (m)	Conc (kg/m^3)	Vol Frac
0	0		0	187.201	0.093769
0.010929	0.463039		0.010507	189.573	0.094957
0.02889	0.750483		0.046945	122.427	0.061324
0.049834	0.984077		0.082846	94.0276	0.047099
0.05778	1.05928		0.095093	57.3612	0.028732
0.07785	1.22855		0.129848	53.5349	0.026816
0.086669	1.29553		0.143242	41.1199	0.020597
0.090163	1.32117		0.178335	39.8593	0.019966
0.110177	1.45849		0.19139	32.9193	0.016489
0.115558	1.49345		0.227137	34.923	0.017493
0.135812	1.61748		0.239538	33.5501	0.016805
0.144448	1.66753		0.276046	37.223	0.018645
0.16497	1.78067		0.287686	38.8994	0.019485
0.173337	1.82474		0.324976	38.2037	0.019136
0.194157	1.92989		0.335834	38.2773	0.019173
0.202227	1.9691		0.373896	34.6867	0.017375
0.223354	2.06805		0.383982	33.5288	0.016795
0.231116	2.1032		0.422802	30.6057	0.01533
0.252554	2.19717		0.432131	29.7323	0.014893
0.260005	2.22887		0.47169	27.3214	0.013685
0.281752	2.3187		0.480279	26.6328	0.01334
0.288895	2.34741		0.520558	24.625	0.012335
0.310948	2.43381		0.528427	24.0588	0.012051
0.317784	2.45983		0.569406	22.3743	0.011207
0.319921	2.46798		0.576575	21.8905	0.010965
0.342267	2.54975		0.618235	20.469	0.010253
0.346673	2.56573		0.624723	20.0418	0.010039
0.369321	2.64599		0.667045	18.8366	0.009435
0.375562	2.66773		0.672871	18.4489	0.009241
0.398502	2.74607		0.715836	17.4231	0.008727
0.404451	2.76604		0.72102	17.064	0.008547
0.427676	2.84254		0.764611	16.1876	0.008108
0.433341	2.86088		0.769168	15.8503	0.007939
0.456845	2.93568		0.813369	15.0986	0.007563
0.46223	2.95254		0.817316	14.7791	0.007403
0.486008	3.02579		0.862113	14.1315	0.007078
0.491119	3.04129		0.865464	13.8276	0.006926
0.515165	3.11311		0.910841	13.2666	0.006645
0.520008	3.12736		0.913613	12.9776	0.006501
0.544317	3.19787		0.959555	12.4884	0.006255
0.548897	3.21097		0.961761	12.2144	0.006118

y (m)	v (m/s)		y (m)	Conc (kg/m^3)	Vol Frac
0.573464	3.28026		1.00826	11.7844	0.005903
0.577787	3.29229		1.00991	11.5259	0.005773
0.602606	3.36046		1.05694	11.1442	0.005582
0.606676	3.3715		1.05806	10.9022	0.005461
0.631743	3.43861		1.10562	10.5597	0.005289
0.635565	3.44872		1.1062	10.3349	0.005177
0.660875	3.51485		1.15429	10.0238	0.005021
0.664454	3.52409		1.15435	9.81703	0.004917
0.690004	3.58928		1.2025	9.34271	0.00468
0.693343	3.5977		1.25065	8.91953	0.004468
0.719128	3.66202		1.2988	8.60081	0.004308
0.722232	3.66968		1.34916	8.43195	0.004224
0.748248	3.73315		1.39952	8.32581	0.00417
0.751121	3.74009		1.44989	8.22724	0.004121
0.777364	3.80277		1.50025	8.13529	0.004075
0.78001	3.80902		1.55061	8.04885	0.004032
0.806476	3.87094		1.60098	7.96529	0.00399
0.8089	3.87656		1.65134	7.84821	0.003931
0.835584	3.93775		1.7017	7.5133	0.003763
0.837788	3.94275		1.75207	7.20183	0.003607
0.864689	4.00325		1.80243	7.33187	0.003673
0.866678	4.00768		1.84549	7.01472	0.003514
0.893791	4.0675		1.85279	7.43557	0.003724
0.895567	4.07139		1.90316	7.39032	0.003702
0.922889	4.13057		1.95352	7.32575	0.003669
0.924455	4.13393		2.00388	7.21641	0.003615
0.951985	4.19248		2.05425	7.10756	0.00356
0.953345	4.19535		2.10461	7.00083	0.003507
0.981077	4.25331		2.15497	6.89734	0.003455
0.982234	4.2557		2.20534	6.79766	0.003405
1.01017	4.31307		2.2557	6.70202	0.003357
1.01112	4.31502		2.30607	6.6105	0.003311
1.03925	4.37182		2.35643	6.54674	0.003279
1.04001	4.37334		2.35643	6.52303	0.003267
1.06834	4.4296		2.40679	6.46324	0.003237
1.0689	4.43071		2.40679	6.43952	0.003226
1.09742	4.48643		2.45714	6.38346	0.003197
1.09779	4.48715		2.45716	6.35979	0.003186
1.1265	4.54236		2.5075	6.30716	0.003159
1.12668	4.5427		2.50752	6.28164	0.003146
1.15557	4.5974		2.55786	6.23101	0.003121

Vita

Arturo Sepulveda Fernandez was born September 2nd, 1968. The ninth child of Carlos Hector and Thelma Sepulveda, he graduated in Industrial Mechanical Engineering in 1991 from Instituto Tecnologico de Chihuahua (ITCH), after several years of work and experience he completed his Masters in Manufacturing Engineering at the University of Texas at El Paso (UTEP) in 2009. Currently he is working on his PhD on Environmental Science and Engineering (ESE) at UTEP with an emphasis on heat absorption analysis by falling particles at high temperatures for concentrating solar power systems. While completing his Mechanical Engineering degree he joined the Universidad Autonoma de Chihuahua as an English teacher; right after completing his Mechanical degree he has worked in the private industry working in the Automotive and construction fields. Working for Delphi Automotive Systems he was responsible for the Prototype area of Saginaw Steering Systems division at the Mexico Technical Center (MTC), also developed functions as Sr. Project Engineer and worked as a Program Manager for the Thermal systems division leading cross functional teams to develop new automotive products for international companies. In the private industry also participated in the construction business with his company designing and developing HVAC systems for industrial, commercial and residential programs.

Permanent address: 131 Sun Season Re
Santa Teresa NM, 88008

This thesis/dissertation was typed by Arturo Sepulveda Fernandez